Performance Assessment Modeling and Sensitivity Analyses of Generic Disposal System Concepts

Fuel Cycle Research & Development

Prepared for
U.S. Department of Energy
Used Fuel Disposition

S. D. Sevougian, G. A. Freeze,
W. P. Gardner, G. E. Hammond, P. Mariner

Sandia National Laboratories

Spetember 11, 2014

FCRD-UFD-2014-000320
SAND2014-17658P

Sandia National Laboratories is a multi-program laboratory managed and operated by Sandia Corporation, a wholly owned subsidiary of Lockheed Martin Corporation, for the U.S. Department of Energy's National Nuclear Security Administration under contract DE-AC04-94AL85000.

APPENDIX E

FCT DOCUMENT COVER SHEET [1]

Name/Title of Deliverable/ Milestone/Revision No.	Performance Assessment Modeling and Sensitivity Analyses of Generic Disposal System Concepts, M3FT-14SN0808032
Work Package Title and Number	Generic Disposal System Analysis, FT-14SN080803
Work Package WBS Number	1.02.08.08
Responsible Work Package Manager	Geoff Freeze (Name/Signature)
Date Submitted	September 12, 2014

Quality Rigor Level for Deliverable/Milestone[2]	☒ QRL-3	☐ QRL-2	☐ QRL-1 Nuclear Data	☐ Lab/Participant QA Program (no additional FCT QA requirements)

This deliverable was prepared in accordance with Sandia National Laboratories
(Participant/National Laboratory Name)

QA program which meets the requirements of

☒ DOE Order 414.1 ☐ NQA-1-2000 ☐ Other

This Deliverable was subjected to:

☒ Technical Review ☐ Peer Review

Technical Review (TR)
Review Documentation Provided

☐ Signed TR Report or,
☐ Signed TR Concurrence Sheet or,
☒ Signature of TR Reviewer(s) below

Peer Review (PR)
Review Documentation Provided

☐ Signed PR Report or,
☐ Signed PR Concurrence Sheet or,
☐ Signature of PR Reviewer(s) below

Name and Signature of Reviewers

Teklu Hadgu

NOTE 1: *Appendix E should be filled out and submitted with the deliverable. Or, if the PICS:NE system permits, completely enter all applicable information in the PICS:NE Deliverable Form. The requirement is to ensure that all applicable information is entered either in the PICS:NE system or by using the FCT Document Cover Sheet.*

NOTE 2: *In some cases there may be a milestone where an item is being fabricated, maintenance is being performed on a facility, or a document is being issued through a formal document control process where it specifically calls out a formal review of the document. In these cases, documentation (e.g., inspection report, maintenance request, work planning package documentation or the documented review of the issued document through the document control process) of the completion of the activity, along with the Document Cover Sheet, is sufficient to demonstrate achieving the milestone. If QRL 1, 2, or 3 is not assigned, then the Lab / Participant QA Program (no additional FCT QA requirements) box must be checked, and the work is understood to be performed and any deliverable developed in conformance with the respective National Laboratory / Participant, DOE or NNSA-approved QA Program.*

ACKNOWLEDGEMENTS

The authors greatly appreciate the contributions of the WIPP program, and the associated managers and technical staff of Sandia Orgs. 06211 and 06212, toward the testing of PFLOTRAN capabilities, as well as the impetus to add additional capabilities. This includes Sean Dunagan, Christi Leigh, Todd Zeitler, Chris Camphouse, and Sungtae Kim, with a special thanks to HeeHo Park. Also, Kris Kuhlman of Sandia Org. 06224 provided valuable advice and insights, as did Peter Lichtner of OFM Research, the original developer of PFLOTRAN.

EXECUTIVE SUMMARY

The Used Fuel Disposition Campaign (UFDC) of the U.S. Department of Energy (DOE) Office of Nuclear Energy (NE) is conducting research and development (R&D) on generic deep geologic disposal systems (i.e., repositories) for high-activity nuclear wastes (i.e., used nuclear fuel (UNF) and high-level radioactive waste (HLW)) that exist today or that could be generated in future fuel cycles. This report describes specific activities in FY2014 toward the development of an enhanced generic disposal system modeling and analysis capability that utilizes high-performance computing (HPC) environments to simulate important multi-physics phenomena and couplings associated with the potential behavior of a geologic repository for UNF and HLW.

The new Generic Disposal System Analysis (GDSA) Framework employs the HPC-capable PFLOTRAN multi-physics code (Hammond et al. 2014) to support the evaluation of repository and subsystem performance in the presence of coupled thermal-hydrologic-chemical processes, and the HPC-capable uncertainty sampling and propagation code DAKOTA (Adams et al. 2013a) for sensitivity analysis and multi-realization performance assessment, over a range of disposal options (e.g., salt, granite, clay, and deep borehole disposal). The GDSA framework includes multi-physics representations within PFLOTRAN of various coupled processes, including waste degradation, radionuclide mobilization, fluid flow, and radionuclide transport (advection, dispersion, diffusion, sorption, and radionuclide decay and ingrowth) through the engineered barriers and the bedded salt natural barrier to a well location in the aquifer.

In 2014 enhancements were made to the GDSA Framework process model capabilities, including the addition and testing of (1) a new multiphase fluid and heat flow process model, (2) dispersive transport through the addition of a diagonal hydrodynamic dispersion tensor, (3) a soil matrix compressibility model, (4) a hydrogen gas generation source term computed as a function of Fe corrosion and microbial degradation organics in waste packages, (5) generalization of sorption through isotherms, (6) on-the-fly swappable constitutive relations (i.e. gas and liquid equations of state, etc.), and (7) increasingly flexible radioactive decay and ingrowth within the aqueous and sorbed phases. This enhanced performance assessment (PA) modeling capability is demonstrated in FY2014 with deterministic and probabilistic simulations of a generic repository in bedded salt host rock, by comparisons of repository performance between a case with heat-generating waste (“thermal” case) and a case without heat generation (“isothermal” case). The simulation results provide preliminary insights into the multi-physics processes and couplings for the long-term behavior of a generic reference-case salt repository, but require additional refinement before being used as a definitive guide for future R&D. These preliminary results indicate that the effect of heat on radionuclide transport to the biosphere is likely not significant in a bedded salt repository, if only TH couplings are considered. However, the impact of THC, THM, and THMC coupling has not been investigated and may have important effects on transport pathways and behavior for the nominal scenario. Also, disturbed scenarios still require investigation with the GDSA Framework. (There are some effects on transport in some rock units for certain random samplings of the parameters in the multi-realization thermal (TH) case.)

In addition to the enhanced GDSA Framework capabilities and the expanded demonstration for the generic salt repository (Section 4), the salt repository reference case (Freeze et al. 2013a) was further revised in FY 2014 to include additional details (Section 3), and the reference cases for generic granite and clay/shale repositories were further advanced in FY 2014, as reported in

Painter et al. (2014) and Wang et al. (2014) for granite, and Zheng et al. (2014) and Jove-Colon et al. (2014) for clay/shale.

The application of an HPC-capable GDSA Framework is a significant advancement in PA modeling capability in that it allows the important multi-physics couplings to be represented directly, rather than through simplified abstractions. It also allows for complex representations of the source term, e.g., the explicit representation of many individual waste packages (i.e., meter-scale detail of an entire waste emplacement drift).

This report fulfills the Generic Disposal System Analysis Work Package Level 3 Milestone – *Performance Assessment Modeling and Sensitivity Analyses of Generic Disposal System Concepts* (M3FT-14SN0808032).

CONTENTS

FIGURES

TABLES

ACRONYMS

CFR	Code of Federal Regulations
DAKOTA	Design Analysis toolKit for Optimization and Terascale Applications
DOE	U.S. Department of Energy
DPC	dual-purpose canister
DRZ	disturbed rock zone
EBS	engineered barrier system
FEP	feature, event, and process
FY	fiscal year
GDSA	generic disposal system analysis
GWd	gigawatt-day
HDF5	hierarchical data format, version 5
HLW	high-level radioactive waste
HPC	high-performance computing
LHS	Latin hypercube sampling
MPI	message passing interface
MTHM	metric tons heavy metal
NBS	natural barrier system
NE	Office of Nuclear Energy
NRC	U.S. Nuclear Regulatory Commission
NWTRB	U.S. Nuclear Waste Technical Review Board
PETSc	Portable Extensible Toolkit for Scientific Computation
PWR	pressurized water reactor
QA	quality assurance
THC	thermal-hydrologic-chemical
THCM	thermal-hydrologic-chemical-mechanical
THCMBR	thermal-hydrologic-chemical-mechanical-biological-radiological
PA	performance assessment

R&D	research and development
SNF	spent nuclear fuel
UFDC	Used Fuel Disposition Campaign
UNF	used nuclear fuel
V&V	verification and validation
WIPP	Waste Isolation Pilot Plant
WF	waste form
WP	waste package

1. INTRODUCTION

This report describes specific activities in FY2014 toward the development of an enhanced disposal system modeling and analysis capability that utilizes high-performance computing (HPC) environments to assess the performance of a generic geologic repository for UNF and HLW. The new Generic Disposal System Analysis (GDSA) Framework employs the HPC-capable PFLOTRAN multi-physics code (Hammond et al. 2014) to support the evaluation of repository and subsystem performance in the presence of coupled thermal-hydrologic-chemical processes, and the HPC-capable uncertainty sampling and propagation code DAKOTA (Adams et al. 2013a) for sensitivity analysis and multi-realization performance assessment, over a range of disposal options (e.g., salt, granite, clay, and deep borehole disposal). The overall objectives of this enhance performance assessment (PA) modeling capability are:

1) Evaluate potential UNF/HLW disposal concepts and sites in various host rock media (such as salt, granite, or clay/shale)
2) Help prioritize generic RD&D activities and, later, site-specific RD&D activities
3) Support safety case development during all phases of repository investigations

Generic Disposal System Analysis (GDSA) Work Package activities completed in Fiscal Year (FY) 2013 and prior years demonstrated the capability to perform generic disposal system simulations for salt, granite, clay/shale, and deep borehole disposal options. These capabilities are documented in Clayton et al. (2011), Freeze and Vaughn (2012), Vaughn et al. (2013a), and Freeze et al. (2013a).

This report describes specific GDSA activities performed in FY2014 to:

- enhance the multiphysics capabilities of PFLOTRAN to better represent processes occurring in the disposal environment,
- further refine the reference modeling cases for the salt, granite, and clay/shale disposal concepts, and
- demonstrate the capabilities of the DAKOTA-PFLOTRAN framework in an HPC environment by simulating a portion of the 3-D domain for the generic salt reference case, for two cases—one with heat-generating waste and one without heat.

This report directly fulfills GDSA Work Package Level 3 Milestone – *Performance Assessment Modeling and Sensitivity Analyses of Generic Disposal System Concepts* (M3FT-14SN0808032) and, by reference, the supporting Milestones: *Generic Crystalline Disposal Reference Case* (M4FT-14LA0808012) (Painter et al. 2014) and *Generic Argillite/Shale Disposal Reference Case* (M3FT-14LB0808021) (Zheng et al. 2014). Section 2 of this GDSA milestone describes the enhanced GDSA Framework capabilities, including the conceptual model framework and the PFLOTRAN-based computational framework. It describes the new process-model capabilities added to PFLOTRAN during FY 2014 and some proposed capabilities for FY 2015. Section 3 describes additions and enhancements to the generic bedded-salt reference case, including an expansion of the simulation domain to better represent flow and transport boundary conditions, and the addition of thermal properties in order to simulate the performance of a salt repository for heat-generating waste. Section 4 presents a new demonstration of the GDSA Framework modeling and analysis capabilities by deterministic and probabilistic simulations of the generic

repository in bedded salt host rock, including comparisons of repository performance between a case with heat-generating waste ("thermal" case) and a case without heat generation ("isothermal" case). Section 5 presents a summary and conclusions.

2. GDSA METHODOLOGY

The development of any geologic repository takes place over a period of years and, as the repository program evolves, the level of completeness and rigor in the associated safety case (Sevougian and MacKinnon 2014; Freeze et al. 2013b; Sevougian et al. 2013a) becomes more robust with additional data from site characterization, repository design, and performance assessment activities. These three key activities combine to form an iterative process wherein the performance assessment from one development phase feeds site characterization and design at the next phase (Figure 2-1). Planning for, and transitioning to, each subsequent phase requires some form of decision-making process, as indicated in Figure 2-1, to prioritize the RD&D activities designed to resolve remaining issues and uncertainties. As implied in Figure 2-1, the performance assessment analysis is the most important quantitative activity to build confidence in this process and to prioritize future repository investigation activities. Therefore, there must be a high degree of confidence in the capabilities of the PA modeling tool(s). This confidence is enhanced when important multi-physics couplings can be directly incorporated into a probabilistic PA framework. This is facilitated when the PA software is designed to be run in a parallel architecture in a high-performance computing (HPC) environment, which in turn provides the following benefits, as a result of shorter computational times:

- Less reliance on conservative assumptions, simplifications, and process abstractions, which increases transparency and confidence with both the regulator and other stakeholders
- More realistic and comprehensive representation in the PA simulations of (1) features, events, and processes (FEPs), including more detailed spatial-temporal representation of geometry (e.g., 3-D spatial heterogeneity), and (2) parameter and model uncertainty, both aleatory and epistemic

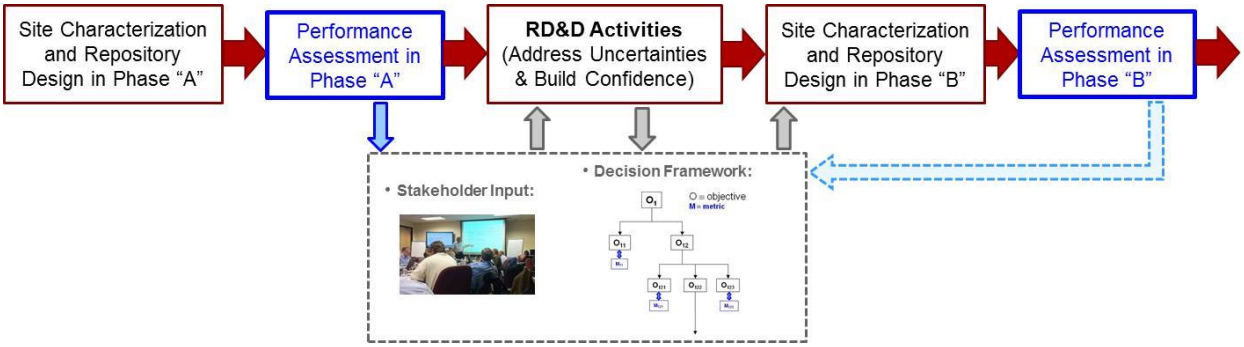

Figure 2-1. Iteration of site characterization, repository design, and performance assessment. {Note: Phases "A" and "B" are generic phases such as "licensing" or "construction".}

Another important aspect of being able to incorporate coupled multi-physics processes directly into PA calculations, is the resulting ability to directly evaluate the importance of these processes to long-term performance. The most complex system behavior occurs at early times as a result of thermal coupling (from the waste heat) with chemical, mechanical, and hydrologic processes. This coupling can greatly increase simulation times but, because long-term system behavior may be insensitive to short term system perturbations, it may be unnecessary to include some of these

coupled processes directly in long-term PA calculations. The decision of whether they must be included directly in PA or simply as an "initial condition" for the long-term postclosure simulations is facilitated by designing a PA framework that can simulate their effects on intermediate performance measures at early times, e.g., on changes in rock properties and fluid fluxes. An example of this is found at early times in salt host rock, wherein creep closure and salt backfill reconsolidation (THM processes) are short time-scale processes that may or may not need to be directly represented in long-term PA calculations. The use of a temporally varying porosity/permeability response surface may be sufficient for long-term PA but, if not, a multi-physics-capable PA framework (such as the GDSA framework) will allow for their direct incorporation in the long-term PA.

The major steps in the GDSA PA methodology are summarized in Figure 2-2. All of these steps are discussed in this report, with an emphasis on the refinement of the reference case (for salt host rock), enhancements to the PA model and code, and a demonstration of postclosure disposal system evaluation for the salt reference case. An important initial step in the development of any PA model is the identification of the important FEPs that must be represented in the PA model and software. Once the key FEPs have been identified and categorized (Freeze et al. 2014; Freeze et al. 2013c), a variety of different analyses may be performed to determine which FEPs are "screened in" to the PA model and which are "screened out" (Sevougian et al. 2012). The PA code/software development will reflect this FEPs screening, as discussed in the next section; however, as mentioned, a key attribute of the GDSA framework is the ability to directly couple robust representations of FEPs in the PA model. Thus, if future R&D indicates a change to an initial FEPs screening decision, this can easily be accommodated by the flexible GDSA model and computational framework (Section 2).

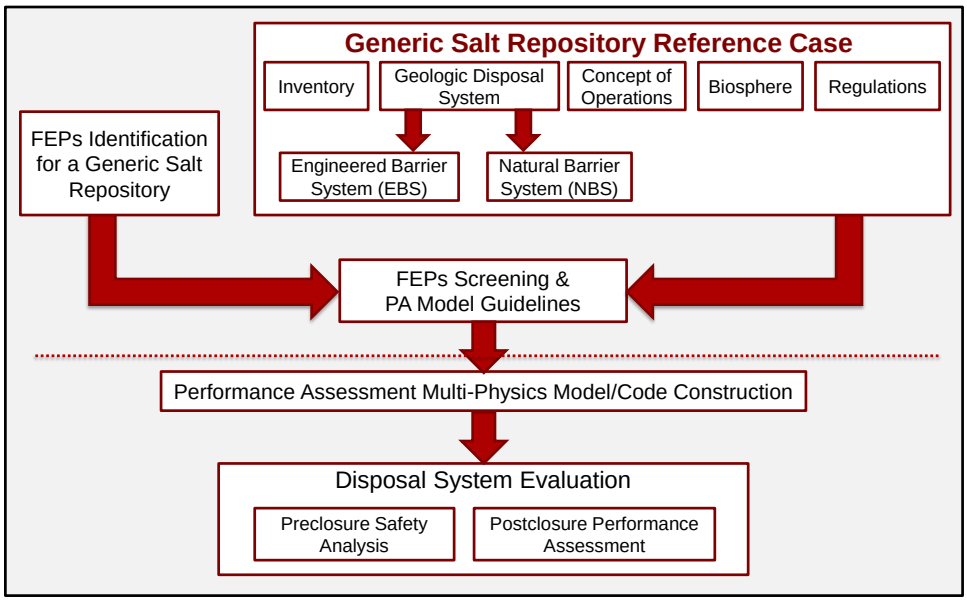

Figure 2-2. PA Methodology.

The enhanced PA modeling capability supporting generic disposal system modeling includes two main components (Freeze and Vaughn 2012, Section 2):

1) A *conceptual multi-physics model framework* that facilitates development of
    - a conceptual model of the important FEPs and scenarios that describe the multi-physics phenomena of a specific disposal system and its subsystem components, and
    - a mathematical model (e.g., governing equations) that implements the representations of the important FEPs and their couplings.
2) A *computational framework* that facilitates integration of
    - the system analysis workflow (e.g., input pre-processing, integration and numerical solution of the mathematical representations of the conceptual model components, and output post-processing), and
    - the supporting capabilities (e.g., mesh generation, input parameter specification and traceability, matrix solvers, visualization, uncertainty quantification and sensitivity analysis, file configuration management including verification and validation (V&V) and quality assurance (QA) functions, and compatibility with HPC environments).

The conceptual model framework is reviewed in Section 2.1 and the computational framework is reviewed in Section 2.2.

2.1 Conceptual Model Framework

This section briefly reviews the development of a generic repository conceptual model applicable to a range of disposal options, such as mined repositories in salt, granite, clay/shale, or disposal in deep boreholes. The major steps in the development of the conceptual model, as shown in Figure 2-2, include

- System Characterization (Reference Case development) – characterization of the regions and features of the disposal system, including property values and quantification of uncertainty
- System Design – specification of a disposal concept, repository, layout, and engineered design features
- FEP and Scenario Analysis – identification and screening of potentially relevant FEPs and scenarios, for inclusion in scenario analysis and PA model(s)
- PA Model Construction – conceptual and numerical implementation of the FEPs and scenarios (i.e., spatial and temporal discretization, parameterization of properties including uncertainty, numerical multi-physics descriptions)

The regions of a generic mined repository are shown in Figure 2-3. They include the Engineered Barrier System (EBS); the Natural Barrier System (NBS) or Geosphere; and the Biosphere. Figure 2-3 also illustrates the nested 3-D nature of the disposal system. The NBS completely surrounds the EBS (which encompasses the waste and emplacement tunnels, shown in red in the figure); radionuclides can be transported from the waste through the EBS and the NBS to the biosphere along multiple flow pathways. The figure also illustrates the presence of shafts and wells, shown in green. Shafts have the potential to provide a direct connection from the EBS to overlying NBS or to the biosphere. Wells have the potential to provide a direct connection from the NBS to the biosphere.

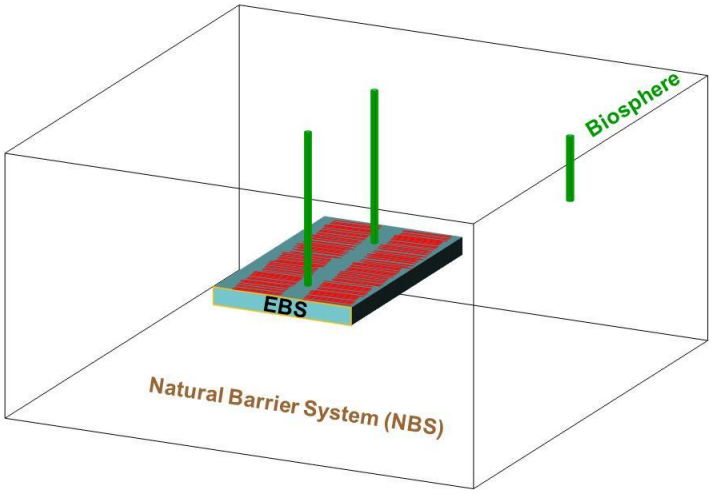

Figure 2-3. Regions of a Generic Disposal System.

For a generic bedded salt repository the major features and processes of each of the regions are illustrated schematically in 1-D in Figure 2-4. The features of the EBS include the wastes (e.g., waste forms and cladding) and engineered features (e.g., waste package, buffer and/or backfill, and seals/liner); the features of the NBS include the disturbed rock zone (DRZ), host rock, and other geological units (e.g., overlying or underlying aquifers); and the features of the biosphere include the surface environment and receptor characteristics (Freeze et al. 2014; Freeze et al. 2013c). Alternate terms that are commonly used to describe a disposal system, "near field" and "far field", are also shown in Figure 2-4. The near field encompasses the EBS and the DRZ (i.e., the components influenced by the presence of the repository). The far field encompasses the remainder of the NBS (i.e., beyond the influence of the repository).

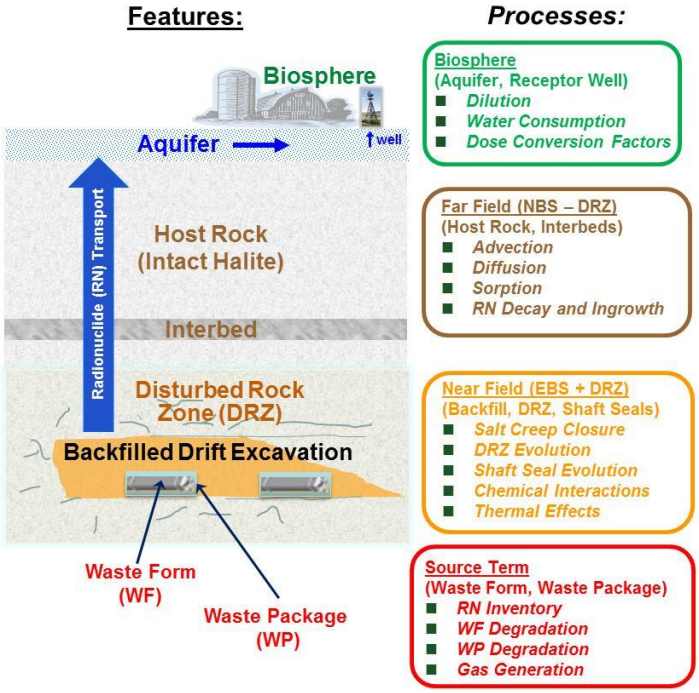

Figure 2-4. Major FEP categories for a generic bedded salt repository.

Figure 2-4 also illustrates schematically how radionuclide movement from the waste form to the receptor is influenced by multi-physics phenomena that can act upon and within each of the regions and/or features, but primarily in the near field region. These multi-physics phenomena include, at a high level, the thermal-hydrologic-chemical-mechanical-biological-radiological (THCMBR) processes and external events (e.g., seismicity) that impact (1) waste form and waste package degradation, (2) radionuclide mobilization from the waste form and radionuclide release from the waste package, (3) radionuclide transport through the near field and far field, and (4) radionuclide transport, uptake, and health effects in the biosphere. In addition to their direct effects on radionuclide transport, the THCMBR processes also influence the physical and chemical environments (e.g., temperature, fluid chemistry, biology, mechanical alteration) in the EBS, NBS, and biosphere, which in turn affect water movement, degradation of EBS components, and radionuclide transport.

FEP and scenario analysis methodologies are described by Freeze et al. (2013b, Section 4.2). A methodology for *categorizing* FEPs has been presented in Sevougian et al. (2014) and Freeze et al. (2014). A methodology for *screening* these potentially important FEPs for inclusion/exclusion with respect to the PA conceptual model (with specific application to bedded salt host rock) has been described by Sevougian et al. (2012). Details of the PA conceptual model used as a current test case for the GDSA framework are described in Section 3, which includes a discussion of the bedded salt reference case and the implementation of that reference case in the current version of the GDSA PFLOTRAN-based computational framework. The current reference cases for mined repositories in granite and clay/shale are described in Wang et al. (2014) and Jove-Colon et al. (2014), respectively. As noted by Sevougian et al. (2013b, Section 1), the current focus of the reference cases is on FEPs for undisturbed scenarios.

As mentioned above, an important attribute underlying the GDSA conceptual PA model is the desire to directly integrate high-fidelity conceptual models of subsystem processes and couplings into the system PA model, thereby reducing the use of abstractions or simplified models and response surfaces. This is facilitated by the HPC compatibility of the multi-physics codes. However, in some cases there will still be conceptual and/or computational model advantages to relying on process model feeds or abstractions to represent some of the most complex multi-physics couplings. This type of approach is illustrated schematically in Figure 2-5, showing some potential process model codes that incorporate THCM coupling. Because of the HPC capability and modular nature of the GDSA framework, the decision of whether to use an abstraction for long-term (e.g., 1,000,000-year) simulations or to include a process directly in the PA framework can be made by testing of the complex coupling within the flexible GDSA framework.

2.2 Computational Framework

The general philosophy and attributes of a PA computational framework are described by Freeze et al. (2013a) and Freeze and Vaughn (2012). As described in these prior reports, the GDSA computational framework includes two major conceptual components:

- System analysis workflow and computational capabilities
- Configuration management

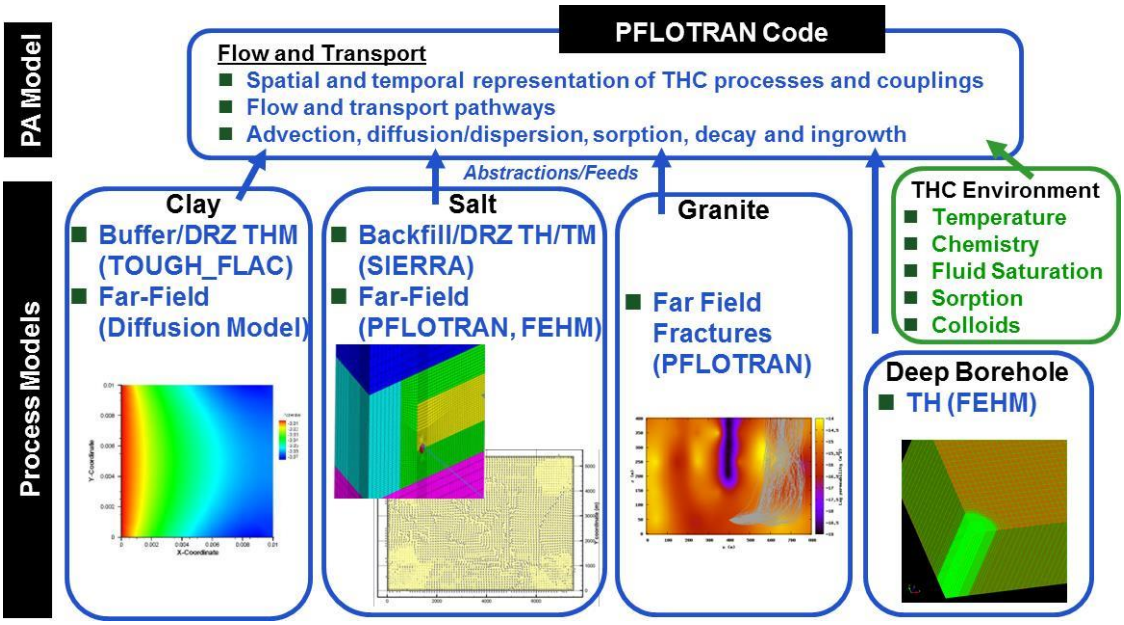

Figure 2-5. Integration of PA Model and Process Models.

As outlined in Freeze and Vaughn (2012, Section 2.3), the first framework component, the system analysis workflow and computational capabilities, controls the development and implementation of the software needed for the execution of deterministic and probabilistic system simulations. Specific functions include:

1. Input development and pre-processing (spatial and temporal discretization, mesh generation, input parameter specification and traceability, including uncertainty)
2. System model development and implementation (mathematical representations of process model FEPs and couplings, uncertainty quantification)
3. Integrated system model execution (numerical representations of FEPs and couplings, data structure and matrix solvers)
4. Output management and post-processing (analysis of results, visualization, sensitivity analyses)

The two key software components that fulfill functions 2 and 3 are the software associated with uncertainty quantification and analysis ("stochastic simulation") and the software associated with simulation of the multiphysics coupled processes ("domain simulation"). As indicated in Figure 2-6, the following open-source codes perform this core set of functions in support of the generic repository PA modeling capability:

- DAKOTA – sensitivity analysis and uncertainty quantification
- PFLOTRAN – THC multi-physics flow and transport

Details of these two codes are presented in Sections 2.2.1 through 2.2.2.

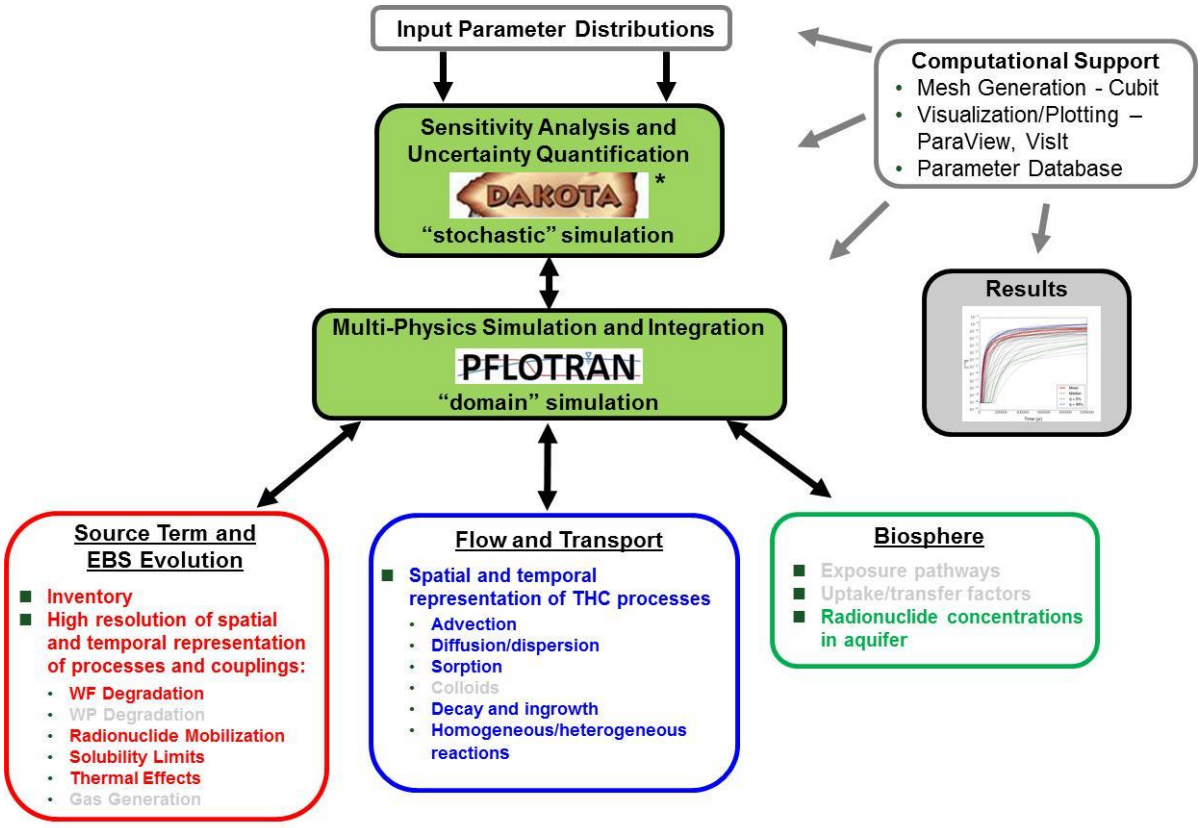

Figure 2-6. High-Level GDSA Computational Framework.

As indicated in Figure 2-6, there are three major components of the domain simulation software:

- Flow and transport – This includes the simulation of fluid-phase flow (either gas or liquid) and solute transport, in both the near-field and far-field domains (see Figure 2-4). Currently, this capability is provided directly by PFLOTRAN in both domains, but could eventually be represented with different codes in the two domains, if warranted (e.g., a separate discrete fracture model/code in the far-field of a granitic repository concept).
- Source Term and EBS Evolution – A single code or a suite of codes to represent the multi-physics processes in the emplacement drifts and near-field surrounding host rock, including heat generation from the inventory, waste form degradation, waste package degradation, coupled THC and/or THCM effects, and radionuclide mobilization and transport.
- Biosphere Transport and Receptor Uptake – A biosphere code to represent the surface and biosphere processes contributing to the dose to a human receptor resulting from radionuclide releases from the NBS. Generally, this is the most "loosely" coupled of the suite of PA codes, with no upstream feedbacks.

More details of these latter two components are presented in Section 2.2.2. Currently, they are implemented in the PFLOTRAN code in a simplified fashion. However, a complex SNF degradation model (Jerden et al. 2014) is planned to be coupled to PFLOTRAN in FY 2015, as described below in Section 2.2.2.1.2.

The computational framework shown in Figure 2-6 also currently includes the following supporting capabilities:

- Input Parameter Specification – eventually in a controlled parameter database, but simply in PFLOTRAN and DAKOTA input files at this time
- Mesh Generation – currently using Cubit (SNL 2013)
- Visualization – currently using VisIt (LLNL 2005)
- Scripting – Python scripts to process output data for analysis

2.2.1 DAKOTA – "Stochastic" Simulation

In the enhanced PA model system analysis workflow, sensitivity analysis and uncertainty quantification (UQ) capabilities are provided by DAKOTA (Design Analysis toolKit for Optimization and Terascale Applications). DAKOTA (Adams et al. 2013a; Adams et al. 2013b) can be used to manage uncertainty quantification, sensitivity analyses, optimization, and calibration. Specific DAKOTA capabilities include (Figure 2-7):

- Generic interface to simulations
- Extensive library of time-tested and advanced algorithms
- Mixed deterministic / probabilistic analysis
- Supports scalable parallel computations on clusters
- Object-oriented code; modern software quality practices

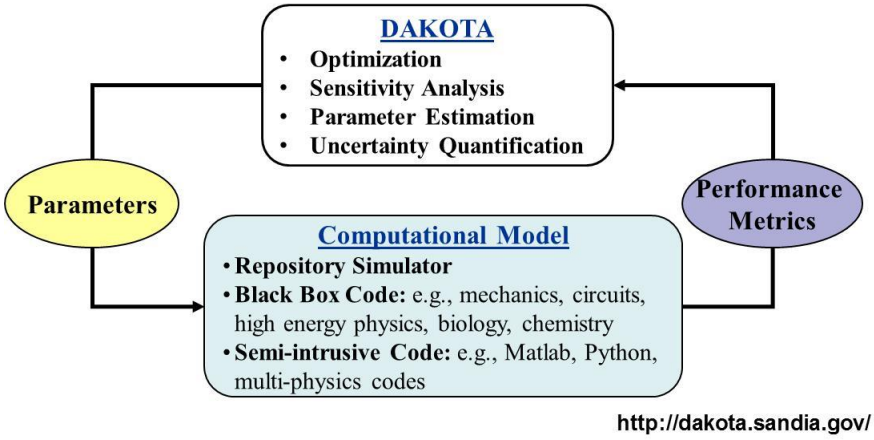

Figure 2-7. DAKOTA Code Workflow and Capabilities.

2.2.2 PFLOTRAN – "Domain" Simulation

PFLOTRAN (Hammond et al. 2014) is an open source, reactive multi-phase flow and transport simulator (see "Flow and Transport" box in Figure 2-6) designed to leverage massively-parallel high-performance computing to simulate earth system processes. PFLOTRAN has been employed on petascale leadership-class DOE computing resources (e.g., Jaguar [at Oak Ridge

National Laboratory (ORNL)] and Franklin/Hopper [at Lawrence Berkeley National Laboratory (LBNL)]) to simulate THC processes at the Nevada Test Site (Mills et al. 2007), multi-phase CO_2-H_2O flow for carbon sequestration (Lu and Lichtner 2007), CO_2 leakage within shallow aquifers (Navarre-Sitchler et al. 2013), and uranium fate and transport at the Hanford 300 Area (Hammond et al. 2007; Hammond et al. 2008; Hammond and Lichtner 2010; Hammond et al. 2011; Lichtner and Hammond 2012a; Chen et al. 2012; Chen et al. 2013).

PFLOTRAN solves the non-linear partial differential equations describing non-isothermal multi-phase flow, reactive transport, and geomechanics in porous media. Parallelization is achieved through domain decomposition using the Portable Extensible Toolkit for Scientific Computation (PETSc) (Balay et al. 2013). PETSc provides a flexible interface to data structures and solvers that facilitate the use of parallel computing. PFLOTRAN is written in Fortran 2003/2008 and leverages state of the art Fortran programming (i.e. Fortran classes, pointers to procedures, etc.) to support its object-oriented design. The code provides "factories" within which the developer can integrate a custom set of process models and time integrators for simulating surface and subsurface multi-physics processes. PFLOTRAN employs a single, unified framework for simulating multi-physics processes on both structured and unstructured grid discretizations (i.e. there is no duplication of the code that calculates multi-physics process model functionals in support of structured and unstructured discretizations). The code requires a small, select set of third-party libraries (e.g., MPI, PETSc, BLAS/LAPACK, HDF5, Metis/Parmetis). Both the unified structured/unstructured framework and the limited number of third-party libraries greatly facilitate software installation and usability for the end user.

Specific PFLOTRAN capabilities for the simulation of generic disposal systems include:

- Multi-physics
  - Multi-phase flow
  - Multi-component transport
  - Biogeochemical processes
  - Thermal and heat transfer processes
- High-performance computing (HPC)
  - Built on PETSc – parallel solver library
  - Massively parallel
  - Structured and unstructured grids
  - Scalable from laptop to supercomputer
- Modular design based on object-oriented Fortran 2003/2008 for easy integration of new process models

In FY 2014, a new multiphase fluid and heat flow process model was implemented within PFLOTRAN that considers conservation of mass for a miscible gas component (e.g. air, $H_{2(g)}$, etc.) in the gas phase and water in the liquid phase. Dissolution of gas in the liquid phase is calculated using Henry's law, while water vapor is tracked in the gas phase. Interchangeable equations of state are employed to calculate fluid mixture densities and viscosities as a function of pressure and temperature. Heat convection (fluid) and conduction (combined matrix and fluid) are modeled through an energy conservation equation. Dispersive transport was added to PFLOTRAN through the addition of a diagonal hydrodynamic dispersion tensor (previously,

PFLOTRAN considered solely advective and diffusive transport). Other enhancements include (1) soil matrix compressibility, (2) a hydrogen gas generation source term computed as a function of Fe corrosion and microbial degradation organics in waste packages, (3) generalization of sorption through isotherms, (4) on-the-fly swappable constitutive relations (i.e. gas and liquid equations of state, etc.) and (5) increasingly flexible radioactive decay and ingrowth within the aqueous and sorbed phases (decay in the mineral phase is a proposed research direction for FY 2015—see Section 2.2.2.1 below).

PFLOTRAN's process models were verified against a suite of test problems developed for the Waste Isolation Pilot Plant (WIPP). For (immisible) multiphase fluid flow, PFLOTRAN results were compared to BRAGFLO (WIPP PA 2013a) and TOUGH (Pruess 1991) simulation results while the code's transport model was verified against NUTS (WIPP PA 1997). Figure 2-8 illustrates a representative comparison of PFLOTRAN's simulation results to those of TOUGH2 (TOUGH28W) and BRAGFLO for gas pressure, liquid pressure, and the production of brine and gas from a production well with a specified bottom-hole pressure—Case #8 in the BRAGFLO V&V document (WIPP PA 2013b).

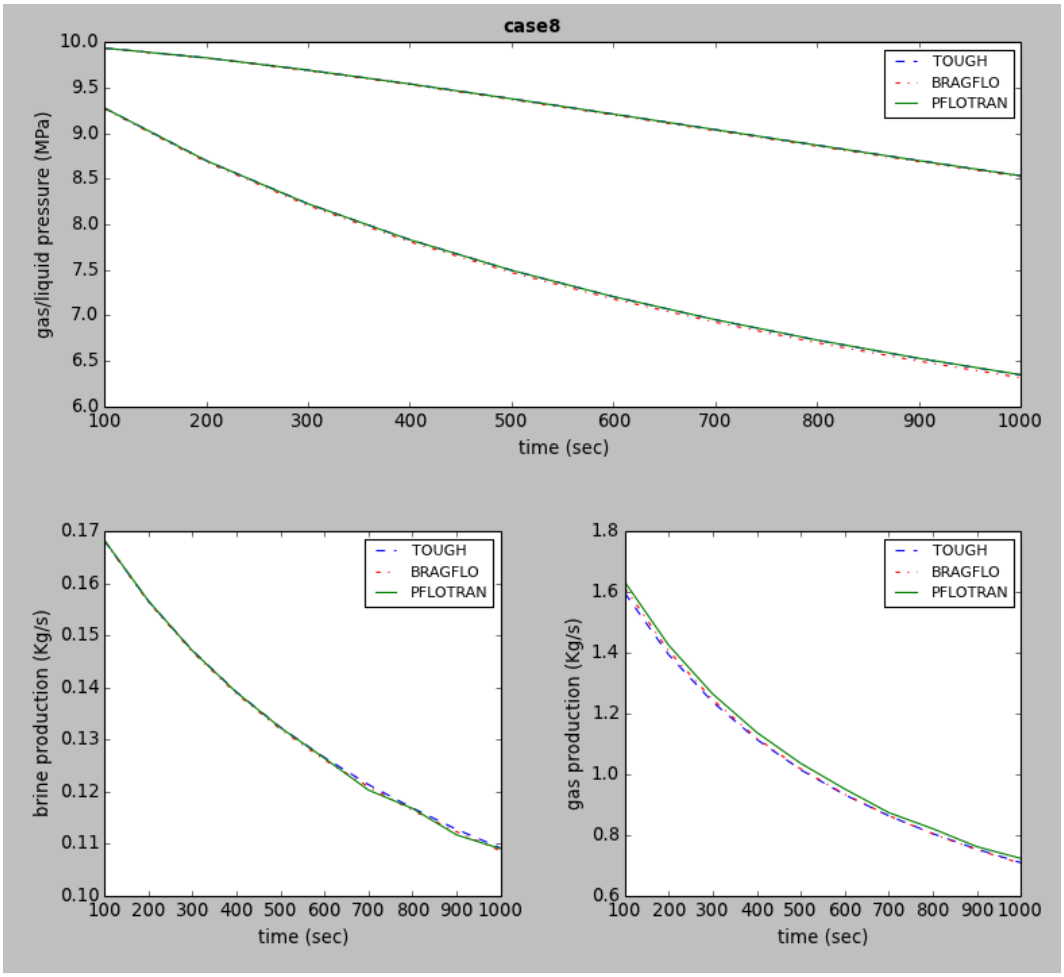

Figure 2-8. Comparison of PFLOTRAN, TOUGH2, and BRAGFLO brine and gas production from a production well with a specified bottom-hole pressure.

2.2.2.1 Source Term and EBS Evolution

As shown in Figure 2-6, in addition to the flow and transport software/model component (described briefly in the previous section, and in detail in Lichtner et al. 2014), a generic disposal system PA model must be able to represent processes contributing to the radionuclide source term. Specific processes to be considered in the Source Term and EBS Evolution component include (consistent with Figure 2-6):

- Waste form degradation
  - Processes and rates for degradation of UNF waste forms (e.g., cladding degradation, gap and grain boundary releases, UO_2 matrix dissolution) as a function of the EBS near-field environment
  - Processes and rates for degradation of HLW waste forms (e.g., borosilicate glass) as a function of the EBS near-field environment
- Waste package degradation
  - Processes, rates, and failure mechanisms (e.g., general and localized corrosion, stress corrosion cracking) as a function of the EBS near-field environment
  - Gas generation and consumption of water associated with waste package degradation
- Radionuclide mobilization
  - Processes for mobilization of radionuclides from degraded waste forms (e.g., equilibrium and/or kinetically rate-limited dissolution in the aqueous phase, alpha radiolysis, growth of a corrosion layer, colloid formation, sorption, diffusion through a boundary layer, etc.)
- Radionuclide solubility limits
  - The concentrations of radionuclides dissolved in the aqueous phase may be limited by solubility. At aqueous dissolved concentrations above the solubility limits, radionuclides precipitate to a solid phase; when concentration falls below the solubility limit (e.g., due to decay and transport), the precipitate will re-dissolve up to the solubility limit.
  - Aqueous solubility is an elemental property. Solubility calculations must account for fractional contributions of all isotopes of the same element and for isotopes that occur naturally in the geosphere.
- Radionuclide decay and ingrowth
  - Radionuclide inventory as a function of time, which includes consideration of decay in various phases (e.g., dissolved, sorbed) and ingrowth of decay chain daughter products
- EBS near-field environment
  - Processes controlling the local near-field THCMBR environment

The relationships between these processes are illustrated schematically in Figure 2-9. As noted above, source term and EBS evolution processes are currently implemented in a simplified fashion directly into PFLOTRAN, as described in more detail below. As the PA model matures, an independent EBS source code or suite of codes may be added to the GDSA PA modeling capability.

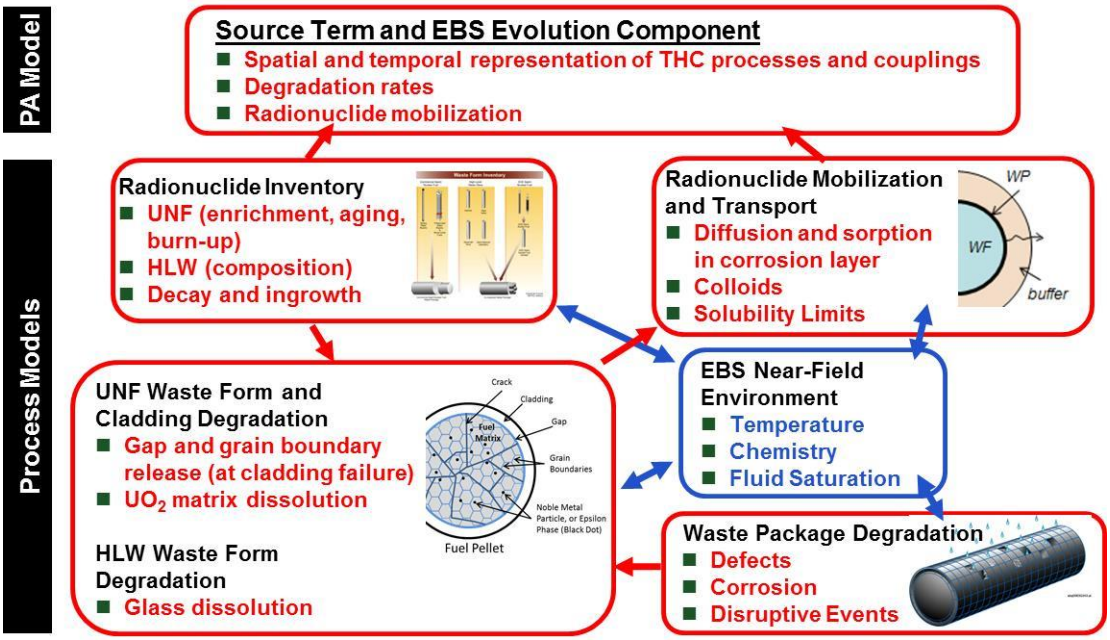

Figure 2-9. Generic Disposal System Source Term and EBS Evolution Processes.

2.2.2.1.1 Current PFLOTRAN Source Term and EBS Implementation

The implementation of the source term and EBS evolution in the GDSA framework currently uses the reactive transport capabilities of PFLOTRAN. The source term derives from a mineral phase (representing an SNF waste form) that kinetically degrades over time. Depending on solubility, the radionuclides released from this waste-form mineral phase are then available to either enter the aqueous phase, where they may be transported through the EBS or precipitate as a secondary mineral phase. The representation of specific source term processes in PLFOTRAN is briefly summarized below. Exact details and property values are presented in Sections 3.2 (which describes the generic salt repository reference case) and 3.3 (which describes the implementation of the reference case in the GDSA framework).

- Waste form degradation
  - The waste form mineral is defined to have a stoichiometry (i.e., radionuclide mole fractions) and density representative of the UNF waste form and to be unstable (i.e., it is specified to have a large dissociation constant (log *K*)). A waste form degradation rate (representative of UO_2 matrix dissolution) can then be specified by adjusting the rate of the dissociation reaction.
  - Gap and grain boundary (fast or instant) release fraction for ^{129}I, modeled as dissolved ^{129}I in the waste form grid cell at the initial time
  - Cladding degradation is not currently modeled in the GDSA framework.
- Waste package degradation
  - Waste package degradation (and associated gas generation) is not included in the current GDSA framework implementation. Instead, waste package degradation is assumed to be instantaneous and no credit is taken for waste package performance.

- Radionuclide mobilization
  - As the waste form mineral degrades, radionuclides are released congruently to the aqueous phase where they may undergo advection, diffusion, sorption, and/or precipitation.
  - Colloid formation and release are not included in the current GDSA framework.
- Radionuclide solubility limits
  - Solubility limits are implemented in PFLOTRAN by defining individual secondary mineral phases for each radionuclide. A radionuclide with a dissolved concentration that reaches its solubility limit precipitates as the equilibrium secondary mineral and can re-dissolve when the dissolved concentration subsequently falls below the solubility limit.
  - Solubility limits in PFLOTRAN are defined by radionuclide rather than by element. To account for fractional contributions of different isotopes (radionuclides) of the same element, PFLOTRAN radionuclide solubility limits are calculated from elemental solubility limits by assuming that the fraction of each radionuclide of an element in the aqueous phase is the same as the fraction of each radionuclide of an element within the waste form. In reality, the radionuclide fractions in the aqueous phase will change over time and space due to decay and ingrowth and due to the different mobilities of the various radionuclides—see Section 2.2.2.1.2 below for planned enhancements that will more properly account for solubility limits when several isotopes are present.
- Radionuclide decay and ingrowth
  - In the aqueous phase, radionuclide decay and ingrowth to daughter radionuclides are simulated using PFLOTRAN chemical reactions. Parent radionuclides are converted to daughters using a first-order forward kinetic reaction.
  - Radionuclide decay and ingrowth in the mineral phases is not included in the current PFLOTRAN implementation. This process could be important for simulation of short-lived radionuclides with slow waste form degradation rates. Thus, as described in Section 2.2.2.1.2, a change will be made in FY 2015 to account for decay/ingrowth in the mineral phase.
- EBS near-field environment
  - Because PFLOTRAN allows for multiphase flow coupled to the energy equation, THC coupling is inherently included. TH couplings are demonstrated by the simulations described below in Sections 4.4 and 4.5. THC couplings will be investigated later, if the effect of major ion chemistry on EBS behavior is deemed to be important. This may be the case when the SNF degradation model (Jerden et al. 2014) is directly coupled to PFLOTRAN (as described in Section 2.2.2.1.1), since the SNF degradation model is a function of pH and certain major ion concentrations such as carbonate and dissolved oxygen. There is no incorporation of the effect of mechanical processes (e.g., salt creep) on the source term in the current GDSA framework, although some mechanical processes (linear elasticity) are incorporated into PFLOTRAN (e.g., see Lichtner et al. 2014).

2.2.2.1.2 Planned Enhancements for PFLOTRAN Source Term and EBS Implementation

To date, GDSA modeling using PFLOTRAN has not included radioactive decay in the precipitate phase and has not sufficiently simulated elemental solubility controls. In FY 2014, ways to address these deficiencies were explored. This section summarizes the working conceptual model for isotope decay, sorption, and secondary precipitation/dissolution and how these processes can be implemented in PFLOTRAN in the future. This section also discusses the integration of PFLOTRAN with the Fortran-based Mixed Potential Model of UNF degradation, planned for FY 2015.

Radioactive Decay and Equilibrium Partitioning

In the main PFLOTRAN code, changes in concentrations within a cell are controlled by rates. The rate of change of a concentration is determined for each isotope species in each phase for each process that affects the concentration within the cell. These rates are summed over all processes to provide the net rates of change for each species at each time step for each cell.

Figure 2-10 is a schematic diagram of the various processes within a single cell that can affect the concentrations of an isotope (^{237}Np in this case). In theory, each of these processes can be defined using rates. However, PFLOTRAN does not simulate radioactive decay in the precipitate phase except through the creation of a new "reaction sandbox" module (Lichtner et al. 2014). In addition, PFLOTRAN also does not automatically account for the effects of elemental solubility on the precipitation/dissolution rates of isotopes. Because these processes are important to PA modeling, it was necessary to devise a plan for including them.

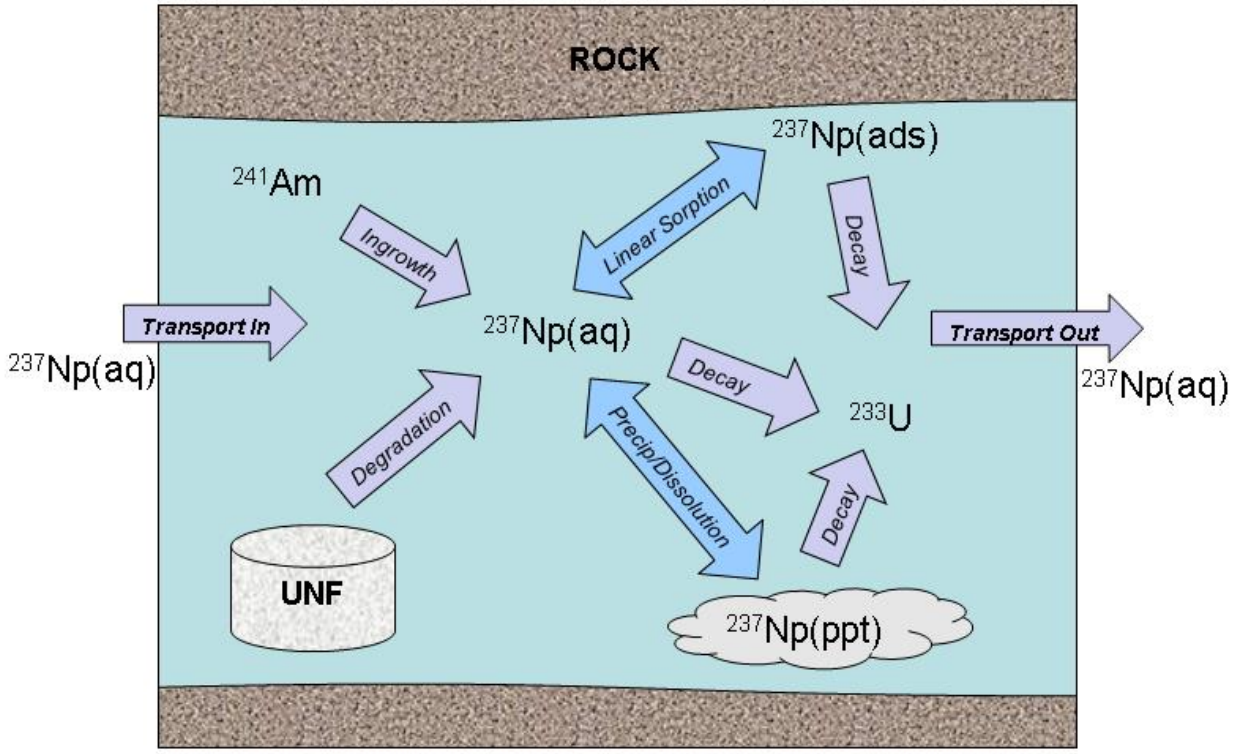

Figure 2-10. Schematic diagram of processes affecting concentrations ^{237}Np in aqueous, adsorbed, and precipitate phases within a single cell.

The plan developed to address these needs is to create a new PFLOTRAN reaction sandbox routine and a new PFLOTRAN process model. The new reaction sandbox routine will be used to calculate the decay and ingrowth of each isotope in each phase, and the new process model will be used to calculate equilibrium solubility partitioning. When implemented, PFLOTRAN will employ the new sandbox routine to calculate net decay rates (i.e., decay rates less ingrowth rates) and the new solubility process model will calculate equilibrium solubility partitioning.

Figure 2-11 presents a flow diagram of the planned calculations. The two main steps are:

- **Step 1**. *Calculate new non-equilibrated isotope concentrations in the cell resulting from time-dependent processes*. The modeled time-dependent processes are depicted with purple arrows in Figure 2-10. This step will require the planned reaction sandbox routine for decay and ingrowth. All rates from time-dependent processes will be summed for each isotope species in each phase, multiplied by the duration of the time step, and added to the initial species concentrations to calculate, in a single implicit Newton solve, new non-equilibrated concentrations for each species in each phase. This step will effectively provide the total concentrations of each isotope in the cell.

- **Step** 2. *Bring the non-equilibrated isotope concentrations in the cell to chemical equilibrium with respect to sorption and solubility*. Sorption of radionuclides and precipitation/dissolution of secondary mineral phases are modeled as equilibrium processes (depicted in Figure 2-10 with blue arrows). Equilibrium processes are not time-dependent. This step will use the planned process model to achieve equilibrium sorption and equilibrium precipitation/dissolution with respect to solubility-controlling phases. It will adjust the isotope concentrations as needed to ensure that elemental solubility limits and mass balances are enforced, sorption reactions are at equilibrium, and intra-element isotope distributions are identical in each phase.

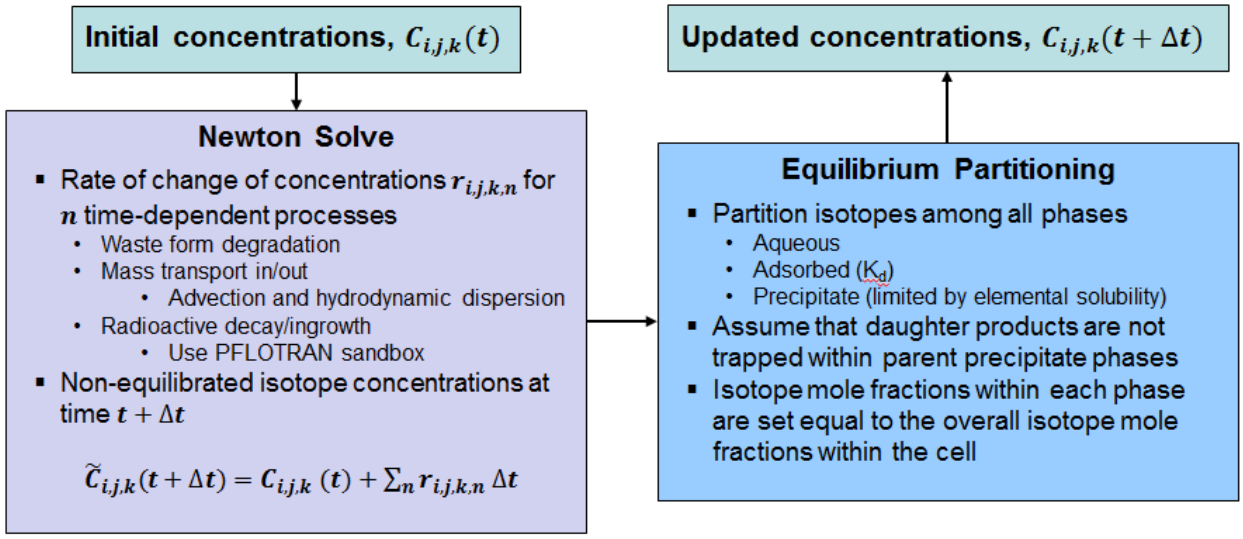

Figure 2-11. Flow diagram for updating isotope concentrations in PFLOTRAN using a new reaction sandbox routine for decay and ingrowth and a new process model for equilibrium partitioning. (Subscripts i, j, and k denote isotope, element, and phase, respectively.)

Radioactive Decay and Ingrowth

Plans have been developed and independently tested for adding advanced features to PFLOTRAN for radioactive decay and ingrowth. This work, planned for implementation in FY 2015, will involve the development of a PFLOTRAN reaction sandbox routine and a radioactive decay database. The new capability will allow for decay of isotopes in the solid phase (e.g., mineral phase) and will improve the implementation and quality assurance of radioactive decay and ingrowth calculations in PFLOTRAN.

Radioactive decay and associated ingrowth of daughter products are not featured capabilities of PFLOTRAN. The `GENERAL_REACTION` block can be used to simulate radioactive decay and ingrowth but only for simple systems and highly soluble isotopes. For example, the input block

```
GENERAL_REACTION
  REACTION 1. I129- <-> 1. Xe129(aq)
  FORWARD_RATE 1.29d-15  ! 1/s
  BACKWARD_RATE 0.d0
```

simulates decay of $^{129}I^-$ to $^{129}Xe(aq)$. For isotopes having more than one modeled aqueous species, each species would need its own decay reaction and an equivalent decay rate. In the `GENERAL_REACTION` block, daughter products are released to the aqueous phase where they are subsequently distributed among their aqueous, solid, and gas species as dictated by the defined chemical reactions. Sorbed isotope species do not require additional decay blocks because their concentrations are functions of aqueous concentrations. For isotopes within a mineral phase, a similar reaction block cannot be defined.

To improve the simulation of radioactive decay and ingrowth, a new PFLOTRAN reaction sandbox routine will be developed. This routine, developed and tested using Mathcad, will return net decay rates for each isotope in each phase (aqueous, sorbed, solid, gas). Instead of reaction blocks, it will use a radioactive decay database that will provide decay rates, daughter products, and isotope daughter branching ratios for each isotope.

The sandbox routine will do the following for each isotope in each cell:

1. Read the isotope concentrations in each phase
2. Read the relevant decay reactions and decay rates from the database
3. Calculate the decay rates
4. Calculate the total ingrowth rates based on the calculated decay rates
5. Calculate and return the net decay rate for each isotope in each phase

The net decay rates from this routine will be calculated in Step 1 ("Newton Solve") of Figure 2-11. These calculations will assume homogeneous decay, i.e., they will assume that daughters initially stay in the same phase as their parents. In reality, some daughters of parents decaying within the solid phase may be highly soluble, and some daughters with aqueous parents will have low solubility. This assumption, however, will not affect the final calculation of equilibrium concentrations because the non-equilibrated isotope concentrations calculated in Step 1 (Figure 2-11) will be redistributed according to the equilibrium solubility and sorption constraints enforced in Step 2 ("Equilibrium Partitioning"). Thus, for example, aqueous ^{237}Np that is initially

produced by the decay of aqueous ^{241}Am will likely immediately precipitate due to the lower solubility of Np and the lower decay rate of aqueous ^{237}Np.

Equilibrium Partitioning

In addition to the plans for developing radioactive decay and ingrowth in PFLOTRAN, a plan has been developed for adding the capability to simulate equilibrium partitioning for elements and isotopes. This work, planned for implementation in FY 2015, will involve adding a new process model to PFLOTRAN. The new capability will allow the user to set elemental solubility limits and use them to simulate element and isotope equilibrium partitioning between phases.

The standard method for simulating solubility controls in PFLOTRAN is to use the chemistry process model. The chemistry process model is a powerful and highly effective tool for simulating a large set of chemical reactions (Lichtner et al. 2014). Reactions are simulated in PFLOTRAN as rate-limited kinetic reactions. Chemical equilibrium is approximated by setting high reaction rates. For a complicated chemical system, a large set of aqueous and mineral reactions must be simulated for each cell at each time step.

Although the chemistry process model is one of the strengths of PFLOTRAN and gives PFLOTRAN the ability to simulate chemical reactive transport, an important drawback is that it typically requires 1) extra effort to ensure that all the desired reactions are included and 2) a large number of parallel processors to perform simulations in a short amount of time. In addition, because the chemistry process model and database were developed for elemental reactions, they are not easily adapted for isotopes. Thus, an alternative solubility process model is needed for simulations where isotopes are involved and where rapid probabilistic scoping calculations are needed for domains where chemical constraints are unknown or poorly understood.

This year, to simplify equilibrium solubility and phase partitioning calculations in PFLOTRAN for radioactive isotopes, a new algorithm was developed and tested in Mathcad for a new optional PFLOTRAN process model to simulate equilibrium partitioning. This model will simulate solubility-controlled mineral precipitation and dissolution for both elements and isotopes. Simulations will be rapid using this process model because equilibrium partitioning of isotopes among all phases is determined using a simple set of explicit, temporally-independent calculations. Instead of identifying and simulating specific minerals and chemical reactions, the user need only define elemental solubility limits and/or their probability distributions. Importantly, the process model will include the ability to calculate the effective solubilities of isotopes for each solubility-controlled element.

This process model will execute after the total non-equilibrated concentrations of each species in each phase are determined in Step 1 of Figure 2-11. Total elemental concentrations and isotope mole fractions in the cell will be calculated from the isotope concentrations provided in Step 1. This information will then be used to determine whether the total concentration for each element is high enough for the element to precipitate. If it is, the aqueous elemental concentration will be set at the solubility limit, the sorbed concentration will be calculated from the solubility, and the amount left over will precipitate. If it is not, the total concentration will simply be partitioned between the aqueous and sorbed phases based on the sorption partition coefficient. As a final step, isotopic distributions will be equilibrated by setting the isotope mole fractions for each element within each phase equal to the overall isotope mole fractions for each element in the cell.

To simulate solubility limits accurately, this process model will require that all isotopes that could have a significant contribution to the aqueous elemental concentration be included in the simulation. Thus, if natural background concentrations of stable and/or unstable isotopes are expected to significantly contribute to elemental aqueous concentrations, they will need to be included in the model. For radioactive isotopes in the source term, it may not be sufficient to exclude an isotope from the model based on low isotopic mole fractions in the source term because in a transport model the isotope in question could be a descendant of a highly mobile ancestor that allowed it to separate from the other isotopes of its element. Excluding potentially significant isotopes from the simulation, however, will err on the side of safety because it will effectively inflate the elemental solubility, resulting in increased mobility for the isotopes of the element that are included in the model.

Coupling to the Mixed Potential Model for UNF Degradation

The rate of degradation of the waste form depends on the properties of the waste form and the conditions of the EBS environment. For PA, a source term model called the Mixed Potential Model (MPM) is being developed to calculate waste form degradation rates as affected by temperature, radiolysis, steel corrosion, chemical composition of water contacting the waste form, and dose rate (burnup) (Sassani et al. 2013; Jerden et al. 2014).

The envisioned use of the MPM in PA is depicted in Figure 2-12. The MPM couples a radiolysis model developed at PNNL (Buck et al. 2013) with a mixed potential model developed at ANL (Jerden et al. 2014). In FY 2015, the MPM will be developed further to include a steel corrosion model for calculating hydrogen generation. The full model for PA will include an instant release fraction model.

The MPM is currently being translated from MATLAB to Fortran 2003 so that it can be integrated into the source term model of the PFLOTRAN GDSA PA model. This initial Fortran code will be able to calculate UNF degradation rates and will account for instant release fractions. Input will include dose rate, temperature, and groundwater composition. When completed, this code will be used in the argillite GDSA PA model to be developed in FY 2015.

2.2.2.2 Biosphere and Receptor

In the enhanced PA model system analysis workflow, the biosphere component model is planned to be implemented using an independent biosphere code (Figure 2-6). However, for the current development phase of the GDSA framework, a biosphere model is not included. Concentrations in a withdrawal well in the aquifer are currently used as the system performance metric. As the PA model matures beyond the generic stage, e.g., during site selection, an independent biosphere code can easily be added to the GDSA framework to evaluate receptor impacts at potential repository sites. This independent biosphere code will be capable of incorporating a number of surface and biosphere processes contributing to the dose to a human receptor resulting from radionuclide releases from the NBS (Figure 2-13). The biosphere transport and receptor uptake processes may be represented explicitly or in an abstracted fashion. In either case, the biosphere calculations are expected to only require one-way (downstream) coupling (e.g., based on radionuclide concentrations in the NBS).

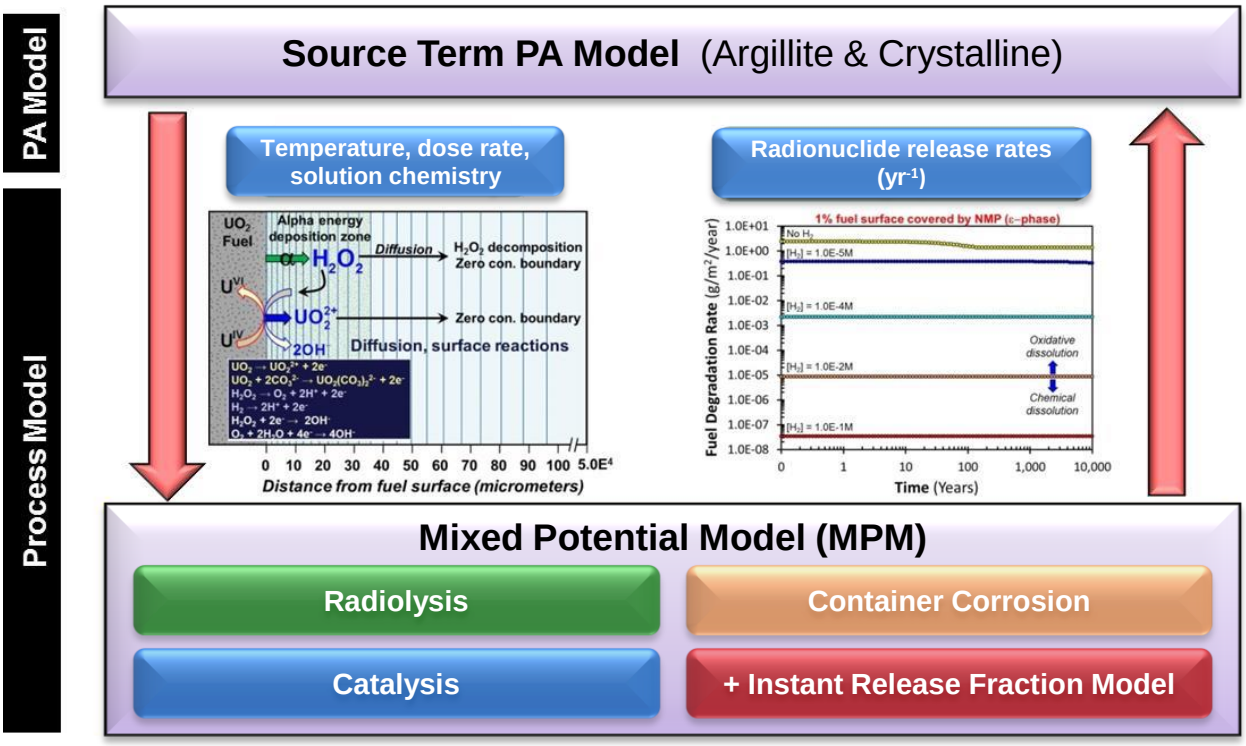

Figure 2-12. General Flow Diagram for the Mixed Potential Model and Source Term PA Model.

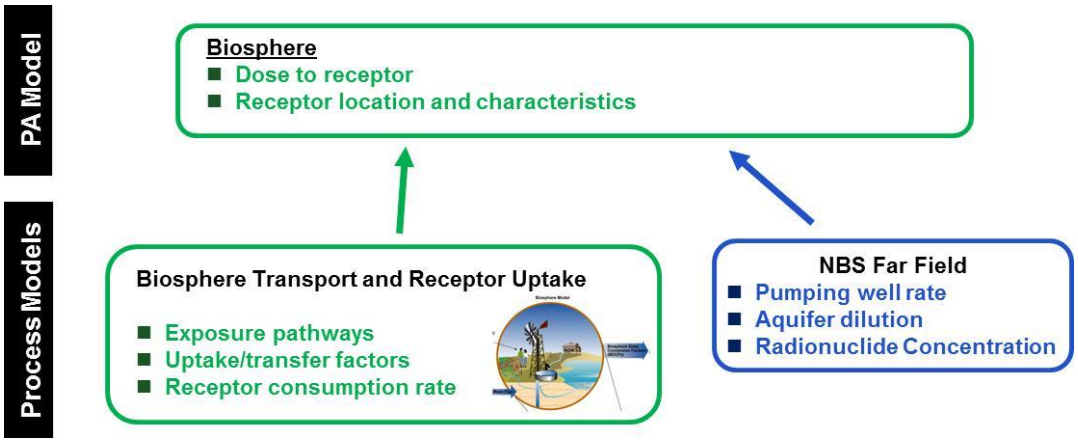

Figure 2-13. Generic Disposal System Biosphere Processes.

3. GENERIC SALT DISPOSAL MODEL AND REFERENCE CASE

Many of the capabilities of the GDSA Framework have been demonstrated previously by application to a model for a generic repository in bedded salt (Freeze et al. 2013a). Because the generic salt repository model was well-developed in Freeze et al. (2013a), only minor changes/additions have been required for FY 2014, e.g., to add thermal properties to test the coupled TH process capabilities of the GDSA Framework in FY 2014, as described in Section 4. Because only minor changes have been made to the salt repository model and its associated reference case, only those updates are reported in this section. For a complete discussion of the entire model and reference case, please see Freeze et al. (2013a). Section numbers shown below differ slightly from Freeze et al. (2013a) but section titles remain the same. Also, some changes to the implementation of the reference case in the GDSA PFLOTRAN-based Framework were adopted in FY 2014. These are documented in Section 4 of this report.

As noted by Vaughn et al. (2013b), the development of conceptual models for *generic* disposal systems has challenges:

> "Normally, a safety case and associated safety assessment address a specific site, a well-defined inventory, waste form, and waste package, a specific repository design, specific concept of operations, and an established regulatory environment. This level of specificity does not exist for a "generic" repository, so it is important to establish a reference case, to act as a surrogate for site/design specific information upon which a safety case can be developed. (A reference case provides) enough information to support the initial screening of FEPs and the design of models for preliminary safety assessments…"

FY 2014 updates to the bedded salt reference case are provided below. Also, as noted by Freeze et al. (2013a), the initial focus of all current generic reference cases (both for the salt reference case described here and the shale/clay and granite reference cases described in Zheng et al. 2014 and Painter et al. 2014, respectively) remains the undisturbed scenario (e.g., performance in the absence of external events) rather than on disturbed scenarios (e.g., human intrusion, igneous activity, seismic activity). This is logical for generic repository analyses because disturbed scenarios are strongly dependent on site-specific information and regulatory considerations.

The generic salt repository model and reference case described in this section has the following major elements (see Figure 2-2):

- Disposal Concept (Section 3.1)
- Waste Inventory (Section 3.2)
- Geologic Disposal System: Engineered Barrier System (Section 3.3)
- Geologic Disposal System: Natural Barrier System (Section 3.4)
- Biosphere (Section 3.5)
- Regulatory Environment (Section 3.6)

3.1 Generic Salt Repository Disposal Concept

There are effectively no changes to the disposal concept from that reported previously in Freeze et al. (2013a); however, the drift emplacement figure has been updated to better reflect the concept of emplacement of waste packages directly on the floors of the disposal drifts, as shown here in Figure 3-1.

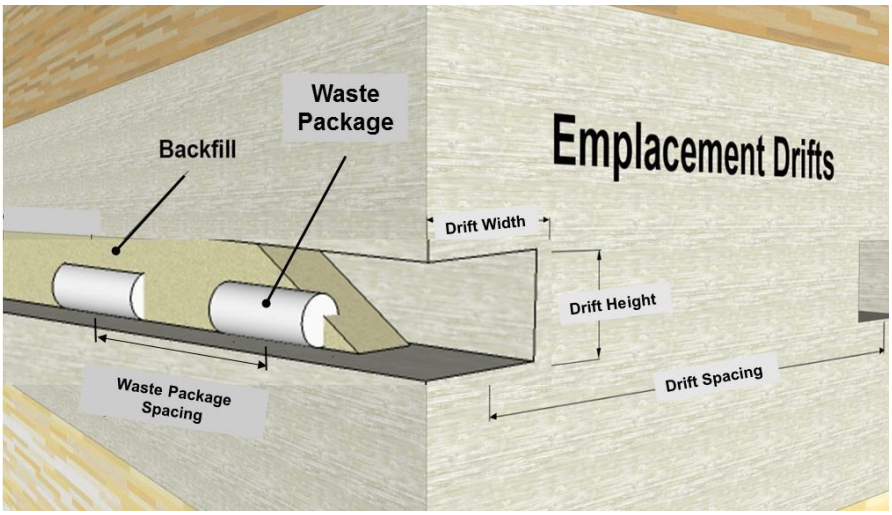

Figure 3-1. Schematic Illustration of an Emplacement Drift in Salt with Waste Packages and Backfill.

3.2 Waste Inventory

The salt reference case waste inventory remains the same as Freeze et al. (2013a). The only related change is to the instant release inventory of ^{129}I, which is discussed below in Section 3.3.1.

3.3 Geologic Disposal System: Engineered Barrier System

The description of the reference case EBS includes the following components, updated where noted from Freeze et al. (2013a, Section 3.2.2):

- Waste Form (Section 3.3.1)
- Waste Package (Section 3.3.2)
- Repository Layout (Section 3.3.3)
- Backfill (Section 3.3.4)
- Seals (Section 3.3.5)

3.3.1 Waste Form

As described in Freeze et al. (2013a), the reference case inventory in the current version of the generic bedded salt reference case is limited to PWR UNF waste. There are two important updates to the UNF waste form model for FY 2014: (1) a change in the fractional UNF waste form degradation rate and (2) a change to the instant release fraction of ^{129}I.

Previously, the fractional UNF waste-form degradation rate was based on information from the Swedish repository program for degradation in chemically reducing environments, specifically in granitic groundwaters (SKB 2010, Table 3-21). However, more pertinent information from the German repository program, which compiled UNF degradation rates for porewaters typically found in salt domes, indicates that the rates from SKB (2010) in granitic environments are highly non-conservative, i.e., much too slow. As discussed in Kienzler et al. (2012, Sec. 5.1.2.2), bromide concentrations found in brines typical of salt domes and bedded salt deposits (e.g., DOE

2009, App. SOTERM, Table SOTERM-2) will counteract the protective hydrogen effect in reducing waters, thereby making the UNF effectively "self-oxidizing" due to radiolysis. This gives UNF degradation rates typical of oxidizing EBS environments in other repository concepts, such as a repository in the unsaturated zone (DOE 2008, Table 2.3.7-19). Based on the information in Kienzler et al. (2012), Table 3-1 shows the new fractional degradation rate constants, λ, being used for the generic salt repository model, where

$$\frac{m(t)}{m_0} = e^{-\lambda t} \qquad \text{Eq. (3-1)}$$

with $m(t)$ being the mass of waste at any time t and m_0 being the initial mass of waste.

Table 3-1. UNF Degradation Rate Constants, λ, in Typical Bromide-Containing Brines[1], Used for the Generic Salt Repository Reference Case.

Case	λ (s^{-1})	λ (d^{-1})	λ (yr^{-1})	Time for 50% Degradation (yrs)	Time for 99% Degradation (yrs)
Deterministic	1.1574×10^{-11}	10^{-6}	3.6525×10^{-4}	~ 1,900	~ 12,500
Probabilistic – Lower	1.1574×10^{-13}	10^{-8}	3.6525×10^{-6}	~ 190,000	~ 1,250,000
Probabilistic – Upper	1.1574×10^{-10}	10^{-5}	3.6525×10^{-3}	~ 190	~ 1,250

[1]from Kienzler et al. (2012, Figures 18 and 19)

Besides the radionuclide releases due to UO_2 matrix degradation, the release of some radionuclides from UNF includes a fast/instant fraction—predominantly from radionuclides located in the fuel and cladding gap and grain boundaries. Currently, the salt reference case uses an instant release fraction of 11.25% for ^{129}I, based on light-water reactor (LWR) SNF destined for the Yucca Mountain repository (SNL 2008, Table 6.3.7-29). However, according to Sassani et al. (2012), this value is more appropriate for used fuels with burn-ups less than 50 GWd/MT. A more comprehensive set of models and values for instant release fraction for PWR SNF at various burn-ups has been compiled by Sassani et al. (2012, Table 3.2-1), with the Johnson 2005 model being recommended for high burn-up fuels, such as the 60 GWd/MT fuel being considered in the salt reference case. Using the Johnson 2005 model, a "best estimate" instant release fraction of 10% or a "pessimistic estimate" instant release fraction of 16% would be chosen for ^{129}I in 60 GWd/MT PWR used fuel. These values may be implemented in future revisions to the salt repository reference case.

3.3.2 Waste Package

The salt reference case waste package remains the same as Freeze et al. (2013a) and still assumes that the waste package fails instantaneously and does not provide any barrier capability. Future iterations of the bedded salt PA model may consider the effects of non-instantaneous waste package failure, as well as different waste canisters (e.g., HLW) and overpacks, including larger-capacity DPCs (Hardin et al. 2013).

3.3.3 Repository Layout

The salt reference case repository layout remains the same as Freeze et al. (2013a) and is based on a 200°C temperature constraint at the waste package surface.

3.3.4 Backfill

The salt reference case backfill remains the same as Freeze et al. (2013a), except that a value for tortuosity, τ, has been assigned and assumed to be given by $\tau = \phi^{1/3} = 0.48$. This is important to properly represent the dominant transport mechanism in salt repositories, i.e., diffusive transport.

3.3.5 Seals

The salt reference case shaft and drift seals remain the same as Freeze et al. (2013a), except that a value for tortuosity, τ, has been assigned and assumed to be given by $\tau = \phi^{1/3} = 0.48$. This is important to properly represent the dominant transport mechanism in salt repositories, i.e., diffusive transport.

3.4 Geologic Disposal System: Natural Barrier System

The natural barrier system (NBS) encompasses the geologic setting of the generic bedded salt repository, including the DRZ. As noted in Freeze et al. (2013a), the reference case bedded salt formation is assumed to be a relatively pure salt unit (e.g., halite) within a vertically and laterally extensive bedded salt formation that includes clay and/or anhydrite interbeds. Stratigraphy and dimensions of the reference case salt repository NBS, shown in Figure 3-2, are updated slightly from Freeze et al. (2013a). In particular, the 5000-m distance from the edge of the repository to the domain boundary in the *x* and *y* directions (based on having a withdrawal well at a regulatory distance of 5 km downstream of the repository) is changed to 5000 m beyond the edge of the 12-m DRZ that abuts the repository on all sides. This adds 24 m to the domain in both the *x* and *y* directions. Another change from Freeze et al. (2013a) is to the regional hydraulic gradient which is changed from 0.001 m/m to 0.0013 m/m and is applied across the entire *y*-*z* plane in the *x*-direction, i.e., it is applied to all formation layers.

The geologic setting of the reference case NBS components is described further in the following subsections, updated when necessary from Freeze et al. (2013a, Section 3.2.3), and with the important addition of a section that provides properties for the overburden sediments layer, i.e., the formation between the aquifer and the ground surface:

- Disturbed rock zone (Section 3.4.1)
- Host rock halite (Section 3.4.2)
- Host rock interbeds (Section 3.4.3)
- Aquifer (Section 3.4.4)
- Overburden sediments layer (Section 3.4.5)
- Pressurized brine reservoirs (Section 3.4.6)
- Thermal and Chemical Environment (Section 3.4.7)

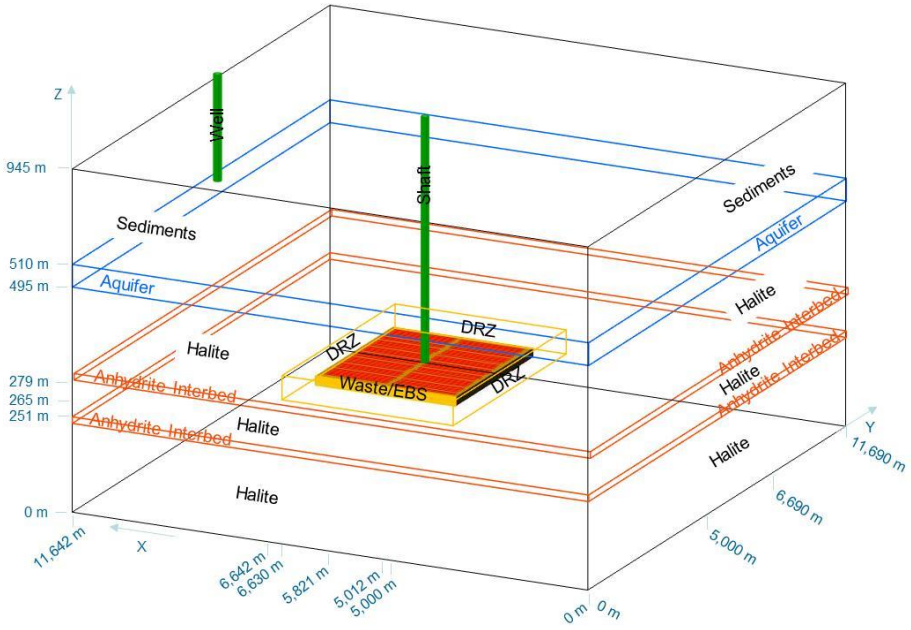

(Not to scale)

Figure 3-2. Salt Repository Reference Case Dimensions.

3.4.1 Disturbed Rock Zone

The salt reference case DRZ remains the same as Freeze et al. (2013a), except that a value for tortuosity, τ, has been assigned and assumed to be given by $\tau = \phi^{1/3} = 0.23$. This is important to properly represent the dominant transport mechanism in salt repositories, i.e., diffusive transport.

3.4.2 Host Rock Halite

The salt reference case host rock halite remains the same as Freeze et al. (2013a), except that a value for tortuosity, τ, has been assigned and assumed to be given by $\tau = 0.01$ (e.g., Olivella 1995, Sec. 7.4). This is important to properly represent the dominant transport mechanism in salt repositories, i.e., diffusive transport.

3.4.3 Host Rock Interbeds

The salt reference case anhydrite interbeds remain the same as Freeze et al. (2013a), except that a value for tortuosity, τ, has been assigned and assumed to be given by $\tau = \phi^{1/3} = 0.22$. This is important to properly represent the dominant transport mechanism in salt repositories, i.e., diffusive transport.

3.4.4 Aquifer

The salt reference case aquifer remains the same as Freeze et al. (2013a), except that a value for tortuosity, τ, has been assigned and assumed to be given by $\tau = \phi^{1/3} = 0.53$. This is important to properly represent the dominant transport mechanism in salt repositories, i.e., diffusive transport.

3.4.5 Overburden Sediments Layer

An 435-m thick overburden of sedimentary and alluvial deposits above the aquifer layer and extending to the ground surface has always been assumed for the generic bedded salt reference case but its properties have not previously been provided. The reference case sediments layer porosity is assumed to be 0.2. The reference case log permeability (m^2) for these sediments assumes a mean of −15 (1×10^{-15} m^2) and a uniform distribution over the range of −21 to −17.1. Tortuosity, τ, is assumed to be given by $\tau = \phi^{1/3} = 0.58$.

3.4.6 Pressurized Brine Reservoir

A pressurized brine reservoir beneath the repository may be important for a disturbed scenario (DOE 1996) but is not currently used for the generic salt reference case, which is only for an undisturbed scenario.

3.4.7 Thermal and Chemical Environment

Only a few minor changes were made to the chemical environment parameters, as noted below. However, thermal properties are now required to run a coupled TH simulation for the salt reference case, as described in Sections 4.4 and 4.5.

3.4.7.1 Diffusion

A tortuosity value has been added to all porous formations, as described in the previous sections. The longitudinal dispersivity has been changed to 50 m in the aquifer and the transverse dispersivity is set to zero. Values of longitudinal dispersivity in other formations are presented below in Table 3-2. [The ability to set different dispersivity values in the *x*, *y*, and *z* directions is a new capability added to PFLOTRAN; however, it still only allows for a diagonal dispersion tensor (all off diagonal values are zero).]

3.4.7.2 Solubility

No changes have been made to elemental solubility values.

3.4.7.3 Sorption

No changes have been made to sorption coefficients.

3.4.7.4 Thermal Properties

The thermal material properties for each material region, i.e., saturated thermal conductivity and specific heat capacity, are summarized in Table 3-2. In addition, the reference-case domain (see Figure 3-2) has an applied geothermal gradient in the vertical *z*-direction, based on a temperature of 20°C at the surface and 28°C at the bottom boundary over the total domain thickness of 945 m (thermal gradient thus equals 0.00847 °C/m). The simulated heat source represented by the decay of the radionuclides in 70,000 MTHM of SNF was taken from Carter et al. (2012) and is reproduced below in Figure 3-3 ("Total" curve). The curves in this figure should be multiplied by (0.4354 MT/assembly × 12 assembly/pkg) to get the decay heat in each waste package cell in the PFLOTRAN grid.

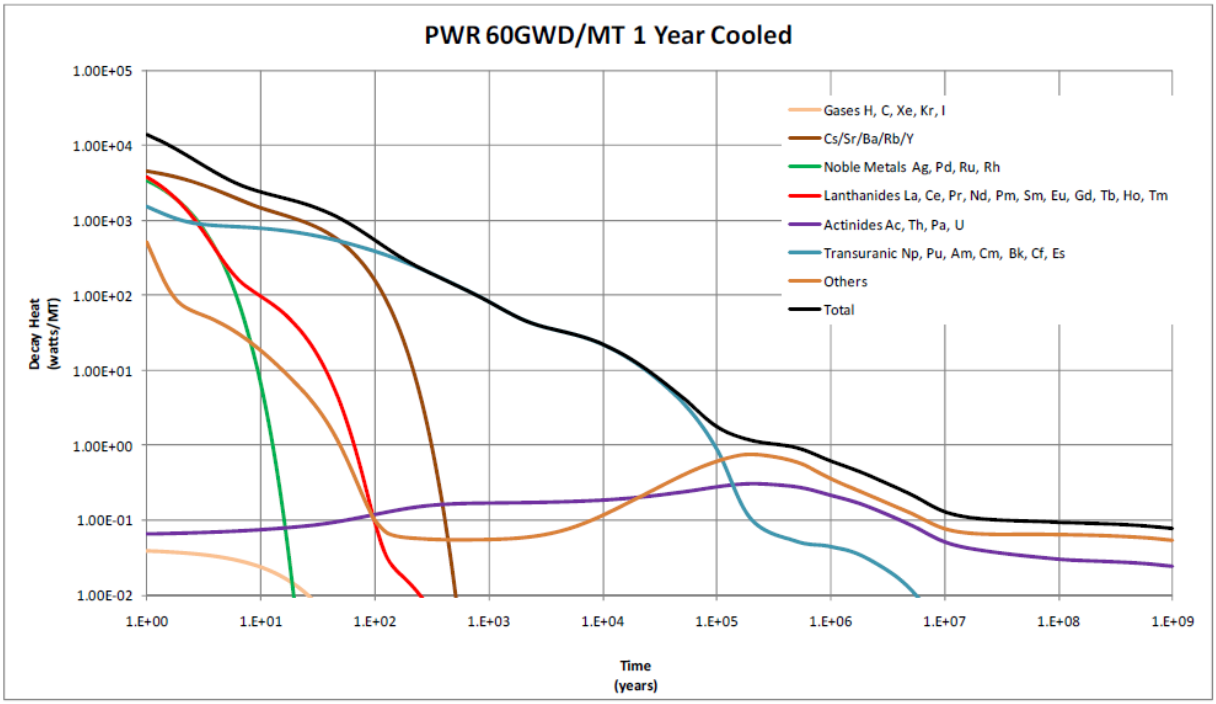

Figure 3-3. PWR 60 GWd/MT Used Fuel Decay Heat (W/MT), from Carter et al. 2012, Fig. 3-11.

3.4.8 Biosphere

As described earlier, there is no biosphere model at present. The primary system performance metric related to the biosphere is the concentration in the aquifer near the point of a withdrawal well at 5 km downgradient of the repository.

3.4.9 Regulatory Environment

Regulatory environment assumptions are the same as in Freeze et al. (2013a).

3.4.10 Summary of Key Parameters in the Salt Reference Case

Table 3-2 summarizes the deterministic ("best estimate") values for the key parameters in the generic bedded salt reference case (from Freeze et al. 2013a, except where noted above and in the footnotes to this table).

Table 3-2. Key Deterministic Parameters for Generic Bedded Salt Reference Case.

Model Region	Permeability (m^2)	Porosity	Tortuosity[1]	Effective Diffusion Coefficient[2] (m^2/s)	Longitudinal Dispersivity (m)[10]	Saturated Thermal Conductivity[4,9] (W/m·°K)	Specific Heat Capacity[5] (J/kg·°K)	Grain Density[7] (kg/m^3)
Waste Package	1.00×10^{-13}	0.500	1.00	6.90×10^{-10}	0.5	16.7	466	5000.0
Backfill	1.00×10^{-18}	0.113	0.48	1.24×10^{-10}	0.2	2.5	927	2170.0
Shaft (sealed)	1.58×10^{-20}	0.113	0.48	1.24×10^{-10}	20.0	2.5	927	2170.0
DRZ	1.12×10^{-16}	0.0129	0.23	6.82×10^{-12}	1.0	4.9	927	2170.0
Halite	3.16×10^{-23}	0.0182	0.01	4.19×10^{-13}	50.0	4.9	927	2170.0
Interbed (anhydrite)	1.26×10^{-19}	0.011	0.22	5.57×10^{-12}	50.0	4.9	927	2960.0
Aquifer[6]	1.00×10^{-13}	0.150	0.53	1.83×10^{-10}	50.0	1.5	959	2820.0[8]
Sediments[3,6]	1.00×10^{-15}	0.20	0.58	2.67×10^{-10}	50.0	1.5	927	2700.0

[1] Tortuosity = $[\text{porosity}]^{(1/3)}$, except for waste package and halite
[2] Effective diffusion coefficient = (free water diffusion coefficient) × (tortuosity) × (porosity)
[3] from Freeze and Cherry 1979, Tables 2.2 and 2.4
[4] Hardin et al. 2012, Tables D-1, D-2, and D-5 (based on Clayton and Gable 2009, Fluor 1985, and Fluor 1986)
[5] Hardin et al. 2012, Table D-3 (based on Clayton and Gable 2009, Fluor 1985, and Fluor 1986)
[6] Hardin et al. 2012, Tables D-1, D-3, and D-5 (based on alluvium from Smyth et al. 1979 and Wollenburg et al. 1982)
[7] Crain's Petrophysical Handbook and PetroWiki (online)
[8] Fox 2008, Table 26 (Culebra dolomite)
[9] Saturation function = Brooks-Corey for all units; however, all material regions are fully saturated, i.e., $S_w = 1$
[10] Transverse dispersivity = 0

4. APPLICATION OF THE SALT DISPOSAL SYSTEM MODEL

This section describes new simulation results from the application of the GDSA framework described in Section 2 to the generic salt repository reference case described in Section 3. In comparison to the isothermal simulations in Freeze et al. (2013a), new simulations shown in this section represent a test of the GDSA framework for a heat-generating repository, in order to demonstrate coupled TH effects. Two cases are shown and compared: (1) an updated isothermal simulation over the full length of the domain in the *x*-direction and (2) a new thermal simulation. The updated isothermal simulation represents an important improvement to the base-case, isothermal domain in Freeze et al. (2013a). In particular, the simulation domain has been extended upstream in the primary *x*-direction of horizontal fluid flow and transport to eliminate an unrealistic zero-gradient boundary condition for diffusive transport at the former "symmetry" boundary in the middle of the repository. The new isothermal (and thermal) simulations also extend the domain to 1 km downstream of the approximate withdrawal well location, to more accurately represent radionuclide transport and to eliminate boundary effects.

4.1 Salt Repository PA Model Domain and Properties

As described in Freeze et al. (2013a), the reference case salt repository is assumed to contain approximately 70,000 MTHM, distributed throughout 84 pairs of emplacement drifts (168 total drifts), where each drift is 809 m long and contains 80 waste packages of 12-PWR UNF with a 10-m center-to-center spacing between waste packages that are 5 m in length. The biosphere (receptor location) is assumed to be located at the ground surface directly above the withdrawal well, at a distance of 5,000 m laterally from the edges of the emplacement drifts.

The current GDSA simulation domain for the salt reference case includes a single drift pair containing 160 waste packages, i.e., it is a three-dimensional "slice" of the full model domain, as indicated by the gray shading in Figure 4-1 (cf. Figure 3-2). Also, as mentioned, 1 km is added to the downstream end of the model domain (cf. Figure 3-2) to avoid boundary condition effects at the withdrawal well location. The resulting 3-D model domain is 12,642 m long (464 grid cells) in the *x*-direction, 20 m wide (5 grid cells) in the *y*-direction, and 945 m high (92 grid cells) in the *z*-direction, as shown in Figure 4-2 (*x*-*z* plane, side view) and Figure 4-3 (*x*-*y* plane, top or plan view). The model domain includes the material regions shown in Figure 4-2 and Figure 4-3, along with their dimensions, which correspond to the EBS and NBS features described in Section 3: waste package (which includes the waste form); backfill; drift seals; DRZ; sealed shaft; intact halite units; anhydrite interbeds; an aquifer; and overburden sediments. The model domain also includes a slice of the central access hallway, which is assumed to be backfilled, salt pillars adjacent to the modeled drift, which are assumed to be similar to the DRZ, and a groundwater sample well, which provides dissolved radionuclide concentrations that are used as a surrogate performance indicator for dose.

The model domain and regions shown in Figure 4-2 and Figure 4-3 are reproduced in Figure 4-4 at a scale and orientation consistent with the model results, i.e., directly from the PFLOTRAN simulation grid. Also, shown in Figure 4-4 is a not-to-scale blow-up of 8 out of the 160 waste packages in a single drift pair.

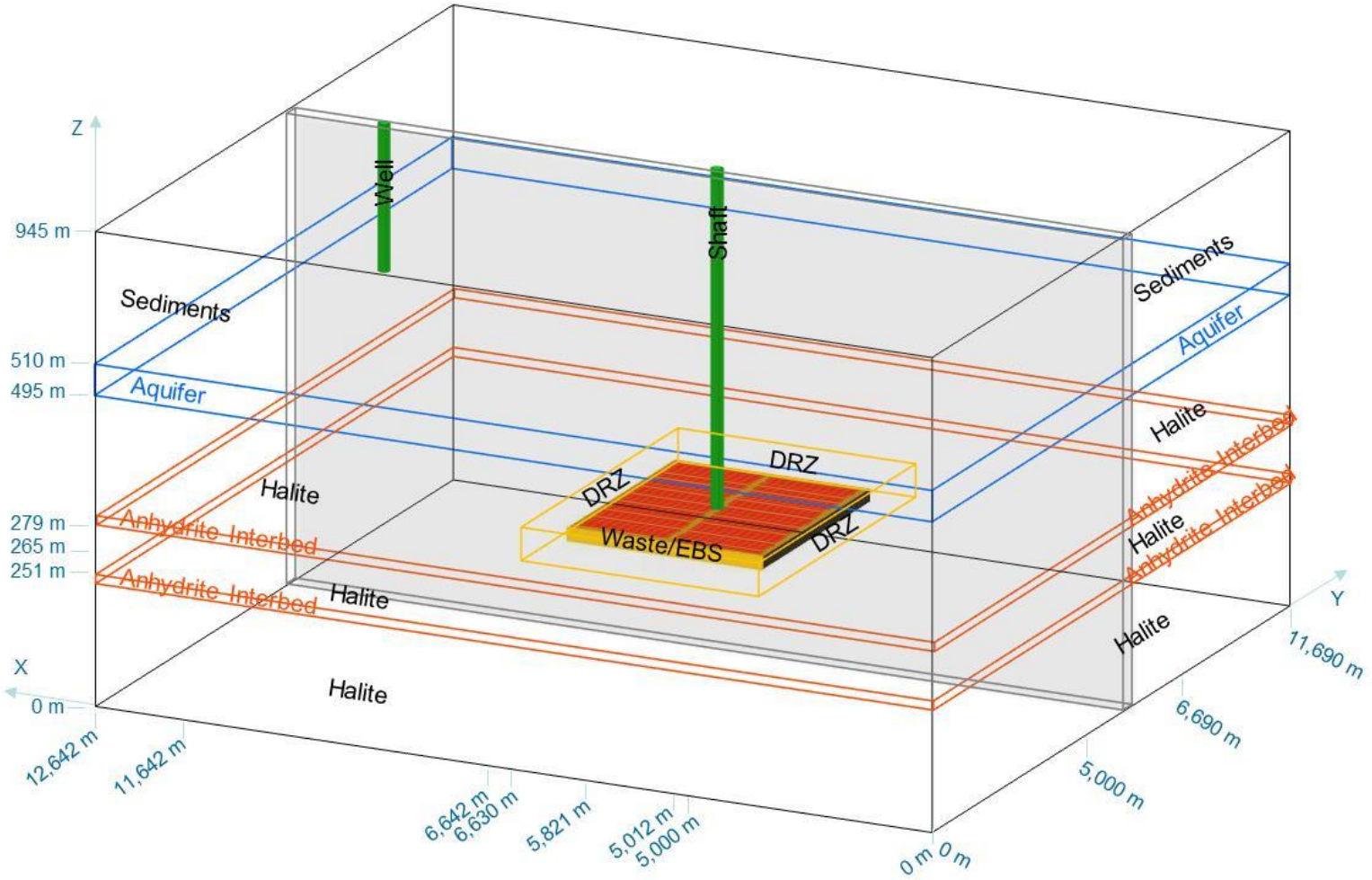

(Not to scale)

Figure 4-1. GDSA Simulation Domain (gray shading) for the Salt Reference Case.

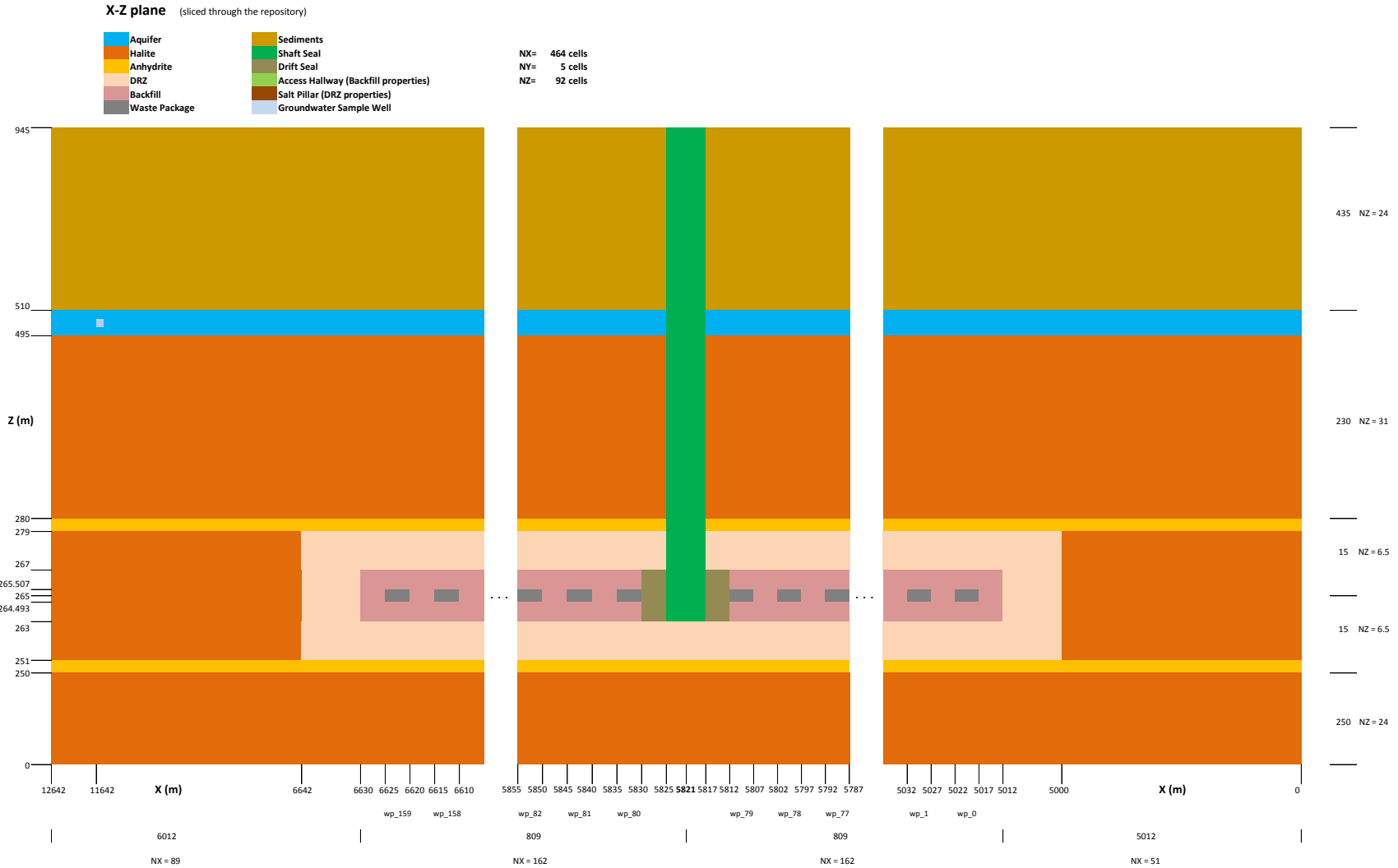

(Not to scale)

Figure 4-2. Salt Repository Reference Case Model and Material Regions x-z Plane (side view of domain—parallel to regional fluid flow).

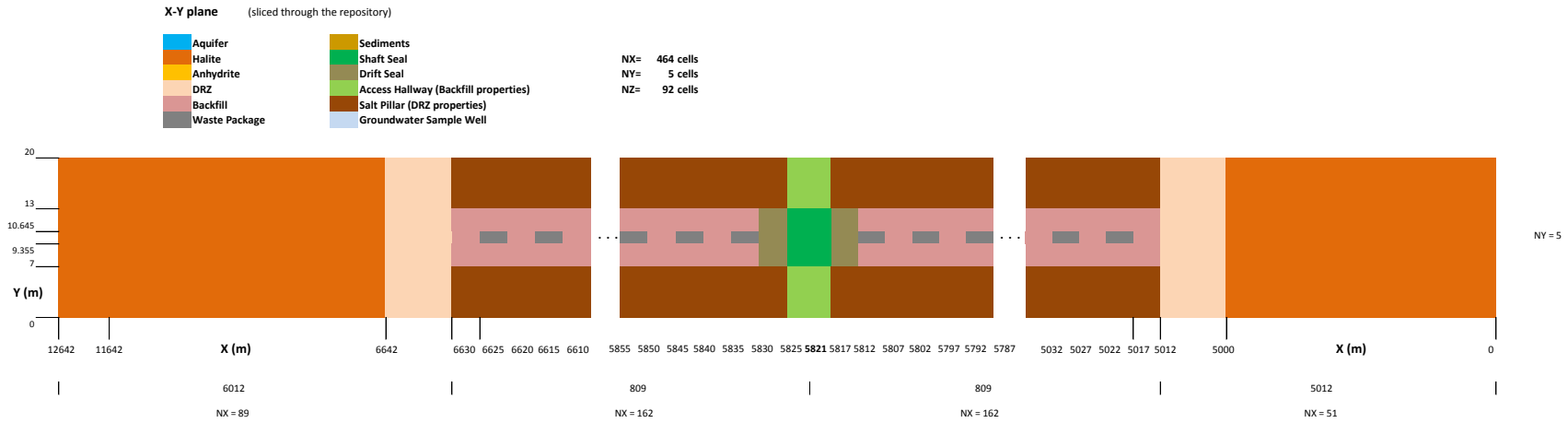

(Not to scale)

Figure 4-3. Salt Repository Reference Case Model and Material Regions x-y Plane (plan view of domain at z = 265 m).

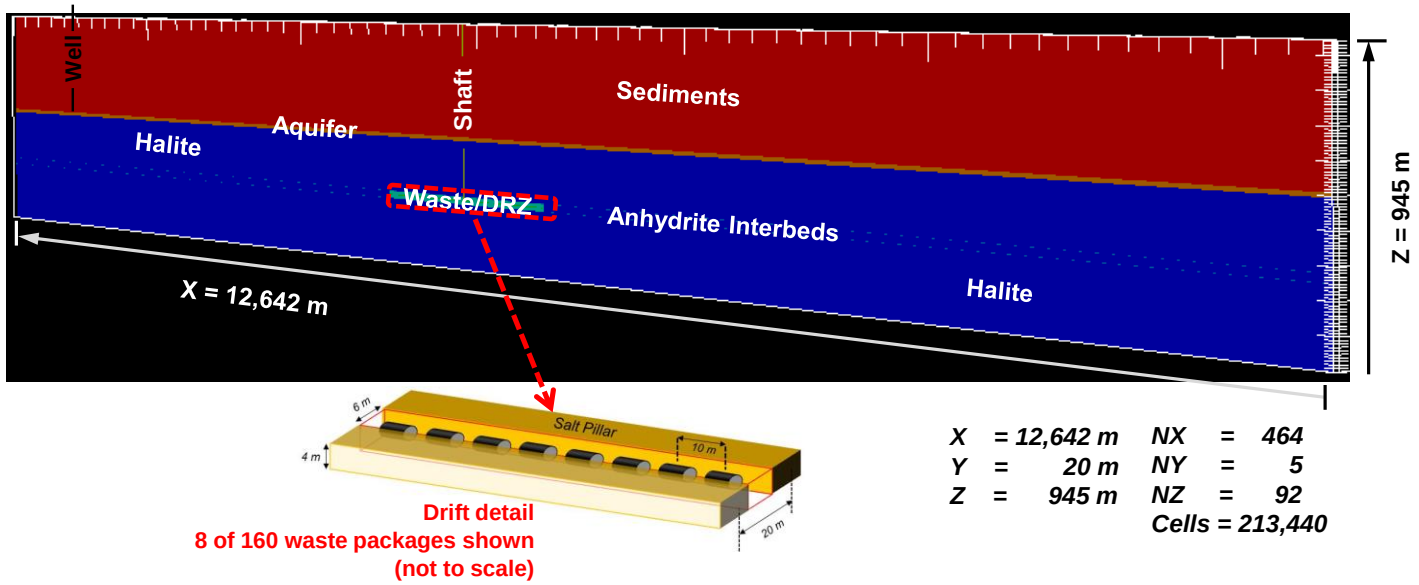

Figure 4-4. PFLOTRAN model domain and blow-up of drift domain.

Boundary Conditions – Flow boundary conditions are implemented to simulate regional groundwater flow in the *x* direction (west to east). Separate hydrostatic pressure profiles are applied along the west (x = 0 m), east (x = 12,642 m), top (z = 945 m), and bottom (z = 0 m) faces. No flow boundaries are specified along the north (y = 20 m and south (y = 0 m) faces as these are symmetry boundaries. A regional hydraulic gradient of 0.0013 is applied across the domain from west to east (Section 3.4). The initial flow conditions throughout the domain in all simulations derive from hydrostatic conditions and the regional hydraulic gradient.

Solute transport boundary conditions are specified as Dirichlet/zero gradient (i.e., specified concentration for inflow and zero diffusive gradient for outflow) at the east, west, and bottom boundaries and Dirichlet (specified concentration) at the top of the aquifer. The north and south boundaries are zero flux (consistent with the no flow boundary above). The initial concentration conditions include a very low background aqueous concentration of 10^{-20} molal (mol/kg H_2O) for all radionuclides, and zero secondary mineral volume fraction in all the domains except the waste emplacement drift. Initial mineral concentrations in the waste emplacement drift are specified as part of the initial condition.

The symmetry boundaries assigned on the north and south boundaries are not rigorously correct, as these are not true planes of symmetry. Although these boundary conditions result in conservatively high radionuclide concentrations (see Section 4.2), they are sufficient for the purposes of the demonstration of the enhanced salt repository simulation capability at this stage.

For the deterministic simulation, the model regions were assigned reference case property values as given in Table 3-2. The implementation of the reference case in PFLOTRAN required the following additional considerations/revisions for the reference case:

Radionuclide Inventory – The modeled inventory is a subset of the 10 reference case radionuclides identified in Table 3-1 of Freeze et al. (2013a). The reduced inventory for simulation includes five radionuclides, four from the neptunium decay chain ($^{241}Am \rightarrow {}^{237}Np \rightarrow {}^{233}U \rightarrow {}^{229}Th$) and the fission product ^{129}I. These 5 radionuclides are considered sufficient for a PA model capability demonstration.

Waste Package Volume – Each of the 160 modeled waste packages is represented by a PFLOTRAN cell. Each rectangular PFLOTRAN waste package cell is discretized (5.0 m × 1.29 m × 1.014 m = 6.54 m^3) to correspond to the volume of a cylindrical waste package (including overpack)—see Section 3.2.2.2 of Freeze et al. (2013a).

Waste Package Porosity and Permeability – Each PFLOTRAN waste package cell is assigned a porosity of 0.30, which remains constant over the duration of the simulation. This porosity is lower than the initial porosity of 0.50 (Table 3-2) to qualitatively account for compaction of the waste package due to salt creep after closure. Each waste package cell is assigned a permeability of 1×10^{-13} m^2, representative of the degraded, compacted waste form and waste package internals.

Waste Package Saturation – The porosity in each PFLOTRAN waste package cell is assumed to be fully saturated with the aqueous phase, consistent with the assumption of instantaneous waste package degradation and no gas generation.

Waste Form Composition – The PFLOTRAN "waste-form mineral" contained within each waste package cell (with a waste-form volume fraction of 0.105 within the waste package cell—see Section 3.2.2.2 in Freeze et al. 2013a) is specified to have a molecular weight, M_{WF}, of

100 g/mol. The resulting initial PFLOTRAN radionuclide mole fractions (moles radionuclide per mole of waste-form mineral), χ_i, in the waste form are calculated based on Table 3-1 of Freeze et al. (2013a), and shown in Table 4-1. The formula is $\chi_i = \omega_i M_{WF}/M_i$, where M_i is the molecular weight of radionuclide species i and ω_i is the mass fraction of radionuclide i in the waste-form mineral phase.

Table 4-1. UNF Radionuclide Mole Fractions for the Reference Case (from Table 1 of Sevougian et al. 2013).

Isotope	Molecular weight, M_i (g/mol)	Mass fraction, ω_i (g / g UNF)	Mole fraction, χ_i (mol / mol UNF)
^{241}Am	241.06	8.68×10^{-4}	3.60×10^{-4}
^{237}Np	237.05	8.61×10^{-4}	3.63×10^{-4}
^{233}U	233.04	9.73×10^{-9}	4.18×10^{-9}
^{229}Th	229.03	4.43×10^{-12}	1.93×10^{-12}
^{129}I	129.00	2.17×10^{-4}	1.68×10^{-4}
Other Isotopes	–	–	0.99911

Also, using the mole fraction of ^{129}I in Table 4-1 and its instant release fraction of 0.1125 (Sec. 3.3.1), and assuming the instant release fraction is instantaneously mixed into the pore volume of the waste package cell, gives an initial ^{129}I molality in the waste package pore volume of 7.27×10^{-4} mol/kg-H_2O, which implies that the remaining ^{129}I mole fraction in the waste-form mineral volume is about 1.5×10^{-4}.

Waste Form Degradation Rate – PFLOTRAN does not currently have a fractional degradation rate option, such as that specified in Eq. (3-1). As a surrogate, the waste-form mineral is assigned a zeroth-order dissolution rate law (far from equilibrium) by assuming a very high solubility product (log K_{SP} = 50) and a kinetic rate constant that approximates the degradation times shown in Table 3-1. In particular, the waste-form mineral was specified to have a kinetic rate constant for dissolution of 4.8×10^{-8} mol/m^2/s and a specific surface area of 1 m^2/m$^3_{BV}$ (where BV means bulk volume). The product of the rate constant and the specific surface area gives a constant bulk waste-form degradation rate of 4.8×10^{-8} mol/m$^3_{BV}$/s or 1.515 mol/m$^3_{BV}$/yr. The molar volume of the UNF waste form is calculated to be about 9.116 cm$^3_{MV}$/mol (where MV means mineral phase volume), based on an assumed UO_2(s) (i.e., waste-form mineral) density of 10.97 g/cm^3 and a waste-form molecular weight of 100 g/mol. This molar volume is equivalent to a molar density of 1.097×10^5 mol/m$^3_{MV}$. This in turn implies a bulk molar concentration for the waste form mineral of 1.152×10^4 mol/m$^3_{BV}$, assuming a mineral volume fraction in the waste-package/waste-form cell of ϕ_{WF} = 0.105 m$^3_{MV}$/m$^3_{BV}$. Dividing the bulk molar concentration of the waste-form mineral by the constant bulk degradation rate implies complete (and linear) degradation of the UNF in about 7,600 years or a half-life of about 3,800 years. These values are similar to the deterministic-case degradation times ($t_{50\%}$ and $t_{99\%}$) given in Table 3-1. For example, using the half-life formula of $t_{1/2} = \ln(2)/\lambda$, a half-life of 3,800 years corresponds to a rate constant in Eq. (3-1) of $\lambda = 1.82\times10^{-4}$ yr^{-1}.

Shaft Cross-Sectional Area – In the rectangular PFLOTRAN grid, the shaft has dimensions of 8 m by 6 m, which gives a cross-sectional area of 48 m^2, as indicated by Figures 4-2 and 4-3. This is somewhat less than the stylized reference-case shaft, which was based on the sum of the

cross-sectional areas (85.7 m^2) of four shafts at the WIPP repository—see Section 3.2.2.3 of Freeze et al. (2013a).

Solubility – As described in Section 2.2.2.1.1, the PFLOTRAN radionuclide solubilities are calculated from the elemental solubilities (Table 3-8 in Freeze at al. 2013a) by assuming that the fraction of each radionuclide of an element in the aqueous phase is the same as the fraction of each radionuclide of an element within the waste form. The resulting radionuclide solubilities are shown in Table 4-2. These solubilities are implemented in PFLOTRAN with reactions of the type

$$^{241}\text{Am(s)} \Leftrightarrow {}^{241}\text{Am(aq)}, \qquad K_{SP} = m_{^{241}\text{Am(aq)}} \qquad \text{Eq. (4-1)}$$

where ^{241}Am(s) is a secondary mineral phase that precipitates when the waste form degrades, $m_{^{241}\text{Am(aq)}}$ is the aqueous phase concentration (molality) of the radionuclide, K_{SP} is the solubility product for the secondary mineral phase ^{241}Am(s), and ideal solution behavior is assumed.

Table 4-2. Radionuclide Solubilities for Simulations of the Generic Salt Repository Reference Case.

Radionuclide	Elemental Solubility (mol/L)	Fraction of Isotope in Waste Form[1]	Radionuclide Solubility (mol/L)	Log K_{SP} ($\log_{10}$ of solubility)
^{241}Am	5.85×10^{-7}	0.820	4.80×10^{-7}	–6.32
^{237}Np	1.51×10^{-9}	1.000	1.51×10^{-9}	–8.82
^{233}U	1.12×10^{-7}	1.52×10^{-8}	1.70×10^{-15}	–14.8
^{229}Th	4.00×10^{-3}	2.19×10^{-4}	Assumed to be unlimited	–
^{129}I	Unlimited	–	–	–

[1]calculated from Carter et al. (2012, Table C-1)

These radionuclide solubilities are assumed to apply throughout the model domain. This assumption is appropriate because solubilities are most important close to the degrading waste forms, where the dissolved concentrations are the highest. For simplicity, the solubilities are constant for the duration of the simulation (i.e., they do not change with changing temperature or brine chemistry).

Secondary Phases – The three solubility-limited radionuclides listed in Table 4-2 precipitate into their corresponding secondary phase (designated as ^{241}Am(s), ^{237}Np(s), and ^{233}U(s)), as the waste form degrades. Currently, these secondary phases are given fast dissolution rates, slightly higher than the original waste-form mineral (see above), with rate constants equal to 10^{-7} mol/m^2/s and specific surface areas of 1 m^2/m^3_{BV}. This ensures that the precipitated ^{241}Am(s), for example, will quickly replenish any ^{241}Am(aq) that is transported away, and maintain the solubility value of ^{241}Am(aq) in the aqueous phase. [Note: ^{129}I, with unlimited solubility, and ^{229}Th, with a high solubility limit—see Table 3-8 of Freeze et al. (2013a), do not require secondary mineral phases.]

Sorption – Element-specific K_d^P values (Table 3-9 of Freeze et al. 2013a) are representative of sorption in anhydrite but are also assumed to apply to all model regions. A probability range for the ^{129}I K_d^P has been added and is given by a uniform distribution from 0 to 1.0 ml/g.

Biosphere – The receptor location is assumed to be 5,000 m from the edges of the DRZ surrounding the underground excavations. However, in the current salt repository demonstration simulation biosphere transport, receptor uptake, and dose calculations are not included. Instead, dissolved radionuclide concentrations calculated at the groundwater sample well location in the aquifer are used as a surrogate for dose as a repository performance indicator. [Note: Aqueous concentrations shown in the remainder of this report are calculated at x = 11,600 m, slightly upstream, by 42 m, of the assumed location of the withdrawal well.]

All other parameter values for the deterministic simulation are taken directly from the reference case, described in Freeze et al. (2013a). For the probabilistic simulations, ten parameter values were sampled, with all other parameters using deterministic values. Specific details of the sampled parameters and distributions are provided in Section 4.3.

4.2 Deterministic Isothermal Simulation Results

The salt repository *isothermal* simulations were run using PFLOTRAN "Richards" option, whose governing equations are documented in Lichtner et al. 2014. The fluid velocity magnitude (in m/yr) and vector fields in all regions of the simulation domain (resulting from the applied hydraulic gradient of 0.0013) are shown in Figures 4-5 and 4-6. Figure 4-5 shows Darcy velocity magnitude at 10 years for essentially the full domain, while Figure 4-6 shows velocity vectors and magnitude at 1000 years for a portion of the domain closer to the repository region. For the isothermal case, the velocity magnitude and direction remains essentially constant for the entire 1,000,000-year simulation time, which may be contrasted with the convection cells that develop in the thermal case discussed in Section 4.3. [Note: The small green "dashes" in these plots represent the velocity in the thin anhydrite interbeds adjacent to the upper and lower boundaries of the repository zone.]

The "deterministic" or "best estimate" properties of the reference case (Table 3-2), with the modifications described in Section 4.1, result in primarily diffusive/dispersive radionuclide transport (i.e., a low system Peclet number, N_{Pe}) through the halite and anhydrite regions, as indicated in Table 4-3—using N_{Pe} = 10 as the division between predominantly diffusive/dispersive transport and advective transport (Lake 1989, Fig. 5-14). The Peclet number in each formation, resulting from the combination of molecular diffusion and kinematic dispersion, is defined as

$$N_{Pe} = \frac{uL_{sys}}{D_{eff} + \alpha_L u} \qquad \text{Eq. (4-2)}$$

where $D_{eff} = \phi\tau D_{w,}$ is the effective diffusion coefficient (from Table 3-2), α_L is the longitudinal dispersivity, u is the Darcy velocity, and L_{sys} is the system length, taken to be 5000 m, i.e., the distance from the edge of the repository to the withdrawal well.

Table 4-3. System Peclet Number, N_{Pe}, in the Various Regions.

Region	Darcy velocity, u (m/s)[1]	Effective Diffusion Coefficent, D_{eff} (m^2/s)	Longitudinal Dispersivity (m)	Longitudinal dispersion coefficient, $D_L = \alpha_L u$ (m^2/s)	Peclet Number, N_{Pe}
Halite	3.17×10^{-19}	4.19×10^{-13}	50.0	1.585×10^{-17}	0.0038
Interbed (anhydrite)	1.90×10^{-15}	5.57×10^{-12}	50.0	9.5×10^{-14}	1.7
Aquifer	1.58×10^{-9}	1.83×10^{-10}	50.0	7.9×10^{-8}	98
Sediments	1.58×10^{-11}	2.67×10^{-10}	50.0	7.9×10^{-10}	75

[1]from PFLOTRAN simulations

Radionuclide transport includes the effects of sorption and decay/ingrowth and, because ^{129}I is non-sorbing in the deterministic case (K_d = 0 ml/g) with no solubility limit, it is expected to be the most consequential radionuclide to reach the biosphere. Thus, most of the plots in this results section are for ^{129}I transport through the repository system. Because of its instant release fraction, ^{129}I concentration is high in the repository region at early times compared to other radionuclides. It can be used to reveal details of the domain discretization, showing 160 emplaced waste packages in two opposing repository drifts—one drift on each side of the central access hallway (Figure 4-7). Typical PA models simulate a single waste package or a stylized "lumped" waste package. However, with the HPC-enhanced PA model capability, simulations can include a detailed representation of individual waste packages.

Spatial profiles of ^{129}I concentration (reported as molality or mol/kg water) in the simulation domain are shown at various times in Figure 4-8. The instant release (or "gap") fraction of ^{129}I, as well as ^{129}I released during waste form degradation, produces a high dissolved concentration at early times (e.g., 1000 years) in the waste-package and backfill regions (Figure 4-8a), which subsequently diffuses into the DRZ and halite (Figure 4-8b). At about 50,000 years, the ^{129}I from the waste form reaches and begins to travel through the aquifer (Figure 4-8c), via upward transport through the shaft seal region. At 200,000 years, ^{129}I has been transported by advection down the length of both the aquifer and overburden sediments and is diffusing upward through the sediments (Figure 4-8d). The importance of advective transport in the sediments (see Table 4-3) is apparent from the shape of the concentration profile in Figure 4-8d, which shows limited ^{129}I transport upstream of the shaft in either the aquifer or sediments. This process of diffusion up the shaft and advection with diffusive spreading in the aquifer and sediments continues throughout the duration of the simulation, resulting in dissolved ^{129}I throughout the sediments layer after about 500,000 years (Figure 4-8e) and at an approximately equal concentration throughout the sediments layer at 1,000,000 years (Figure 4-8f), albeit at a very low concentration of about 7×10^{-10} molal (at the "sediments-midx" location, x = 7500 m, y = 10 m, z = 600 m —see Fig. 4-11).

The transport behavior of ^{129}I in Figure 4-8 is a result of the assumed material properties in the various regions and may or may not occur at a potential repository site, depending on the measured properties. Its main purpose here is to demonstrate the capabilities of the enhanced PA model. Also, the indicated ^{129}I concentrations in Figure 4-8 are conservatively high because the

lateral boundary conditions in the *y*-direction (i.e., at the sides of the 20-m-wide, 3-D slice) are zero-gradient, no-flow. This prevents ^{129}I from leaving the system in the lateral direction. This would only be true of a repository with an "infinite" number of parallel drifts and, thus, does not account for dilution from lateral mass loss, thereby biasing the results towards higher than expected concentrations in the aquifer and overburden. Two other factors that bias the ^{129}I concentrations in both the aquifer and sediment layers toward conservatively high values are (1) the top boundary condition at the surface (z = 945), which is specified (see Section 4.1) as Dirichlet (10^{-20} molal) instead of Dirichlet_zero_gradient (zero flux) and (2) the lack of a specified meteoric infiltration flux at the surface. However, the purpose of these simulations is more of a demonstration of the capabilities of the GDSA framework, rather than as a rigorous investigation of the behavior of actual bedded salt repository system.

The time history of ^{129}I dissolved concentration near the sample well location in the aquifer (Figure 4-9) further illustrates the transport processes in the domain. ^{129}I dissolved concentration requires about 20,000 years to rise above background (10^{-20} molal) due to long diffusive transport times up the shaft seal region. Somewhere around 100,000 years or 200,000 years the concentration history is dominated by advection in the aquifer but with an element of spreading due to diffusion/dispersion that causes a slow increase in the ^{129}I concentration out to 1,000,000 years.

Deterministic simulation results are also shown for ^{237}Np dissolved concentration at 1,000,000 years (Figure 4-10). Sorption processes retard ^{237}Np transport, resulting in much slower transport than ^{129}I, such that by the end of simulation at 1,000,000 years, ^{237}Np has not diffused much beyond the DRZ and has not reached the aquifer. Preferential diffusion up the shaft seal region is apparent in Figure 4-10, caused by the higher effective diffusion coefficient in the shaft relative to the DRZ, halite, and interbed (Table 3-10); however, the diffusion rate is still not high enough for ^{237}Np to reach the aquifer during this time.

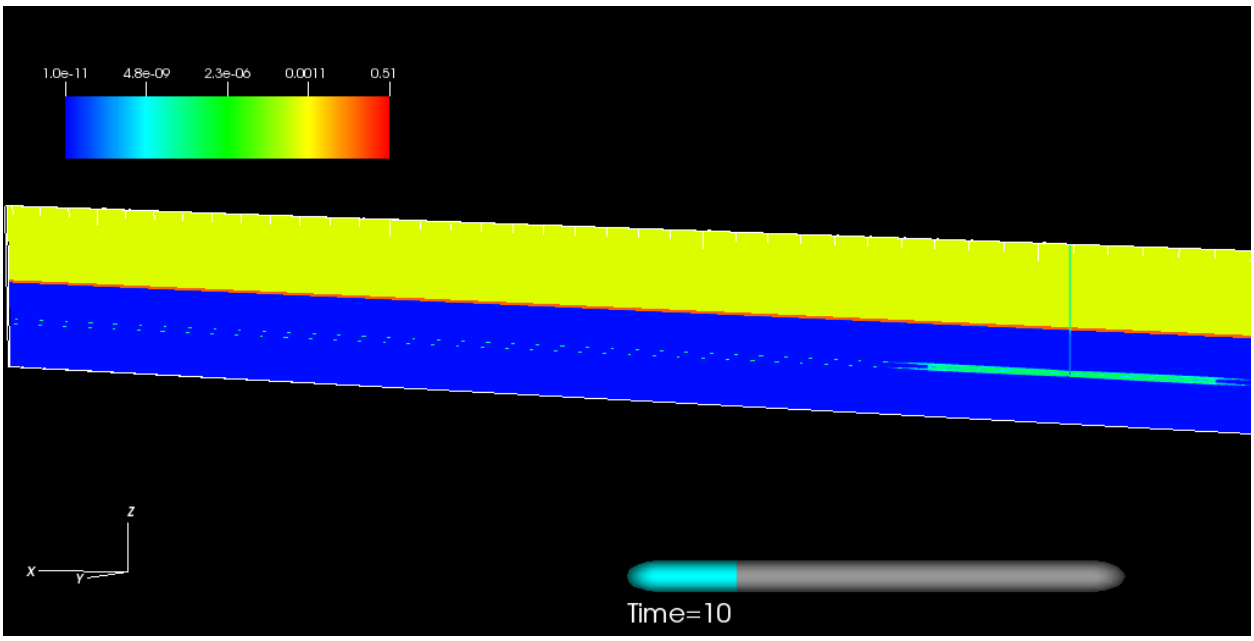

Figure 4-5. Fluid Velocity Magnitude Field (m/yr) for the Deterministic Isothermal Generic Salt Repository Domain.

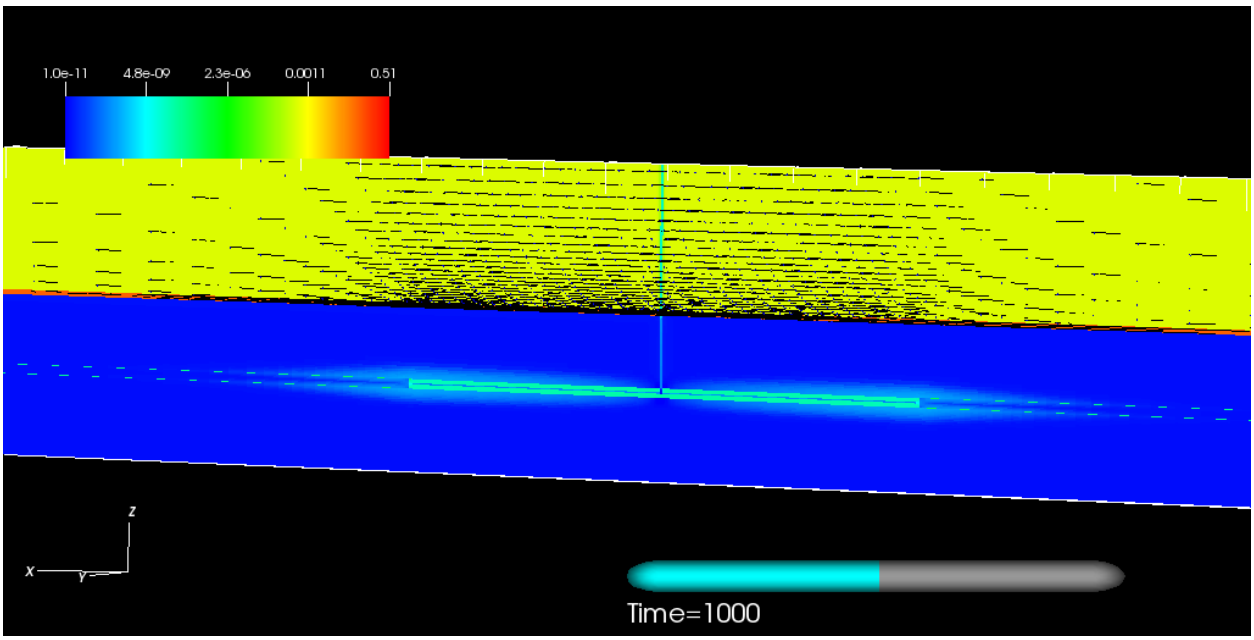

Figure 4-6. Fluid Velocity Vector and Magnitude Field (m/yr) at 1000 years for the Deterministic Isothermal Generic Salt Repository Domain.

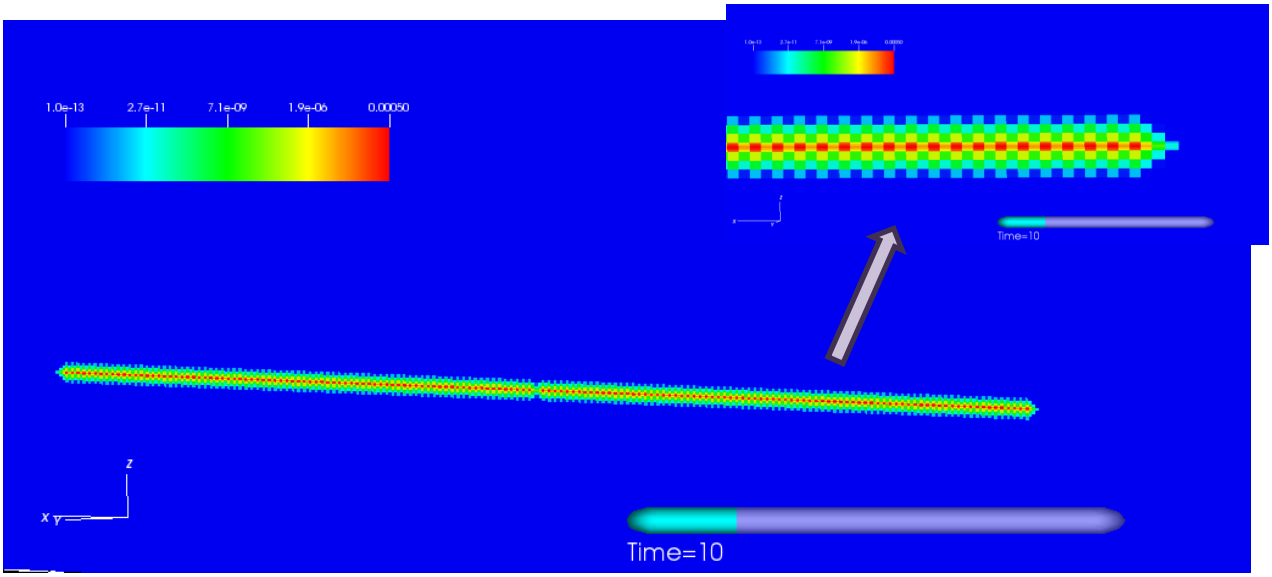

Figure 4-7. ^{129}I dissolved concentration at 10 years, show waste package and drift detail.

a)

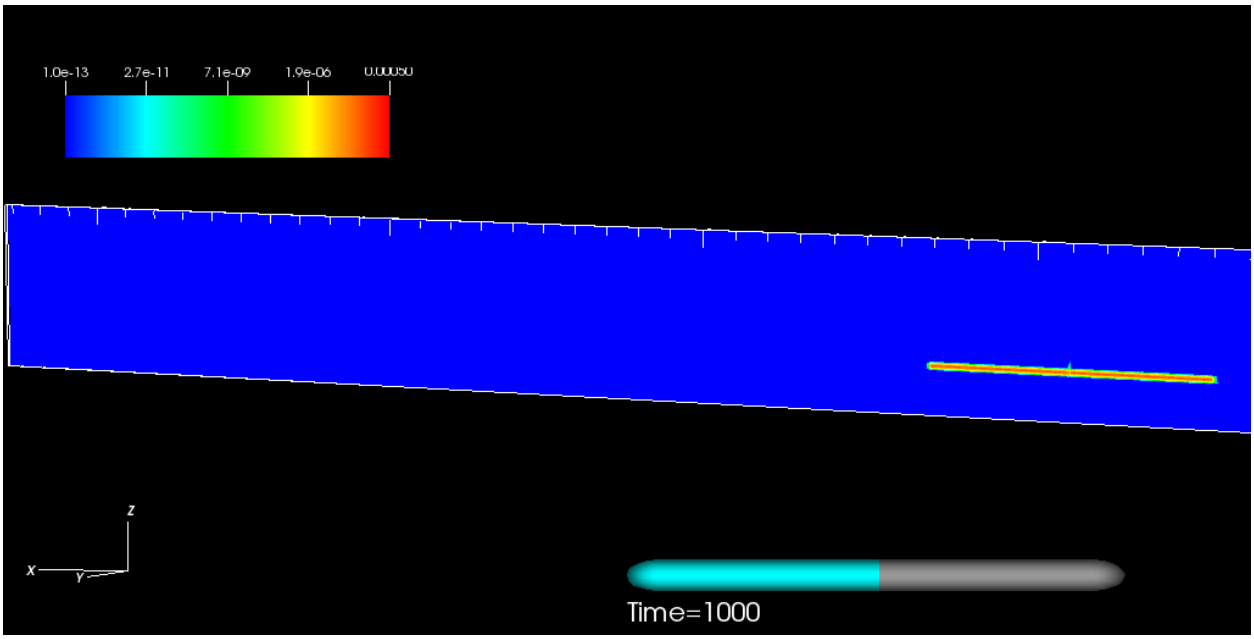

b)

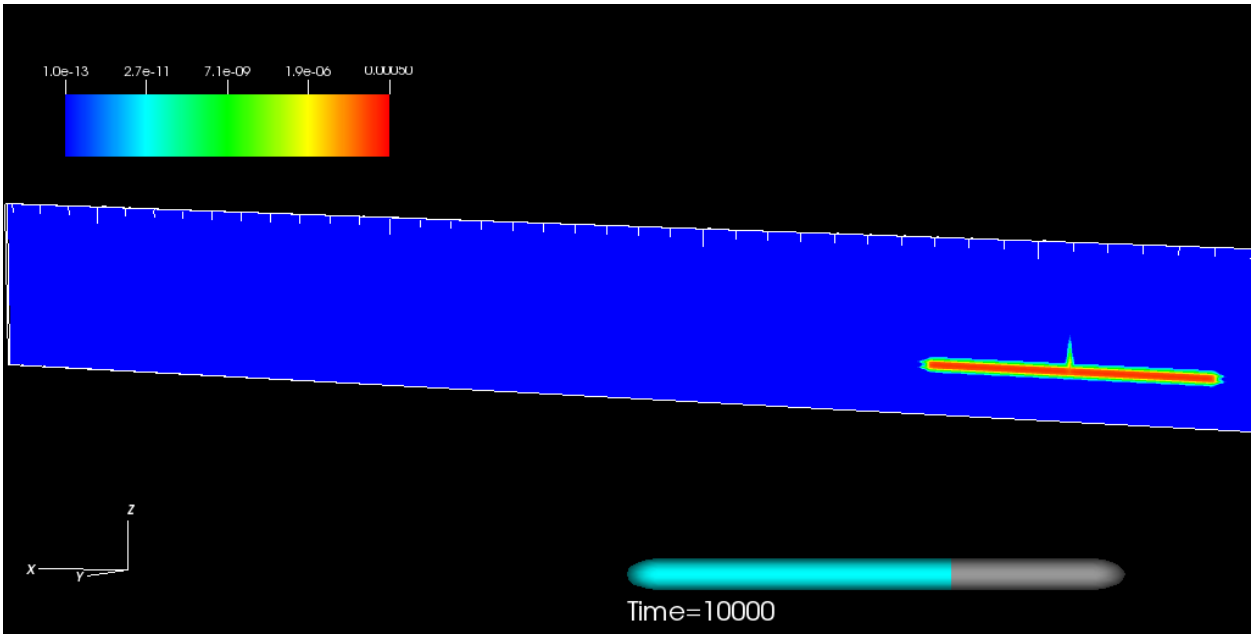

Figure 4-8a,b. ^{129}I Dissolved Concentration at Specified Times for the Deterministic Isothermal Generic Salt Repository Simulation.

a) Time = 1000 years, b) Time = 10,000 years

c)

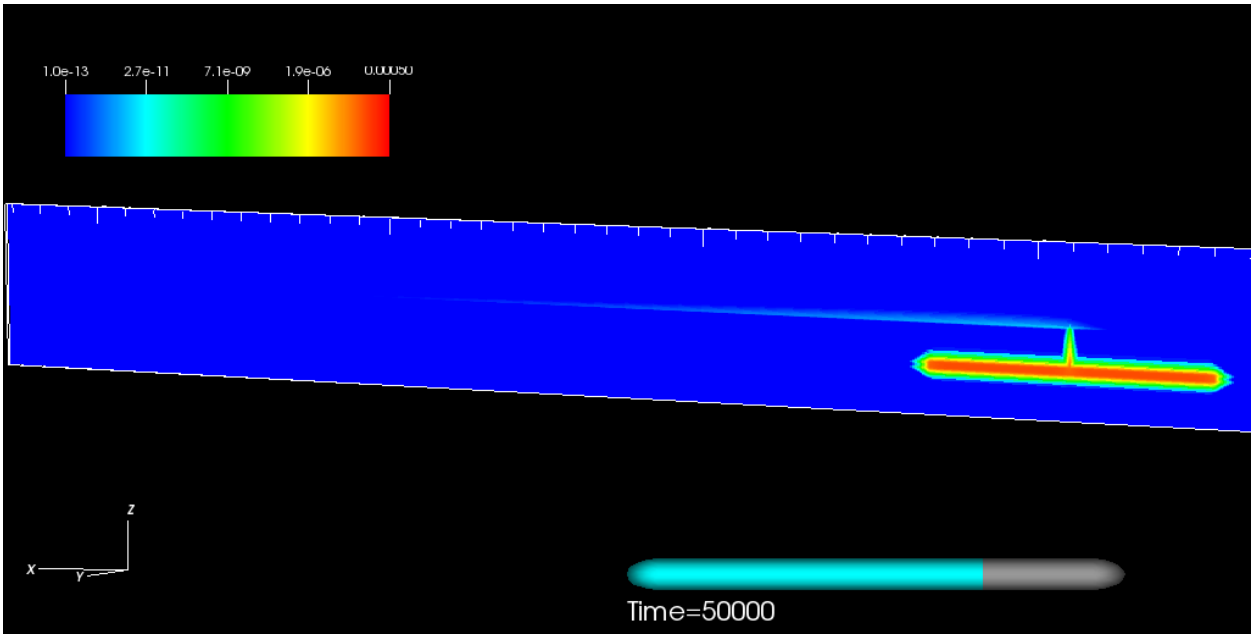

d)

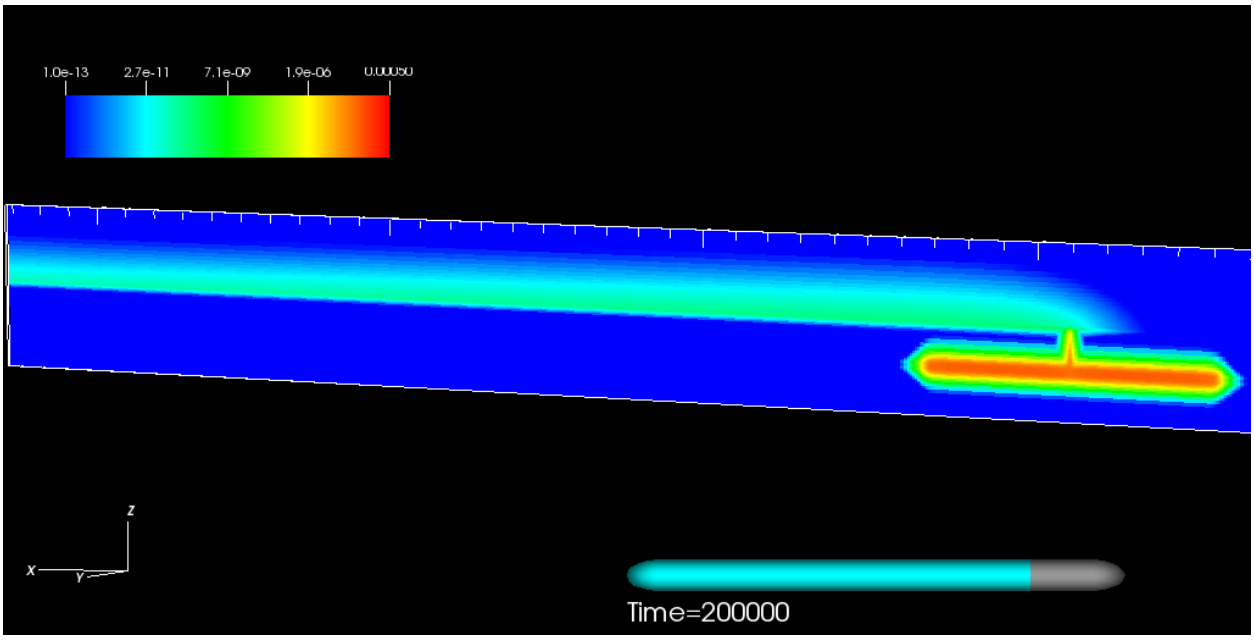

Figure 4-8c,d. ^{129}I Dissolved Concentration at Specified Times for the Deterministic Isothermal Generic Salt Repository Simulation.

c) Time = 50,000 years, d) Time = 200,000 years

e)

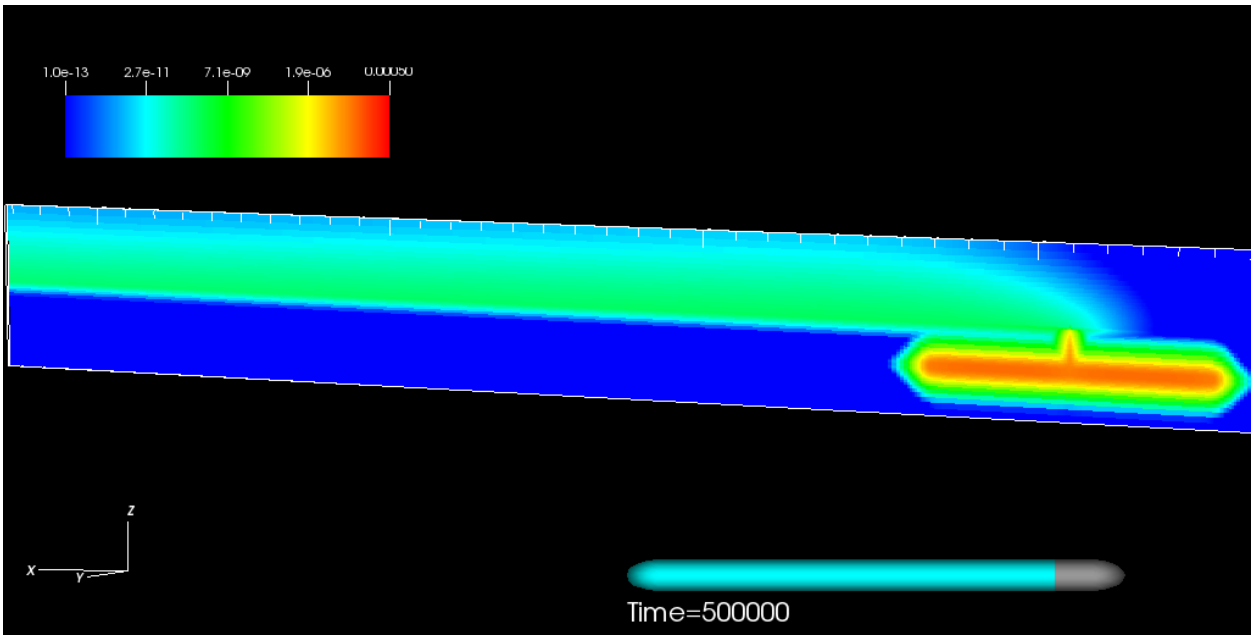

f)

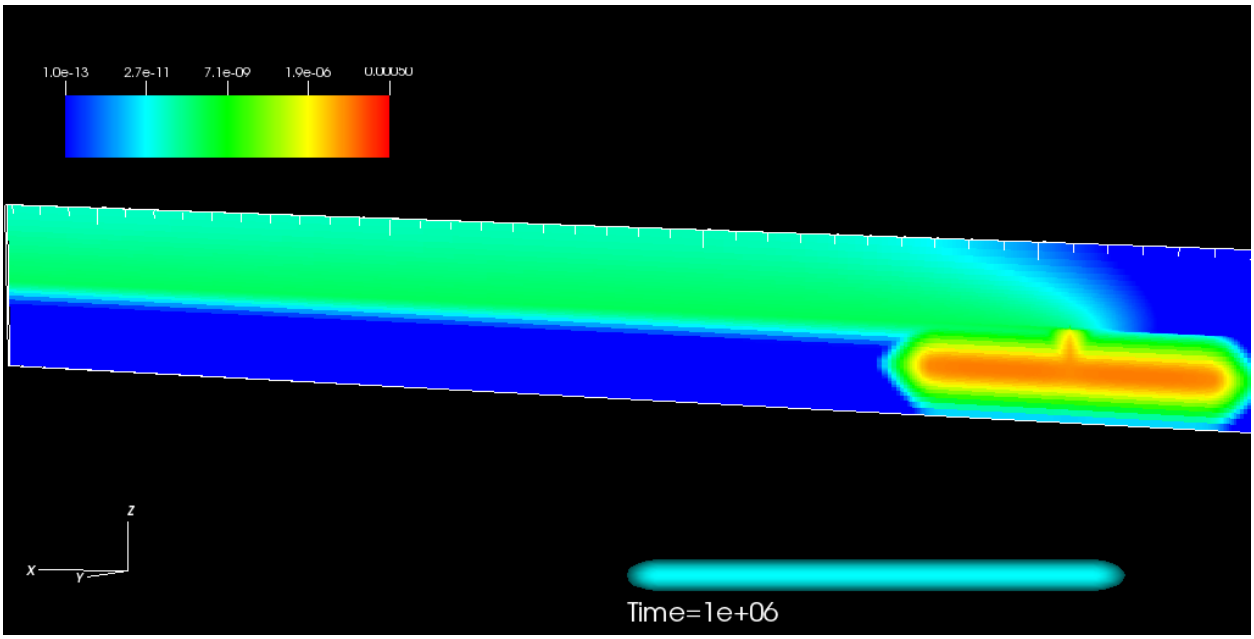

Figure 4-8e,f. ^{129}I Dissolved Concentration at Specified Times for the Deterministic Isothermal Generic Salt Repository Simulation.
e) Time = 500,000 years, f) Time = 1,000,000 years

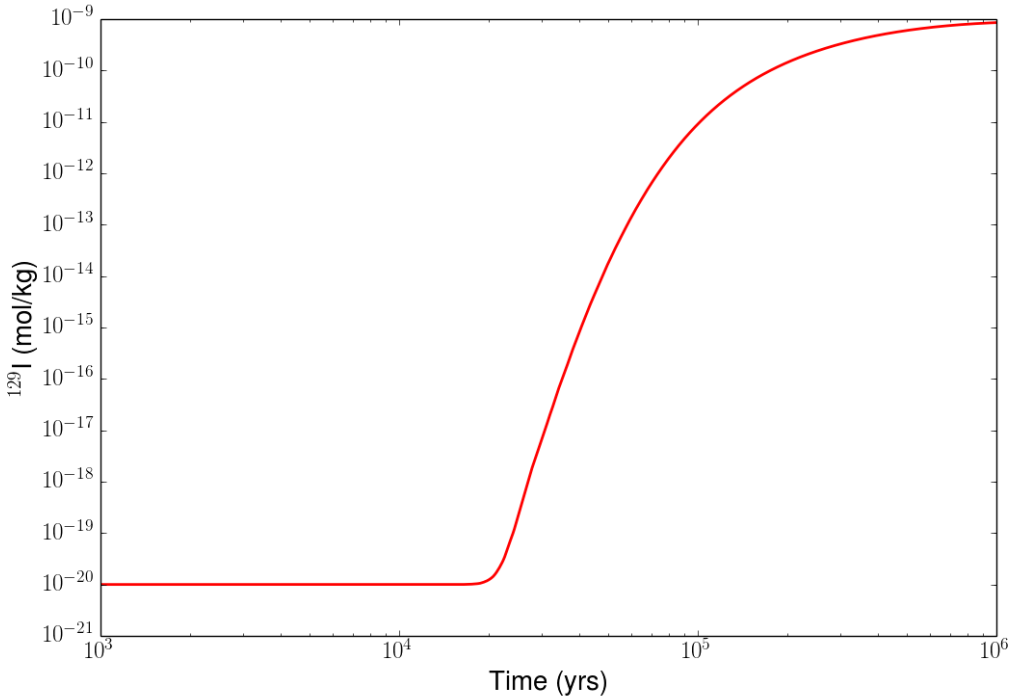

Figure 4-9. ^{129}I Dissolved Concentration in Aquifer at x = 11,600 m for the Deterministic Isothermal Generic Salt Repository Simulation.

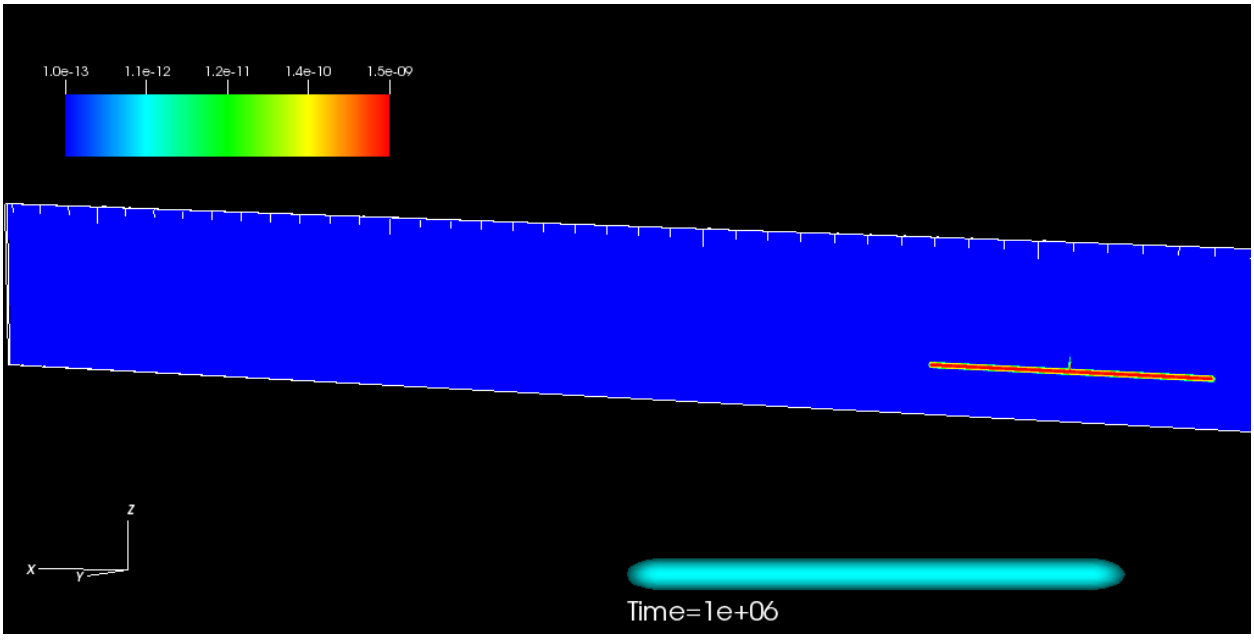

Figure 4-10. ^{237}Np Dissolved Concentration at 1,000,000 years for the Deterministic Isothermal Generic Salt Repository Simulation.

4.3 Probabilistic Isothermal Simulation Results

Probabilistic isothermal simulations of the salt repository demonstration problem were carried out to test the capabilities of the GDSA framework. Fifty realizations were run, with parameter sampling (using Latin Hypercube Sampling (LHS)) and sensitivity analyses performed using DAKOTA. The ten parameters selected for sampling are shown in Table 4-4.

Table 4-4. Salt Repository Reference Case Probabilistic Properties.

Model Parameter	Deterministic Value	Probability Range	Distribution Type
Waste form degradation rate constant (mol/m^2/s)	4.8×10^{-8}	1.00×10^{-10} – 1.00×10^{-7}	Log uniform
^{129}I K_d^P (ml/g)	0.0	9.28×10^{-7} – 7.84×10^{-3}	Log uniform
^{237}Np K_d^P (ml/g)	5.5	1.0 – 10.0	Log uniform
Waste Package Porosity	0.30	0.05 – 0.50	Uniform
Backfill Porosity	0.113	0.010 – 0.200	Uniform
Shaft Porosity	0.113	0.010 – 0.200	Uniform
DRZ Porosity	0.0129	0.0010 – 0.1000	Uniform
Halite Porosity	0.0182	0.0010 – 0.0519	Uniform[1]
Anhydrite Interbed Permeability (m^2)	1.26×10^{-19}	1.00×10^{-21} – 1.00×10^{-17}	Log uniform[2]
Aquifer Permeability (m^2)	1.00×10^{-13}	1.00×10^{-14} – 1.00×10^{-12}	Log uniform

[1]The uniform distribution is a simplification of the cumulative distribution reported in Freeze et al. (2013a, Section 3.2.3.2)
[2]The log uniform distribution is a simplification of the Student-t distribution reported in Freeze et al. (2013a, Section 3.2.3.3)

Probabilistic results were output at ten different observation points as indicated in Figure 4-11. Of those ten points, plots and results are presented here for all but the waste package observation point, which is not particularly revealing. The primary analyzed results at these observation points are time histories of ^{129}I dissolved concentrations for the 50 realizations of the probabilistic parameter sampling. These 50 time histories or "horsetail" plots (Figure 4-12) are then post-processed with DAKOTA subroutines to provide (1) scatterplots of ^{129}I concentration versus sampled input parameter values, for each parameter in Table 4-4 and (2) partial rank regression plots showing the strength of dependency (effectively the derivative) of the variation in ^{129}I concentration versus variation in each sampled parameter. The ^{129}I concentrations used in both the scatterplots and partial rank regression plots is the set of 50 maximum concentrations over the entire 1,000,000-year time span (which, based on Figure 4-12, turns out to be the set of concentrations at 1,000,000 years). Scatterplots show the visual dependency of output variation to input variation, while partial rank regression charts quantify this dependency. Most of the basic analysis here relies on examination of the partial rank correlation coefficients (PRCCs), which are generally more revealing than the simple scatterplots. However, one set of scatterplots is shown here to demonstrate how they are confirmatory to the trends in the partial rank regression analysis.

Horsetail plots of ^{129}I concentration (molal) are provided in Figure 4-12. Corresponding bar charts of the partial rank correlation coefficients (PRCCs) are provided in Figure 4-13. The PRCC bar charts all show similar dependencies of ^{129}I concentration on input parameter variation, except for an important difference related to shaft seal porosity for the "anhydrite-near" and "halite-near" points. This is because ^{129}I reaches the anhydrite-near and halite-near

observation points by a different pathway than ^{129}I for the other seven observation points. The pathway of ^{129}I transport to these two locations is strictly via upward diffusion from the repository zone to these points. No advective transport is involved. On the other hand, for the other seven observation points (aquifer-near, sediments-near, anhydrite-midx, halite-midx, aquifer-midx, sediments-midx, and aquifer monitor well) the ^{129}I transport pathway is via diffusion upward through the shaft seal region, followed by advectively dominated transport through the aquifer and sediments.

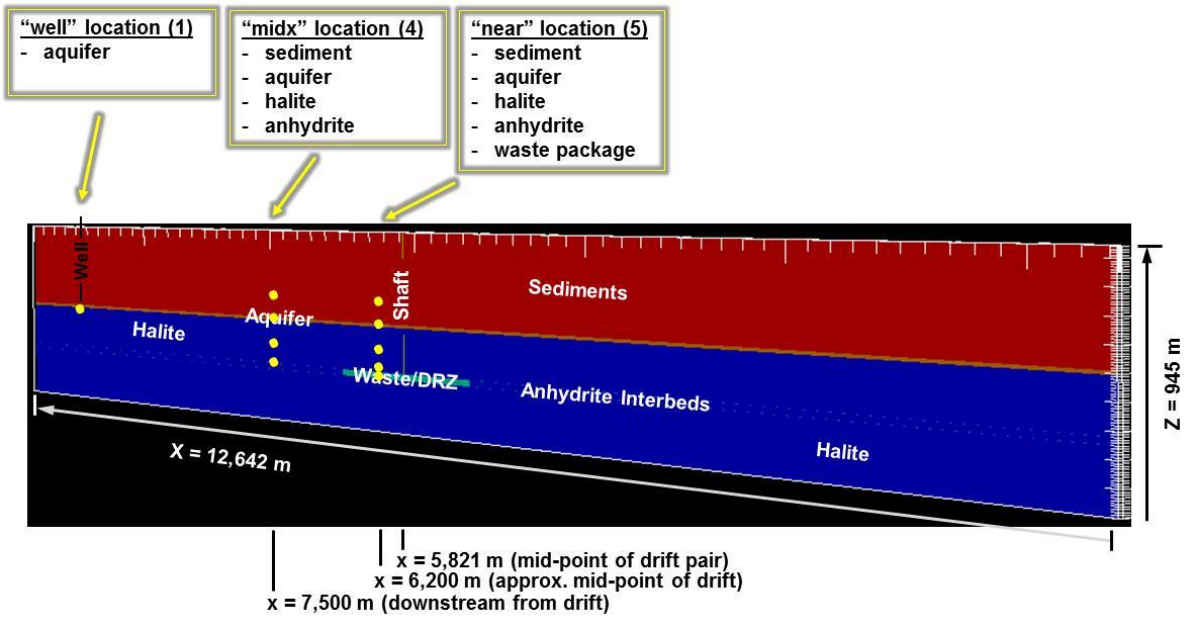

Figure 4-11. Location of Observation Points for Sensitivity Analyses for the Probabilistic Isothermal Generic Salt Repository Simulation.

^{129}I concentration variations at the anhydrite-near and halite-near observation points share strong dependencies on two of the same varied input parameters, with both points showing a strong positive correlation to the waste-form degradation rate and a strong negative correlation to the DRZ porosity. For both observation points the positive dependence on the waste-form degradation rate is because this rate strongly influences the source concentration that drives the diffusion gradient toward the observation point (i.e., the concentration in the waste-package/waste-form cell, which is the upstream boundary condition for diffusive transport). They both have a strong negative correlation to DRZ porosity for the same reason—i.e., the influence of source cell concentration. In particular, the greater the DRZ porosity (recall that the DRZ is directly adjacent to the repository zone) the faster the transport away from the source cells and, thus, the lower the concentration in the upstream source cell at long times. This lower source concentration then causes a lower concentration at the observation point because of the lower diffusion gradient from source to observation point. The halite-near location also has a strong negative dependence on the ^{129}I K_d. This is because of the long diffusive transport time and associated diffusive spreading of the ^{129}I wave front. This type of dependency on ^{129}I K_d is also shared with two other observation points, the anhydrite-midx and halite-midx points, which have a transport pathway that is also highly dependent on diffusion. In particular, as noted below, ^{129}I reaches these two points via relatively transport along the aquifer and then slow downward diffusion.

The other seven observation points (aquifer-near, sediments-near, anhydrite-midx, halite-midx, aquifer-midx, sediments-midx, and aquifer monitor well) all show mostly similar PRCC behavior because they all are influenced by the same transport behavior, which is diffusion upward through the shaft seal region, followed by advectively dominated transport through the aquifer and sediments. This causes all seven points to exhibit a strong positive correlation to shaft seal porosity, since the rate of ^{129}I mass transfer to the aquifer is higher when the effective diffusion coefficient in the shaft region, $(D_{eff})_{shaft} = (\phi\tau)_{shaft}D_w$, is higher. Even the anhydrite-midx and halite-midx show this type of dependency on shaft seal porosity, although the actual magnitudes of their ^{129}I concentrations are very low (Figures 4-12e and 4-12f). In other words, the ^{129}I that reaches these observation points is by diffusive transport up the shaft seal, followed by relatively fast advection through the aquifer, and then slow diffusion downward from the aquifer to these points—as mentioned above with regards to the influence of the sampled ^{129}I K_d^P parameter. Also, all of these seven observation points have a positive correlation to the waste-form degradation rate for the aforementioned reason regarding the source concentration. Furthermore, they all show a negative correlation to both DRZ and halite porosity, which affect the source concentration, as described above. The negative correlation of ^{129}I concentration with aquifer permeability for these seven observation points is further evidence of the importance of advective transport through the aquifer, i.e., the higher the aquifer permeability, the greater the fluid flow rate, which implies a greater dilution of the ^{129}I concentration.

One set of scatterplots is shown in Figure 4-14, for the aquifer monitor well location. The strongest positive trend observable is to shaft seal porosity, as expected from the PRCC bar chart (Figure 4-13i). Similarly, the strongest negative trend is the dependence of ^{129}I concentration on halite porosity, again to be expected based on Figure 4-13i.

The foregoing sensitivity results and analysis provide preliminary insights into the important multi-physics processes and couplings controlling long-term performance for the generic reference-case salt repository. However, these salt repository simulations only represent a preliminary, demonstration-scale problem. Further PA model refinement would be prudent before drawing strong conclusions regarding the relative importance of various parameters for a waste repository in bedded salt. It should also be noted that the sensitivity indicators (e.g., PRCCs) are dependent on the specific performance metric, in this case the peak ^{129}I dissolved concentration at the observation point. For example, the high sensitivity to waste-form degradation rate would likely diminish if the performance metric were total mass transported to the sample well location. Similarly, the sensitivity to ^{129}I K_d^P would likely be even greater if the performance metric were time to peak concentration. However, the current objective was to test the probabilistic simulation and sensitivity analysis capability, not to perform an in-depth analysis of specific processes or parameters.

a)

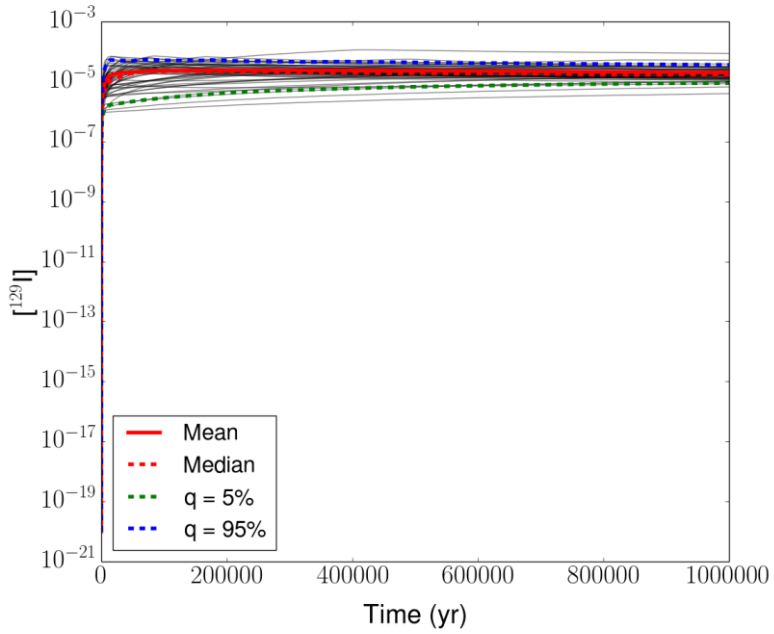

b)

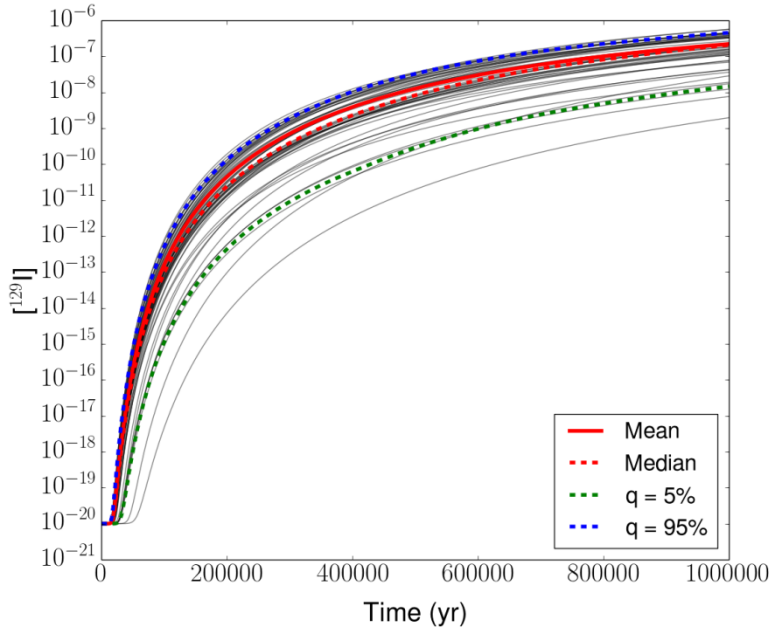

Figure 4-12a,b. Horsetail Plot of ^{129}I Dissolved Concentration at Various Observation Points for the Probabilistic Isothermal Generic Salt Repository Simulation.

a) "Anhydrite Near": x = 6212 m, y = 10 m, z = 279.5 m

b) "Halite Near": x = 6212 m, y = 10 m, z = 375 m

c)

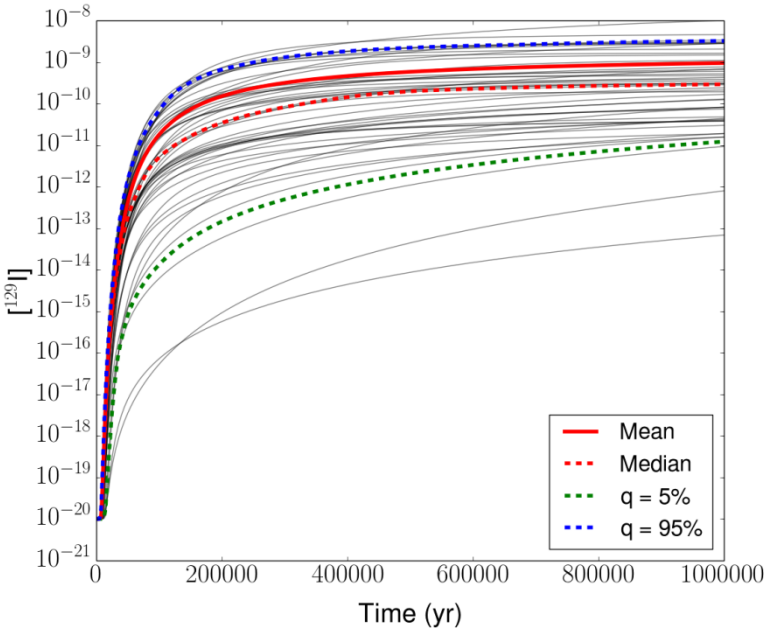

d)

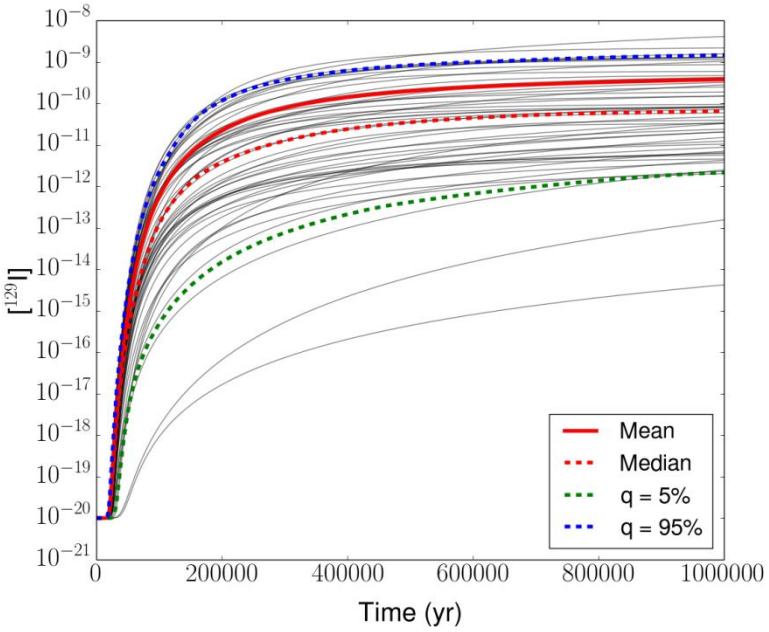

Figure 4-12c,d. Horsetail Plot of ^{129}I Dissolved Concentration at Various Observation Points for the Probabilistic Isothermal Generic Salt Repository Simulation.

c) "Aquifer Near": x = 6212 m, y = 10 m, z = 502.5 m

d) "Sediments Near": x = 6212 m, y = 10 m, z = 600 m

e)

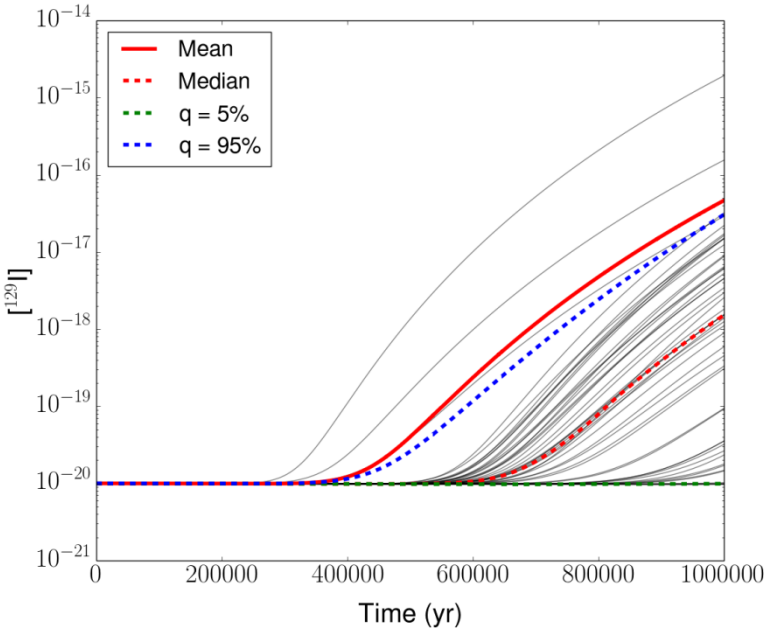

f)

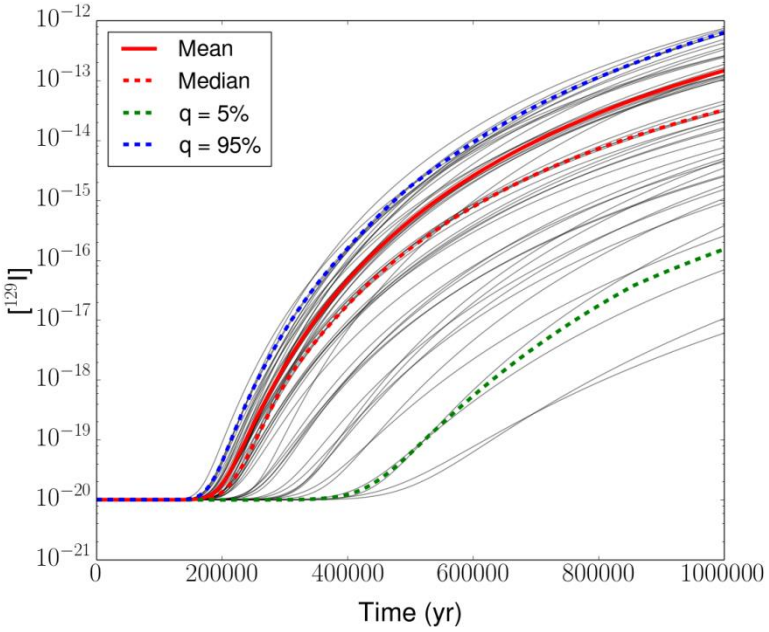

Figure 4-12e,f. Horsetail Plot of ^{129}I Dissolved Concentration at Various Observation Points for the Probabilistic Isothermal Generic Salt Repository Simulation.

e) "Anhydrite Mid-x": x = 7500 m, y = 10 m, z = 279.5 m

f) "Halite Mid-x": x = 7500 m, y = 10 m, z = 375 m

g)

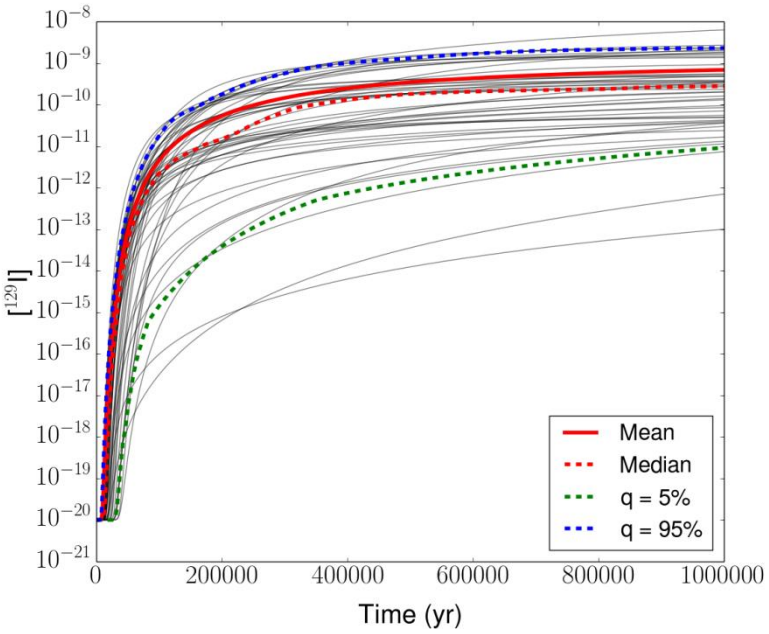

h)

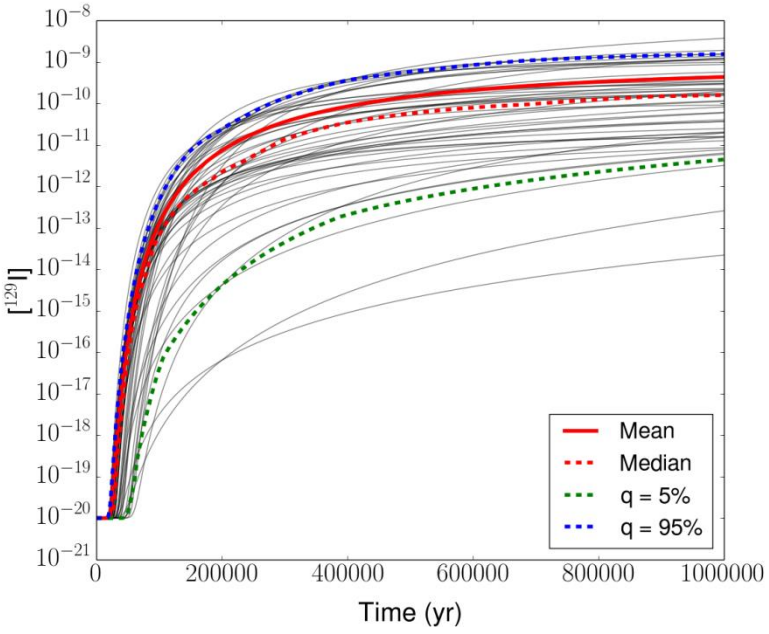

Figure 4-12g,h. Horsetail Plot of ^{129}I Dissolved Concentration at Various Observation Points for the Probabilistic Isothermal Generic Salt Repository Simulation.

g) "Aquifer Mid-x": x = 7500 m, y = 10 m, z = 502.5 m

h) "Sediments Mid-x": x = 7500 m, y = 10 m, z = 600 m

i)

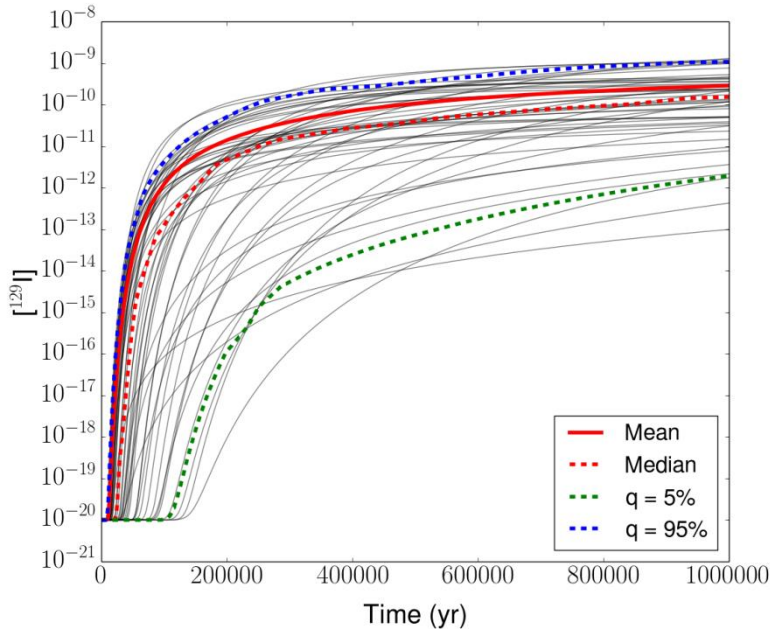

Figure 4-12i. Horsetail Plot of ^{129}I Dissolved Concentration at Various Observation Points for the Probabilistic Isothermal Generic Salt Repository Simulation.

i) Aquifer monitor well location: x = 11,600 m, y = 10 m, z = 502.5 m

a)

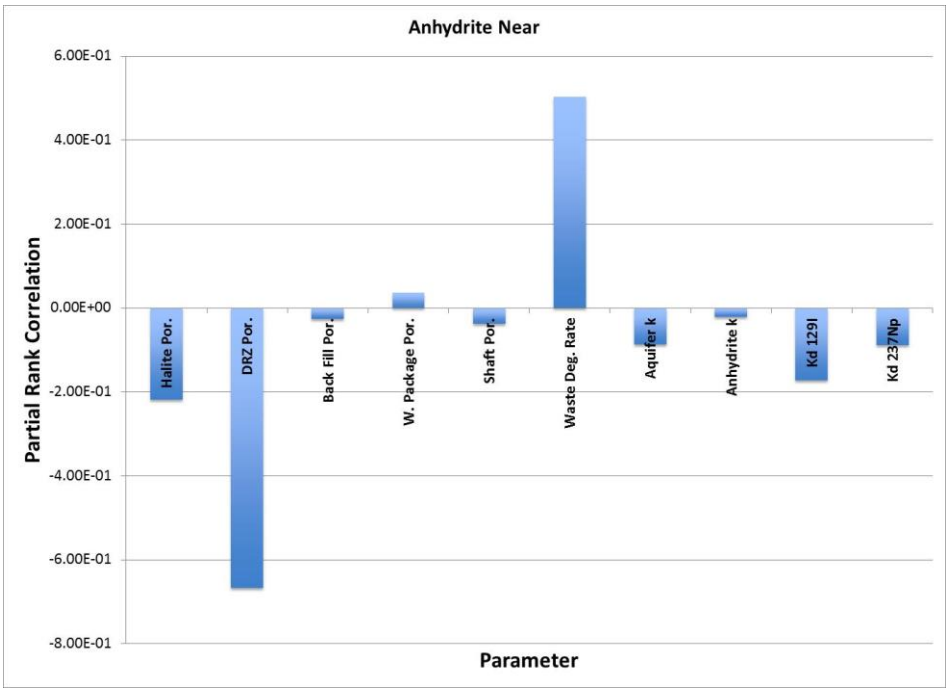

b)

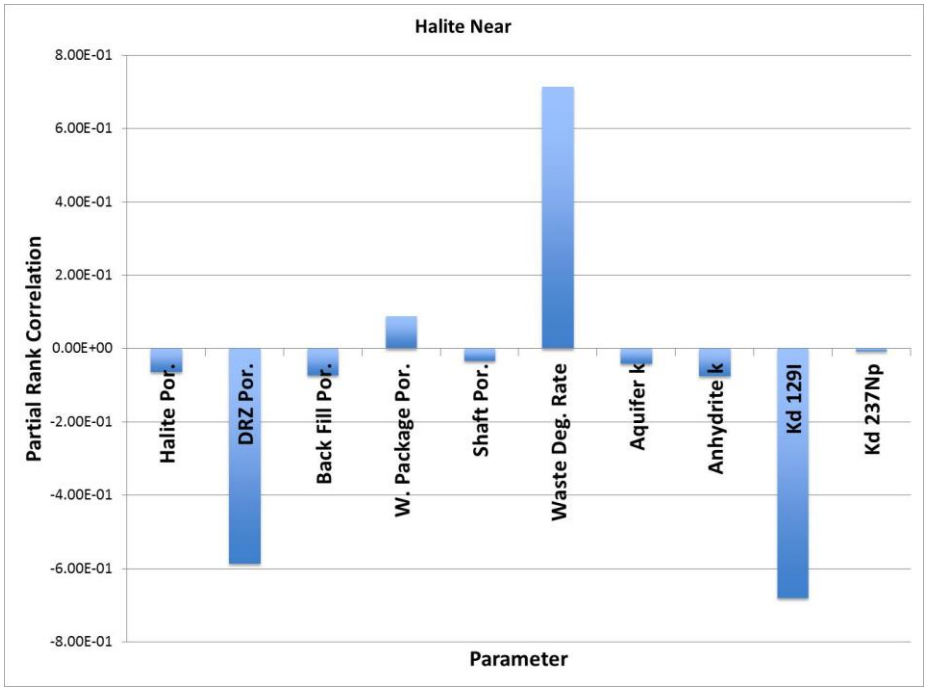

Figure 4-13a,b. Partial Rank Correlation Coefficients for ^{129}I Dissolved Concentration versus Sampled Parameters for the Probabilistic Isothermal Generic Salt Repository Simulation.

a) "Anhydrite Near": x = 6212 m, y = 10 m, z = 279.5 m

b) "Halite Near": x = 6212 m, y = 10 m, z = 375 m

c)

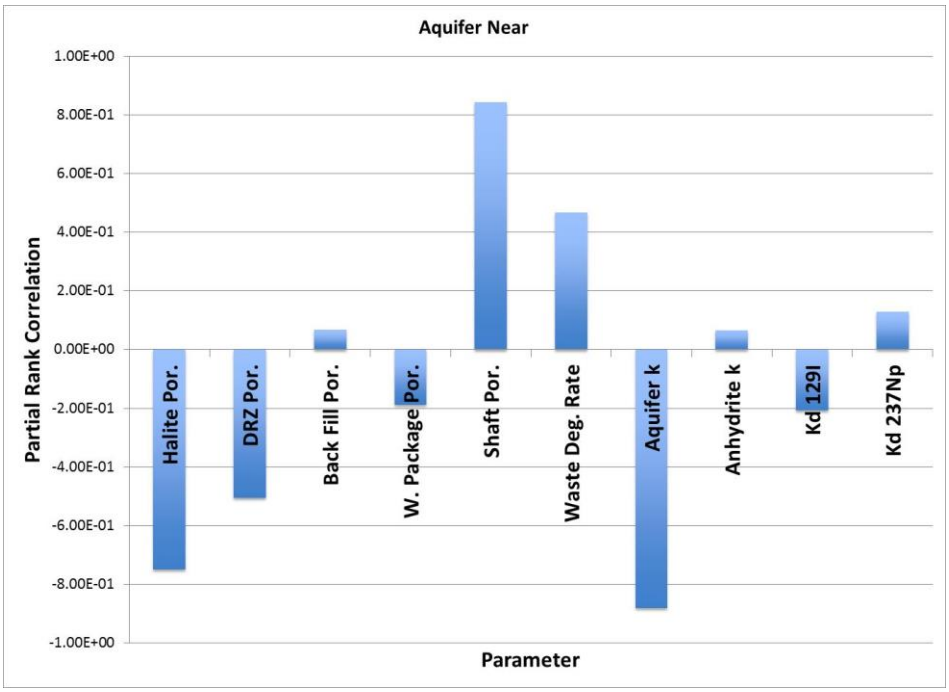

d)

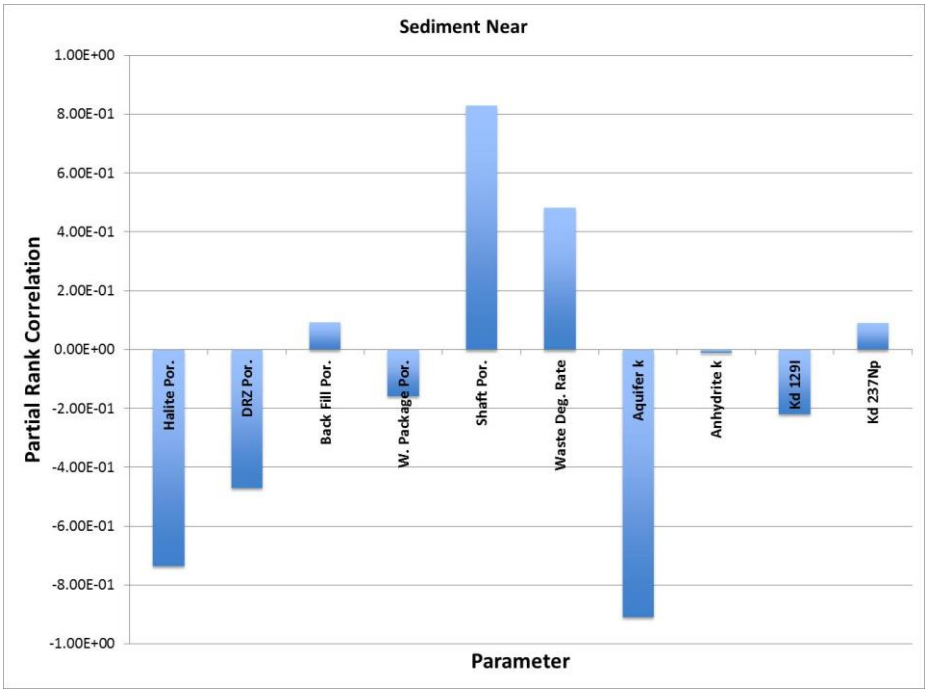

Figure 4-13c,d. Partial Rank Correlation Coefficients for ^{129}I Dissolved Concentration versus Sampled Parameters for the Probabilistic Isothermal Generic Salt Repository Simulation.

c) "Aquifer Near": x = 6212 m, y = 10 m, z = 502.5 m

d) "Sediments Near": x = 6212 m, y = 10 m, z = 600 m

e)

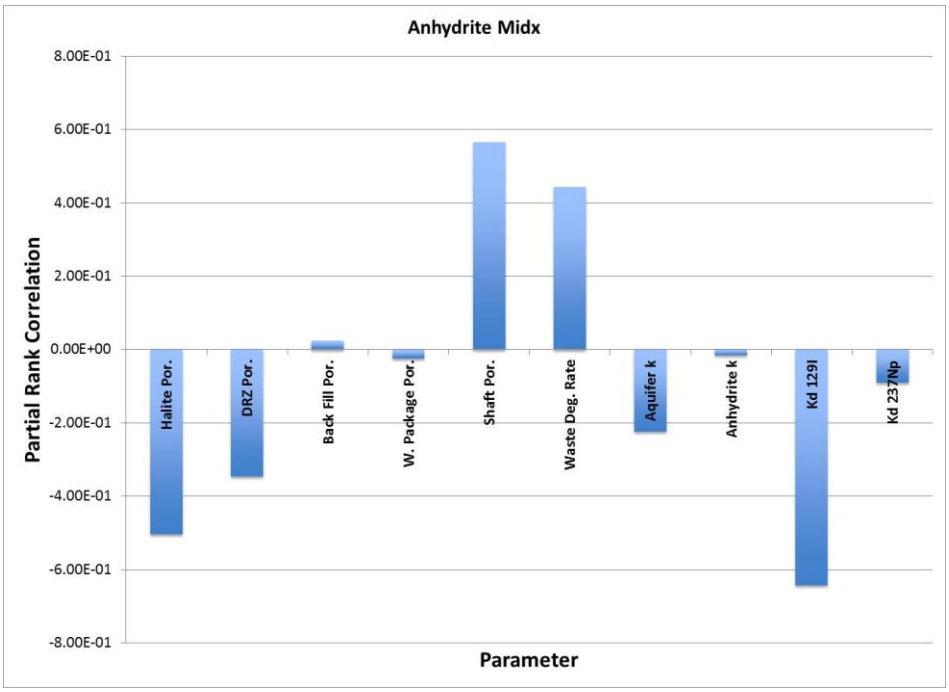

f)

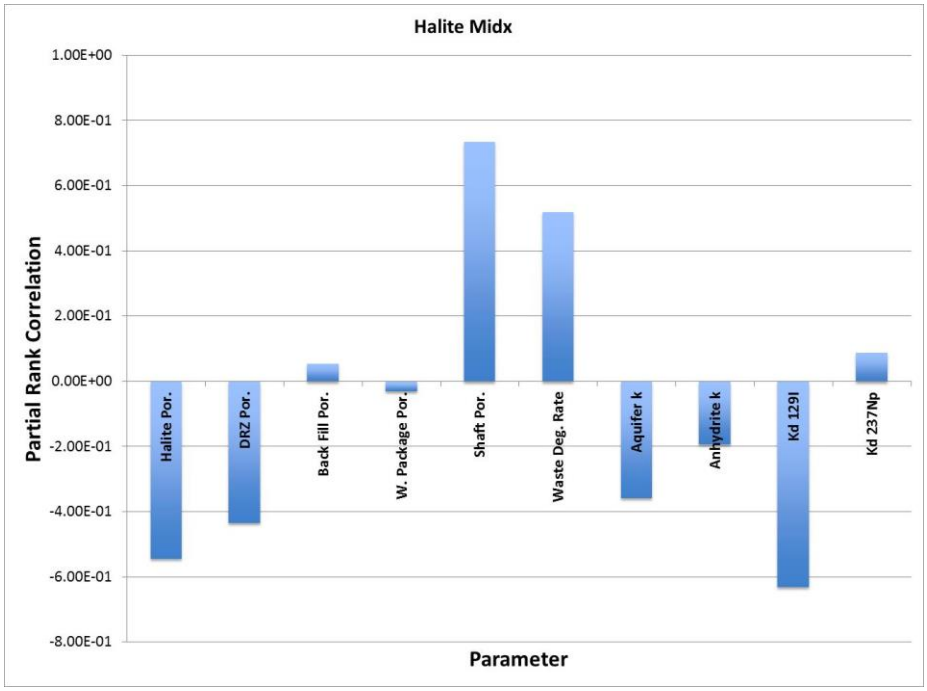

Figure 4-13e,f. Partial Rank Correlation Coefficients for ^{129}I Dissolved Concentration versus Sampled Parameters for the Probabilistic Isothermal Generic Salt Repository Simulation.

e) "Anhydrite Mid-x": x = 7500 m, y = 10 m, z = 279.5 m

f) "Halite Mid-x": x = 7500 m, y = 10 m, z = 375 m

g)

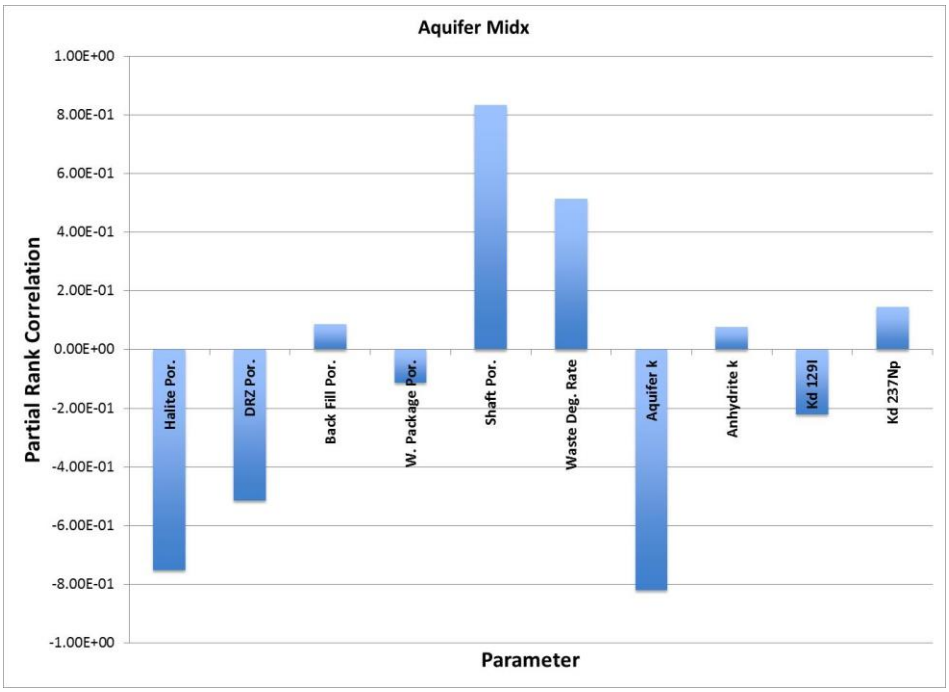

h)

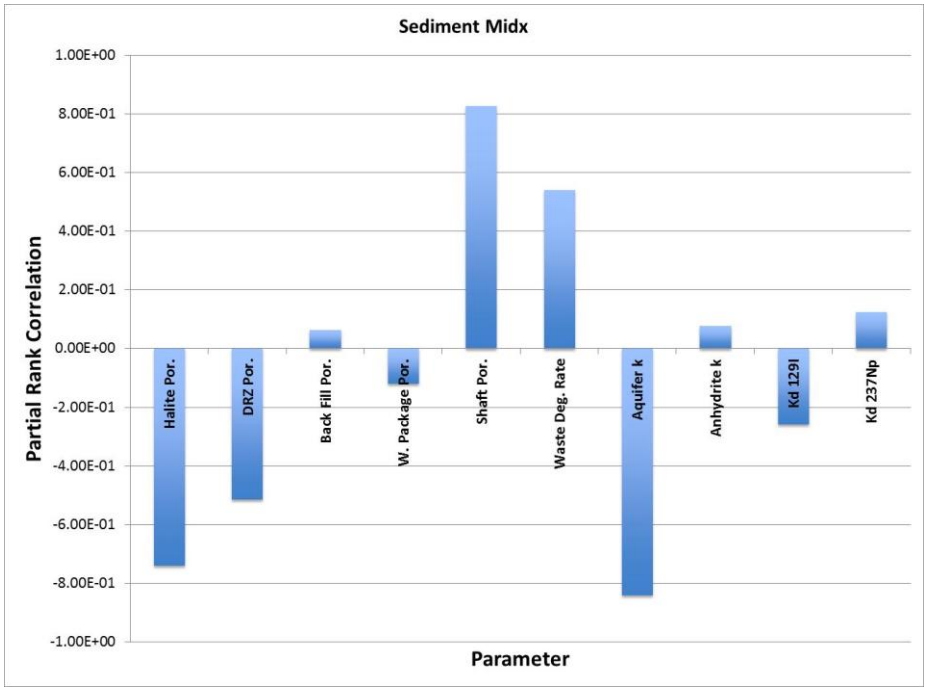

Figure 4-13g,h. Partial Rank Correlation Coefficients for ^{129}I Dissolved Concentration versus Sampled Parameters for the Probabilistic Isothermal Generic Salt Repository Simulation.

g) "Aquifer Mid-x": x = 7500 m, y = 10 m, z = 502.5 m

h) "Sediments Mid-x": x = 7500 m, y = 10 m, z = 600 m

i)

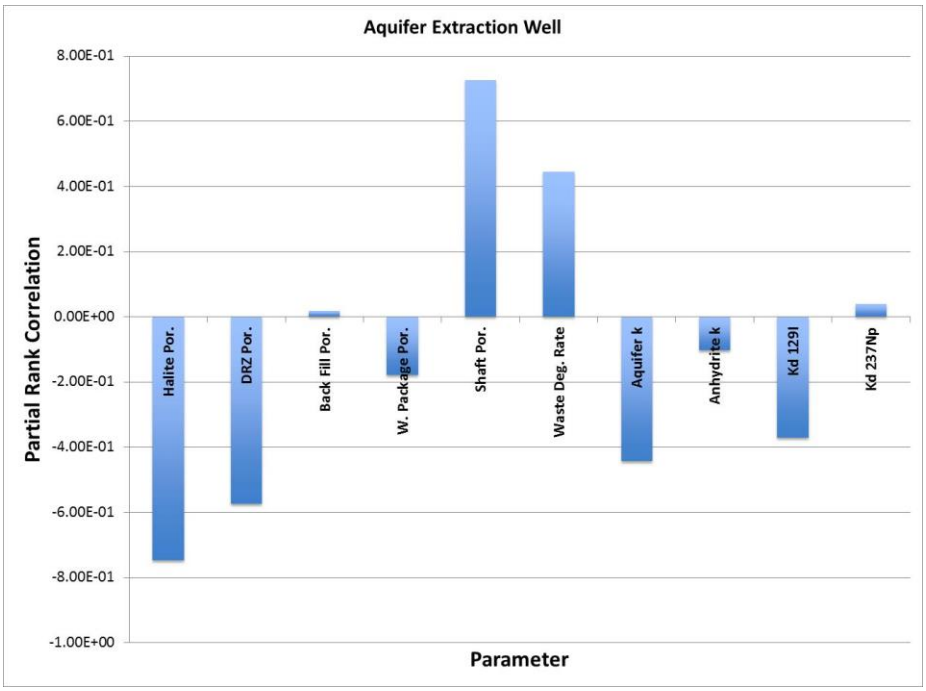

Figure 4-13i. Partial Rank Correlation Coefficients for ^{129}I Dissolved Concentration versus Sampled Parameters for the Probabilistic Isothermal Generic Salt Repository Simulation.

i) Aquifer monitor well location: x = 11,600 m, y = 10 m, z = 502.5 m

a)

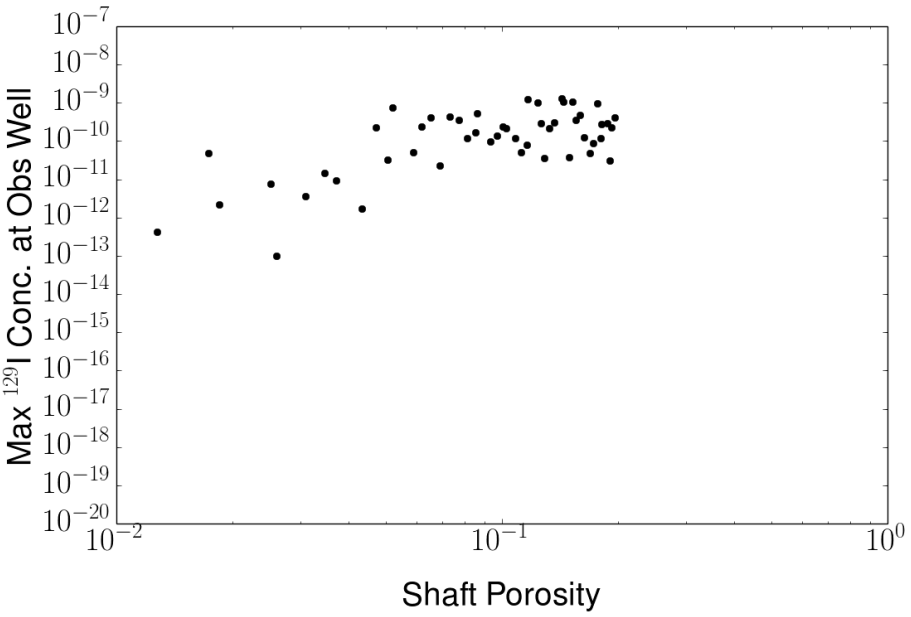

b)

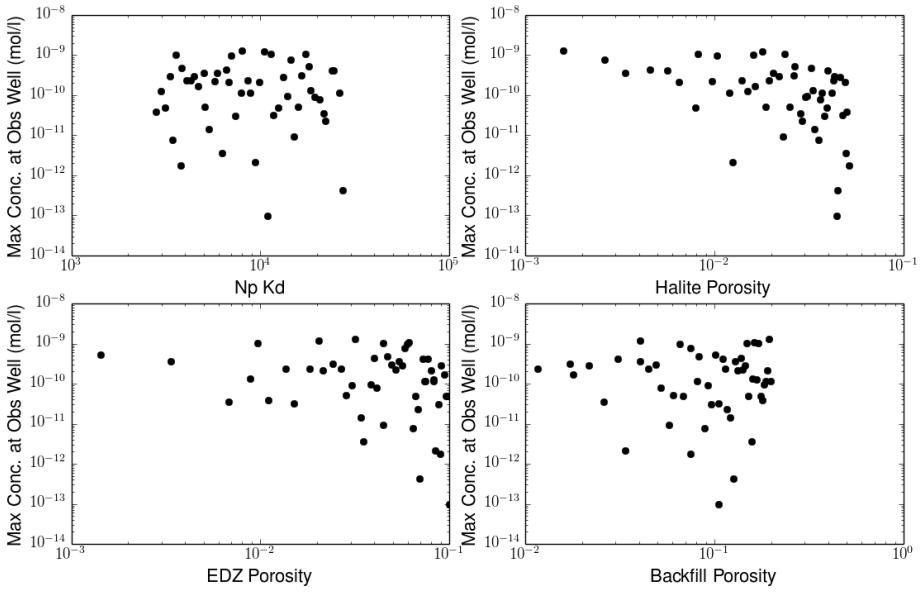

Figure 4-14a,b. Scatterplots for Maximum ^{129}I Dissolved Concentration versus Sampled Parameters for the Probabilistic Isothermal Generic Salt Repository Simulation, at the "Aquifer Monitor Well" Observation Point.

a) ^{129}I vs. Shaft Porosity

b) ^{129}I vs. Np K_d; ^{129}I vs. Halite Porosity; ^{129}I vs. DRZ Porosity; ^{129}I vs. Backfill Porosity

c)

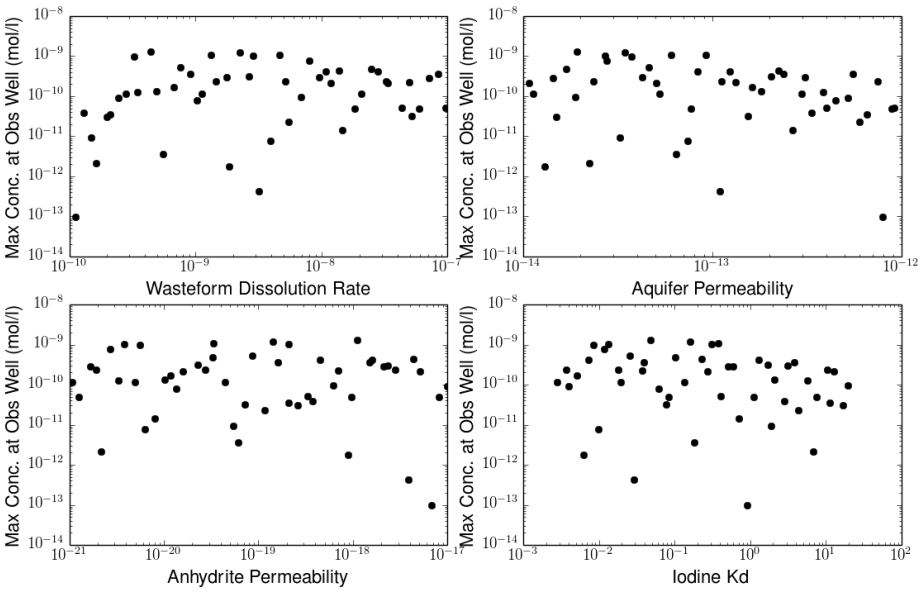

Figure 4-14c. Scatterplots for Maximum ^{129}I Dissolved Concentration versus Sampled Parameters for the Probabilistic Isothermal Generic Salt Repository Simulation, at the "Aquifer Monitor Well" Observation Point.

c) ^{129}I vs. WF Dissolution Rate; ^{129}I vs. Aquifer *k*; ^{129}I vs. Anhydrite *k*; ^{129}I vs. Iodine K_d

4.4 Deterministic Thermal Simulation Results

The salt repository *thermal* simulations were run using PFLOTRAN "GENERAL" option, which models multiphase air-water flow combined with the thermal energy equation (Lichtner 2014). Thermal properties of the various materials and the SNF source-term decay heat are given in Section 3.4.7.4.

The fluid velocity magnitude (in m/yr) and vector fields in all regions of the simulation domain (resulting from the applied hydraulic gradient of 0.0013) are shown in Figures 4-15 and 4-16. Figure 4-15 shows Darcy velocity magnitude at 10 years for most of the simulated domain, while Figure 4-16 shows velocity vectors at 1000 years for portion of the domain closer to the repository region, along with color profiles of the temperature field on a scale of 20°C to 230°C degrees. In comparing Figure 4-15 to the isothermal Darcy velocity magnitude field in Figure 4-5, the primary difference is the halo of increased velocity magnitude surrounding the repository region in Figure 4-15. The cause of this is made clear from Figure 4-16, which indicates a strong component of fluid flux flowing away from the repository region, due to thermal expansion of the fluid. Fluid velocity direction and temperature fields are shown at other times in Figure 4-17. The primary observation from the results in Figure 4-17 comes from parts b, c, and d, the velocity vectors and temperatures at 1000 years, 10,000 years, and 50,000 years, respectively. These plots indicate the development of obvious fluid convection cells in the combined aquifer/sediments region, which can be confirmed by calculating the Rayleigh number. The Rayleigh number can be calculated using:

$$Ra = \frac{\alpha_w \rho_w^2 c_w g k L \Delta T}{\mu K_m} \qquad \text{Eq. (4-3)}$$

where α_w is the thermal expansion coefficient, c_w is the specific heat, k is the intrinsic permeability, L is the length scale of the feature, μ is the viscosity and K_m is the thermal conductivity. Using a permeability of 10^{-15} m^2 for the overburden sediments, the critical Rayleigh number of 2 (associated with the formation of convection cells) is achieved when the bottom of the aquifer reaches a temperature of 35°C. Dissipation of the heat decay pulse lowers the "hot side" temperature far enough by 50,000 years (to a little below 35°C) that the Rayleigh number is reduced to near-critical or below critical, implying the lack of a driving force for convection cells, which is clear from the velocity vectors in Figure 4-17d. (The critical Rayleigh number for this system occurs when the temperature difference across the aquifer-sediment region is greater than about 15°C.)

Spatial profiles of ^{129}I concentration (reported as molality or mol/kg water) in the simulation domain are shown at various times in Figure 4-18. When compared to the comparable plots for the isothermal simulation (Figure 4-8), the thermal expansion of the fluid at early times causes a greater flux of ^{129}I transported laterally from the repository (upstream and downstream in the *x*-direction) in the thermal simulation (cf. Figures 4-18a,b with Figures 4-8a,b). However, later plots for $t > 50{,}000$ years show little effect of the heat pulse in either the repository region or in the aquifer/sediments region (cf. Figures 4-18c-f with Figures 4-8c-f). This is because the ^{129}I takes about 50,000 years to diffuse through the shaft seal region into the aquifer and sediments, which is beyond the time when thermal convection cells are present (see Figure 4-17d). Thus, ^{129}I transport in the aquifer and sediments is not enhanced by these convection cells. Other

conclusions about ^{129}I transport for this thermal simulation are the same as those discussed in Section 4.2 for the isothermal simulation.

The time history of ^{129}I dissolved concentration near the sample well location in the aquifer for the thermal simulation (Figure 4-19) is very similar to the time history of ^{129}I for the isothermal simulation (Figure 4-9), simply because, as mentioned above, the thermal pulse has a minimal effect on transport behavior. However, the ^{129}I does breakthrough to the sample well location slightly earlier in the thermal simulation, probably as a result of the spreading of ^{129}I around the repository region at early times (Figures 4-18a,b) caused by thermal expansion of the fluid in the repository region (Figure 4-15).

Deterministic simulation results are also shown for ^{237}Np dissolved concentration at 1,000,000 years (Figure 4-20). No difference can be observed between this plot and the comparable one for the isothermal simulation (Figure 4-10).

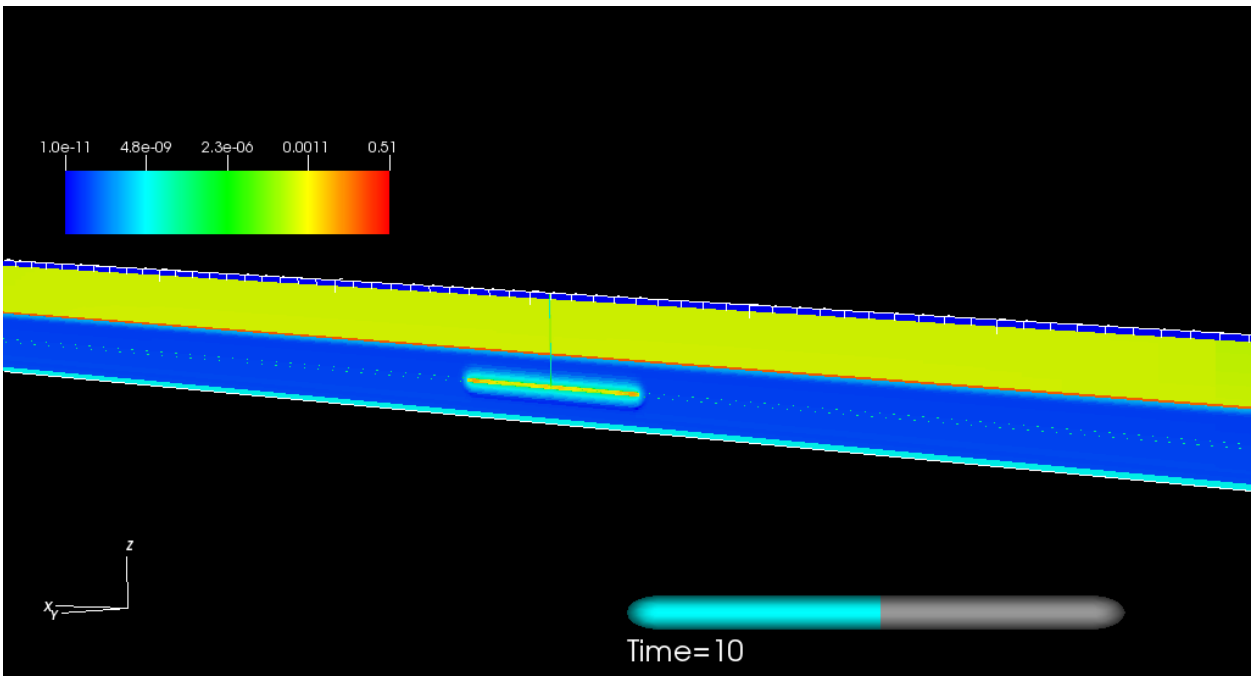

Figure 4-15. Fluid Velocity Magnitude Field (m/yr) for the Deterministic *Thermal* Generic Salt Repository Domain.

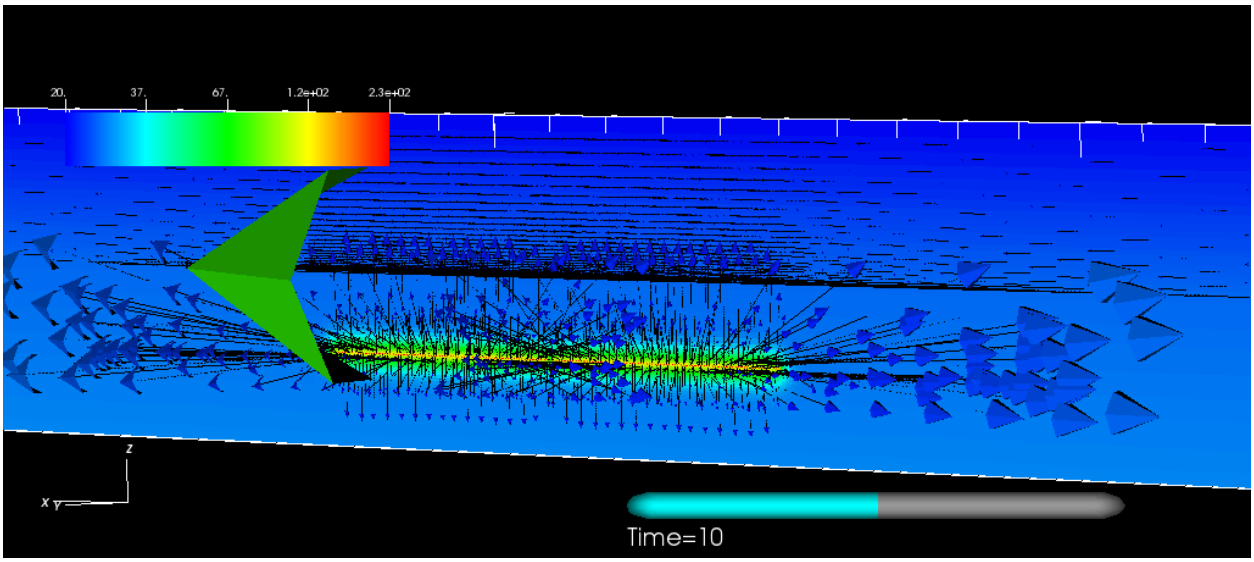

Figure 4-16. Fluid Velocity Vector Field (m/yr) and Temperature Field (on a scale of 20°C to 230°C) at 10 Years after Repository Closure for the Deterministic *Thermal* Generic Salt Repository Domain.

a)

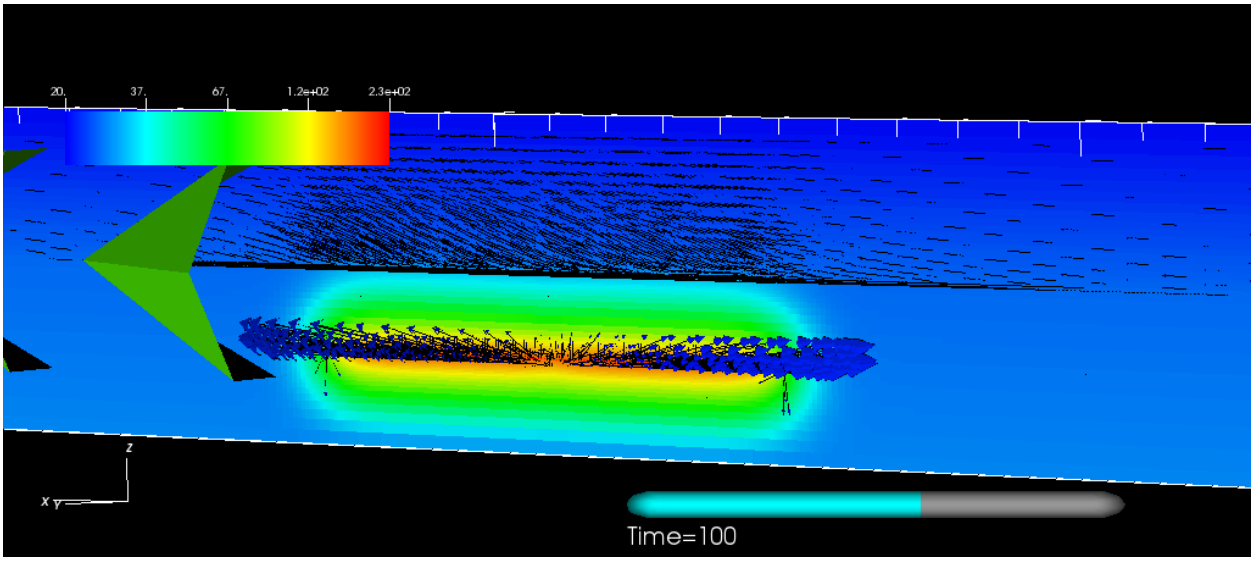

b)

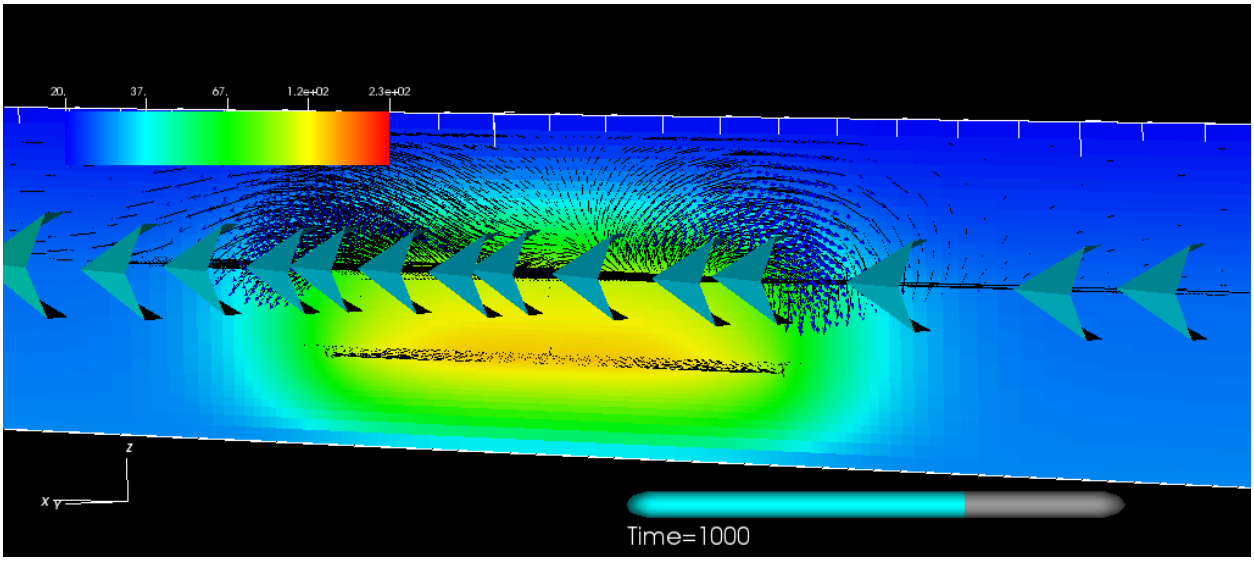

Figure 4-17a,b. Fluid Velocity Vector Field (m/yr) and Temperature Field (on a scale of 20°C to 230°C) at Various Times for the Deterministic *Thermal* Generic Salt Repository Domain.

a) At 100 years

b) At 1,000 years

c)

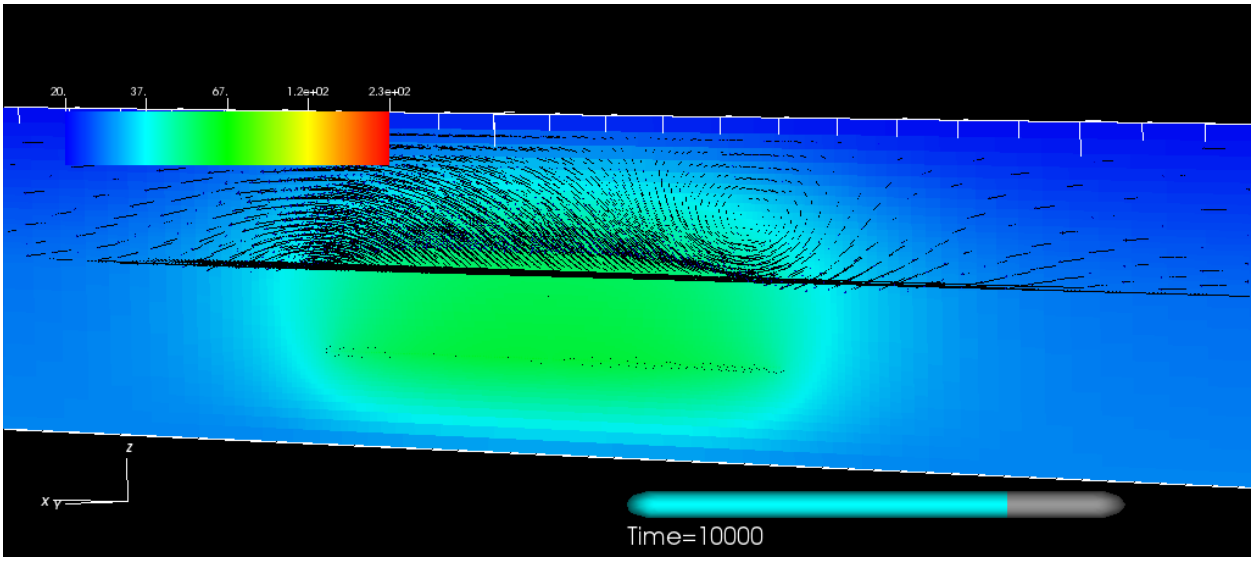

d)

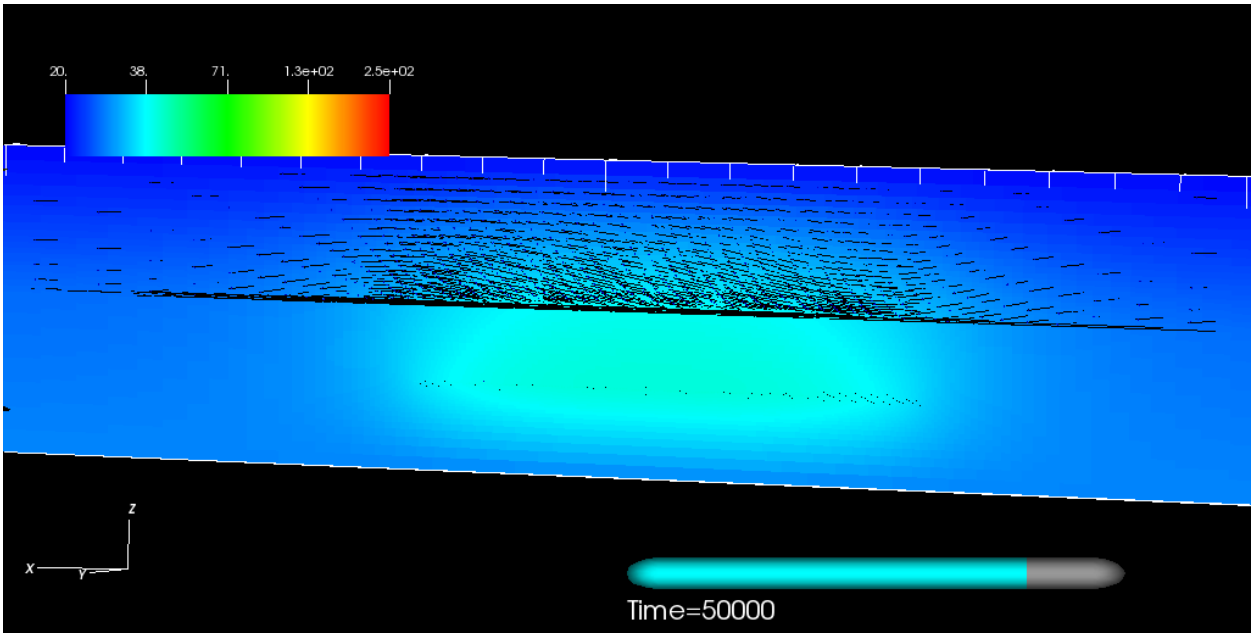

Figure 4-17c,d. Fluid Velocity Vector Field (m/yr) and Temperature Field (on a scale of 20°C to 230°C) at Various Times for the Deterministic *Thermal* Generic Salt Repository Domain.

c) At 10,000 years

d) At 50,000 years

e)

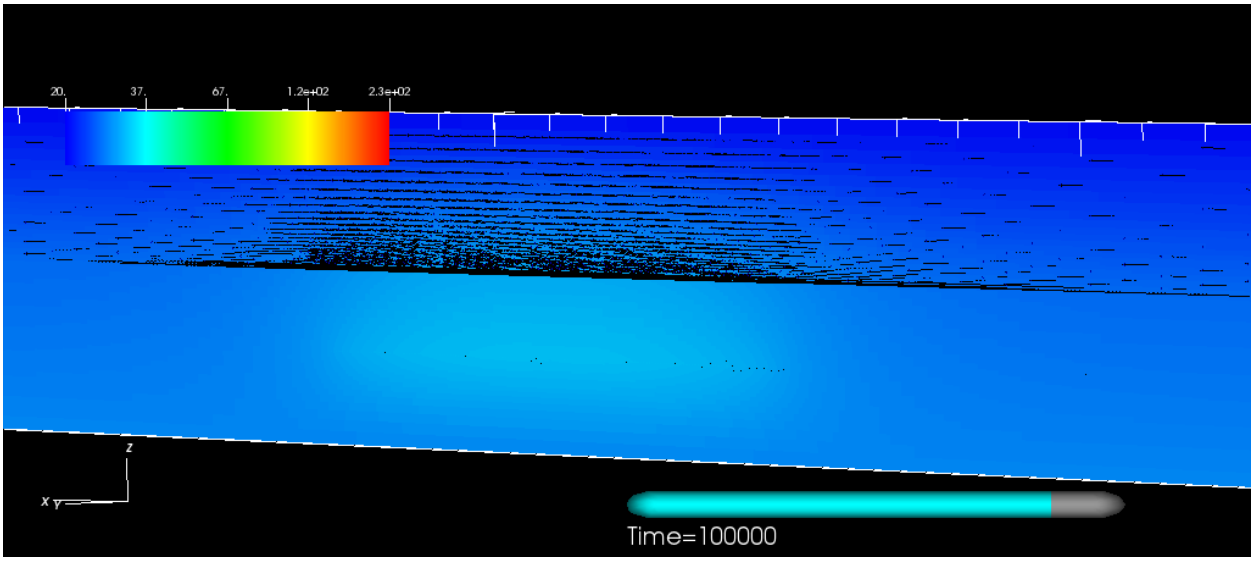

f)

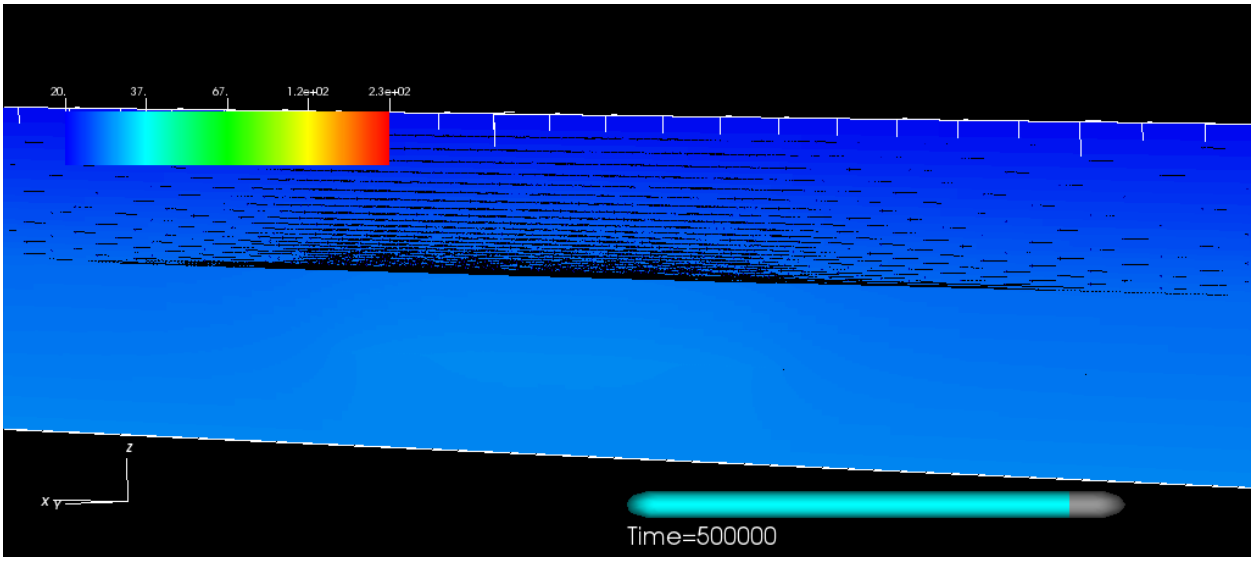

Figure 4-17e,f. Fluid Velocity Vector Field (m/yr) and Temperature Field (on a scale of 20°C to 230°C) at Various Times for the Deterministic *Thermal* Generic Salt Repository Domain.

e) At 100,000 years

f) At 500,000 years

a)

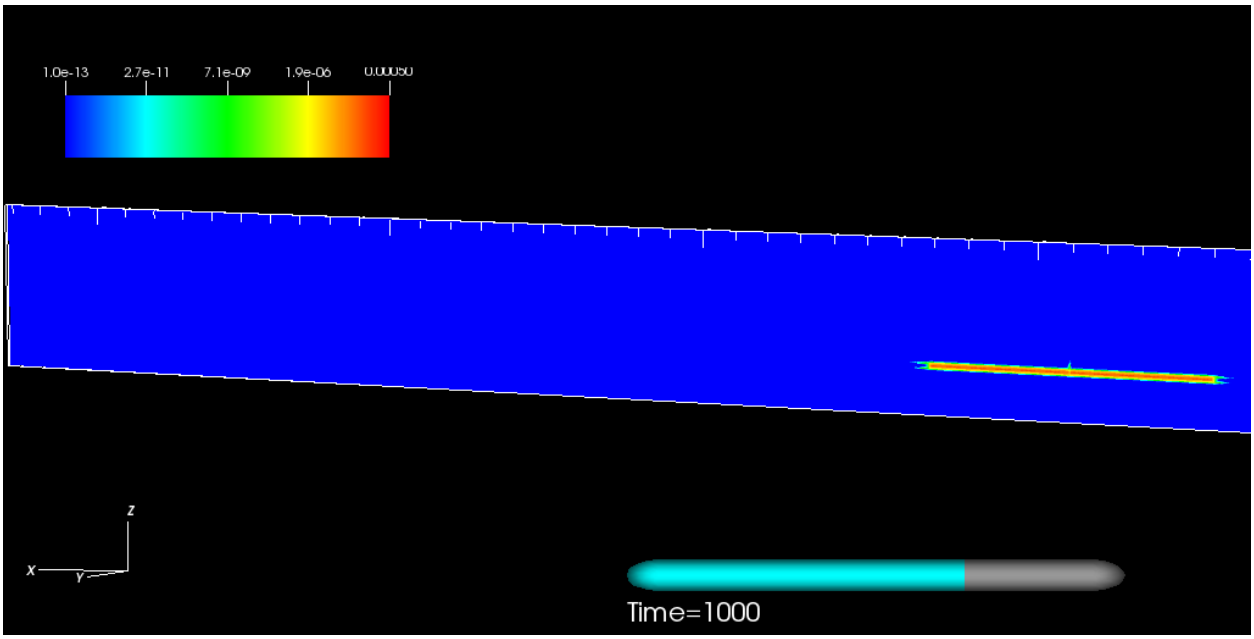

b)

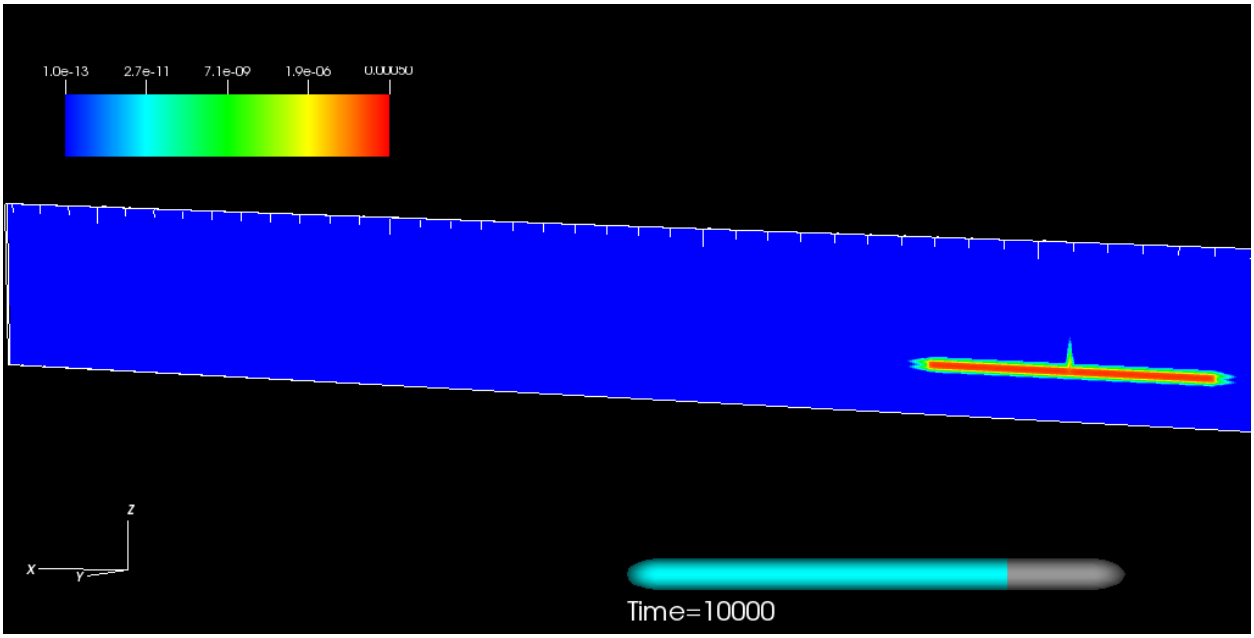

Figure 4-18a,b. ^{129}I Dissolved Concentration at Specified Times for the Deterministic *Thermal* Generic Salt Repository Simulation.

a) Time = 1000 years, b) Time = 10,000 years

c)

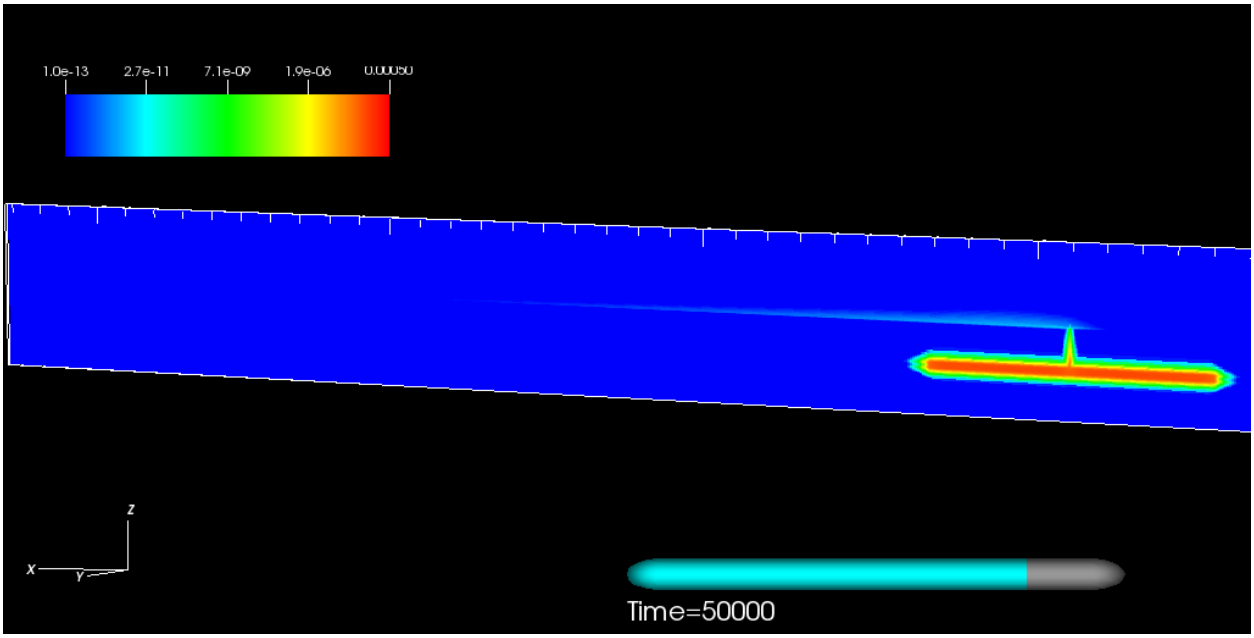

d)

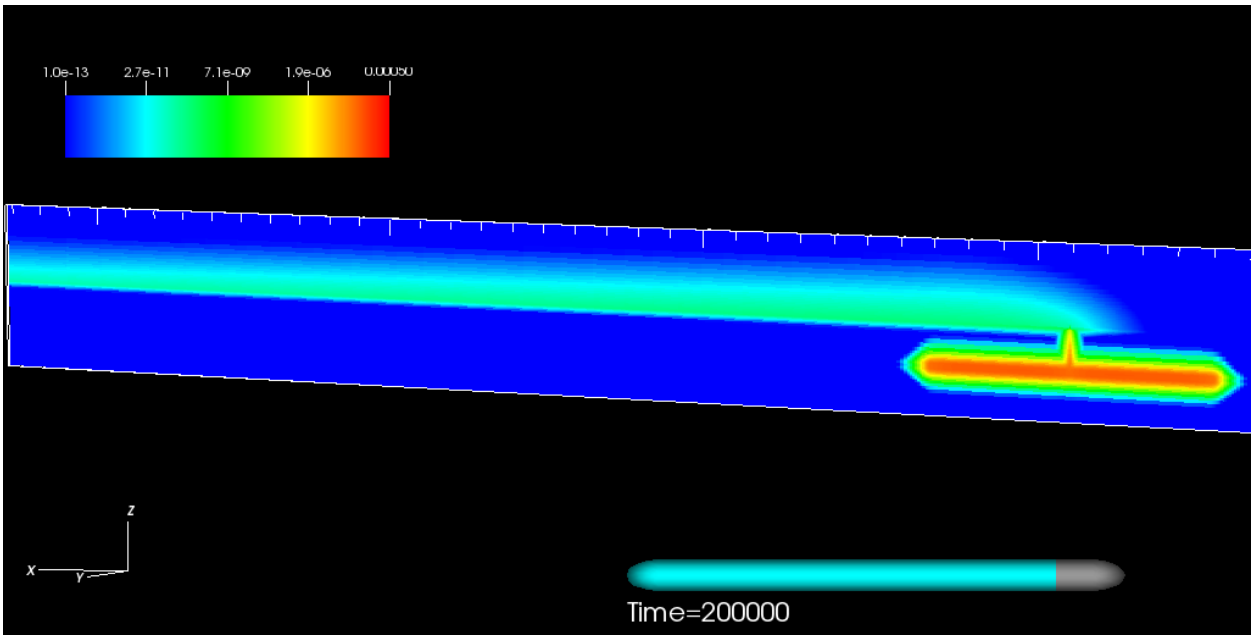

Figure 4-18c,d. ^{129}I Dissolved Concentration at Specified Times for the Deterministic *Thermal* Generic Salt Repository Simulation.

c) Time = 50,000 years, d) Time = 200,000 years

e)

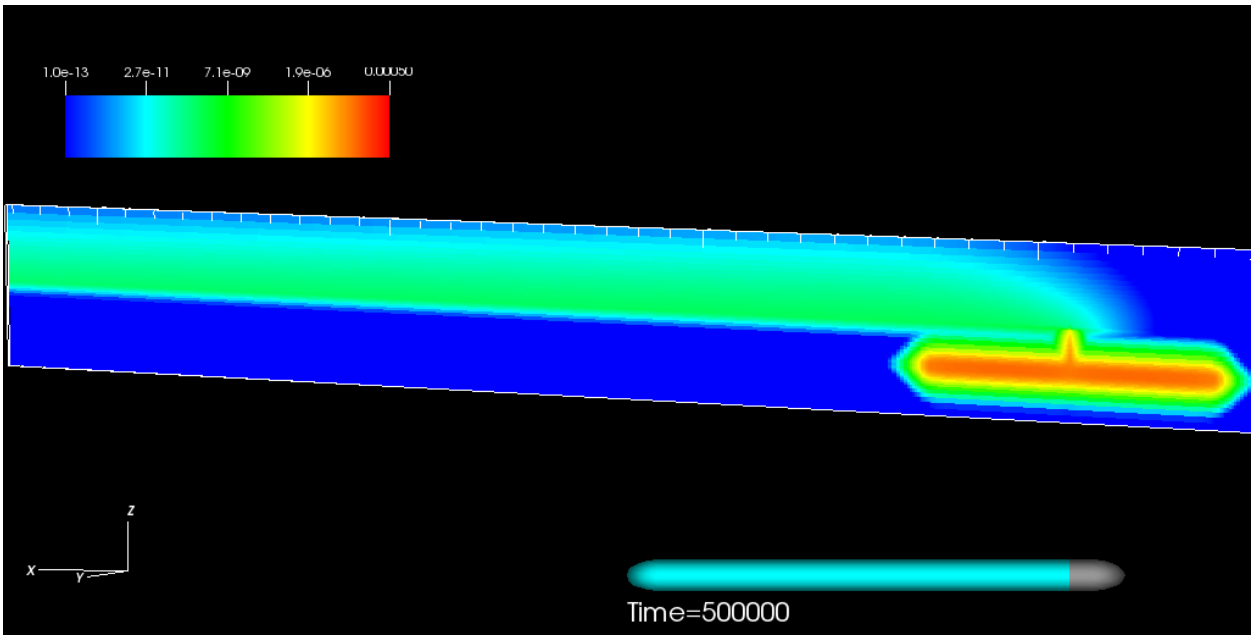

f)

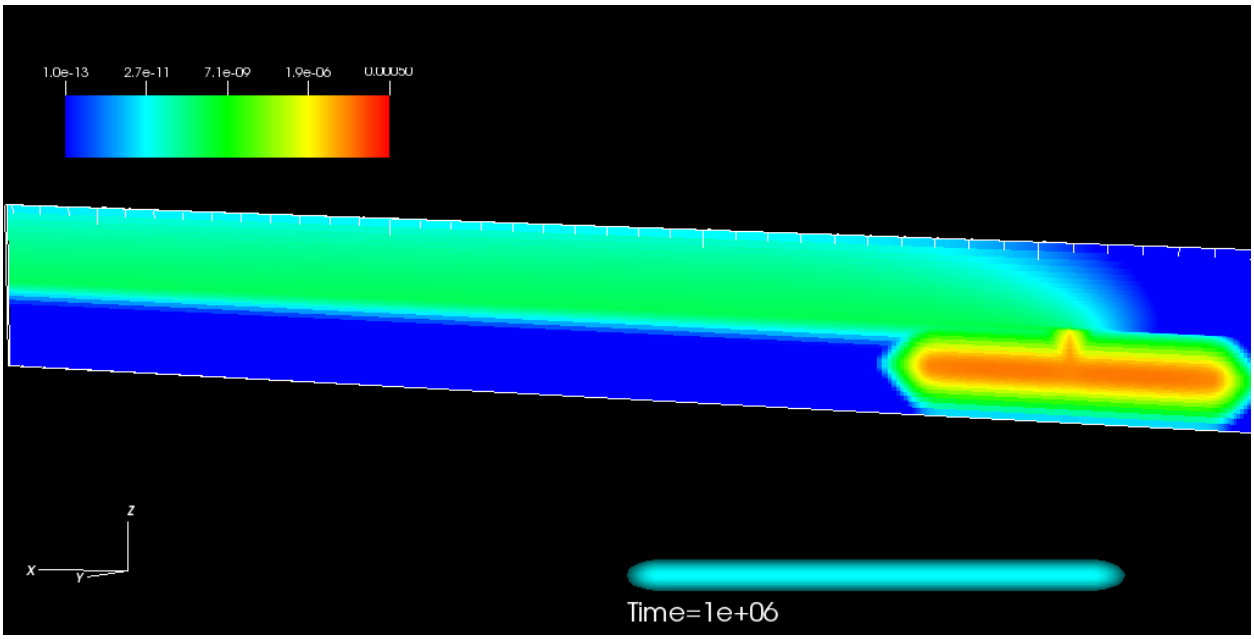

Figure 4-18e,f. ^{129}I Dissolved Concentration at Specified Times for the Deterministic *Thermal* Generic Salt Repository Simulation.
e) Time = 500,000 years, f) Time = 1,000,000 years

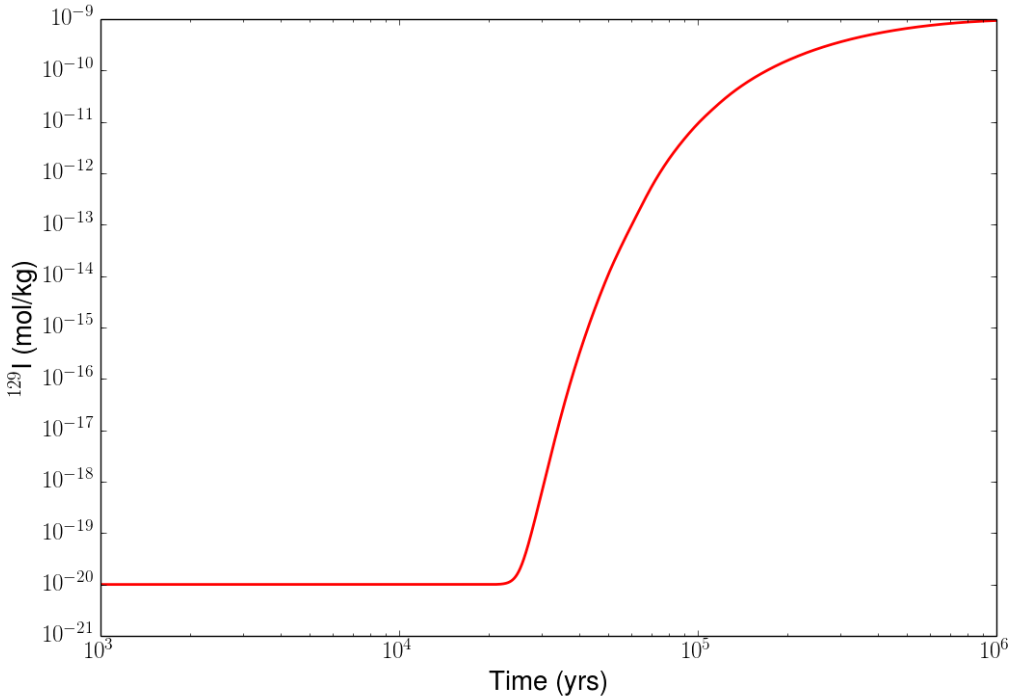

Figure 4-19. ^{129}I Dissolved Concentration in Aquifer at x = 11,600 m for the Deterministic *Thermal* Generic Salt Repository Simulation.

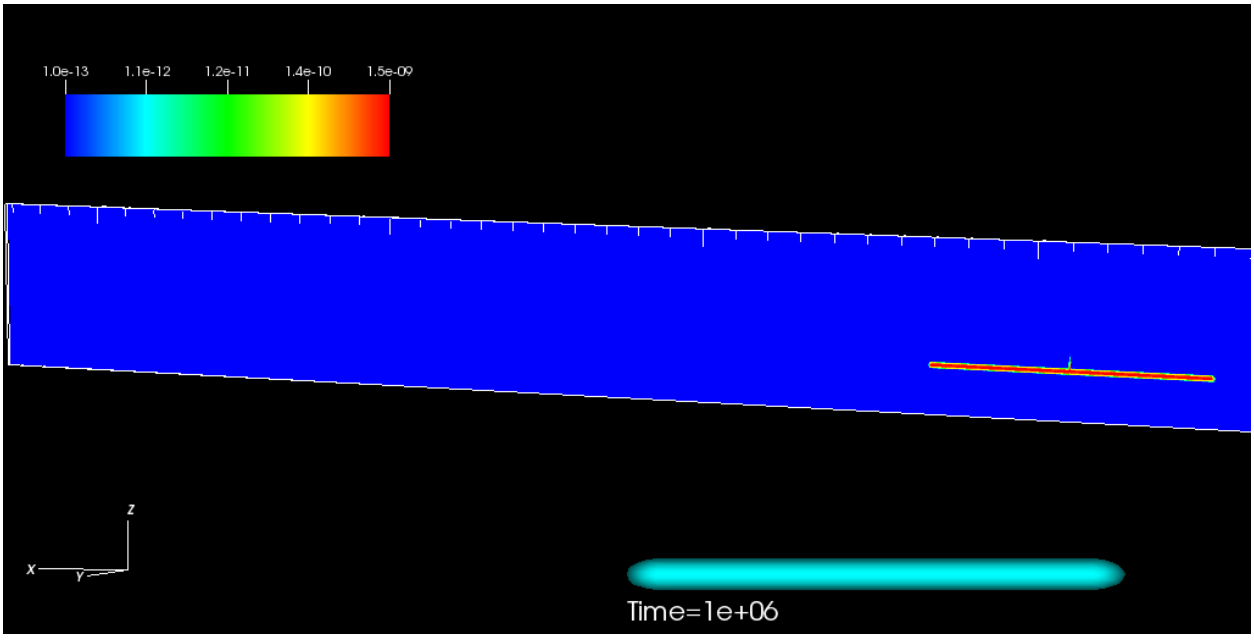

Figure 4-20. ^{237}Np Dissolved Concentration at 1,000,000 years for the Deterministic *Thermal* Generic Salt Repository Simulation.

4.5 Probabilistic Thermal Simulation Results

Probabilistic *thermal* simulations of the salt repository demonstration problem were carried out to test the coupled TH process capabilities of the GDSA framework. Fifty realizations were run, with parameter sampling (using Latin Hypercube Sampling (LHS)) and sensitivity analyses performed using DAKOTA. The ten parameters selected for sampling are shown above in Table 4-4. Thermal simulations, in general, run somewhat longer than the isothermal case described in Sections 4.2 and 4.3 because the coupled processes result in stiffer equations that require smaller timesteps for some of the realizations.

Horsetail plots of ^{129}I concentration (molal) versus time are provided in Figure 4-21. Corresponding bar charts of the partial rank correlation coefficients (PRCCs) are provided in Figure 4-22. The analysis in Section 4.3 for the probabilistic isothermal case is applicable to this thermal simulation, as well, because of the small effect of the thermal pulse on radionuclide transport, as previously discussed in Section 4.4 with regard to the deterministic thermal case. A few subtle differences can be noticed but nothing of importance, except at the "Anhydrite Mid-x" observation point where about 6 of the 50 realizations show nearly immediate breakthrough in the thermal case (Fig. 4-21e) but quite delayed breakthrough in the isothermal case (Fig. 4-12e). This can be explained by examining the early-time fluid flux vectors for the deterministic thermal case (Figs. 4-16 and 4-17a), which show the high early advective flux around the aquifer due to thermal expansion of the fluid. For some of the random samples of the anhydrite permeability distribution near the upper end of its range (Table 4-4), the advective flux in the anhydrite beds is high enough at early times (due to the thermal driving force) to cause rapid transport of the fast release fraction of ^{129}I to the "Anhydrite-Mid-x" location. At least three of these high permeability samples are also noticeable in Figure 4-12e as the three earliest breakthrough curves in that figure.

As in the isothermal case, one set of scatterplots is shown (Figure 4-23), for the aquifer monitor well location. They show similar trends to that shown in Figure 4-14 for the isothermal case.

a)

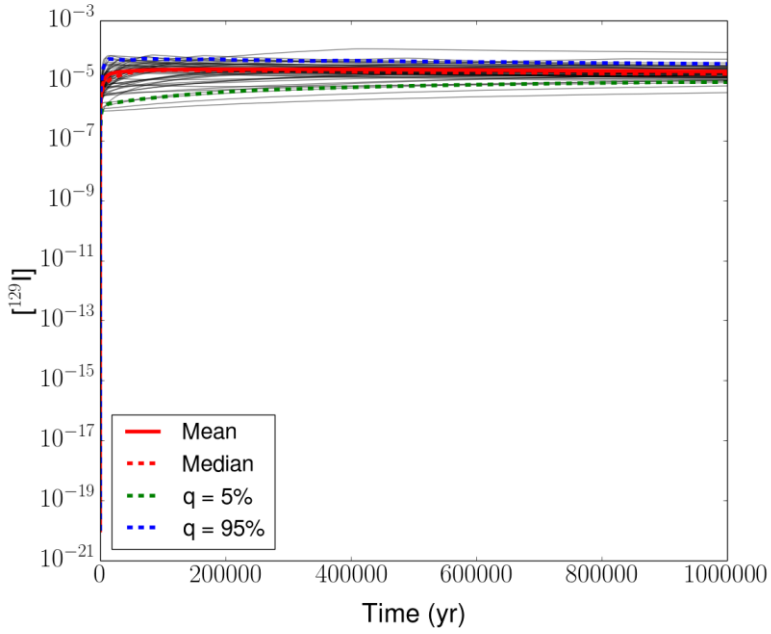

b)

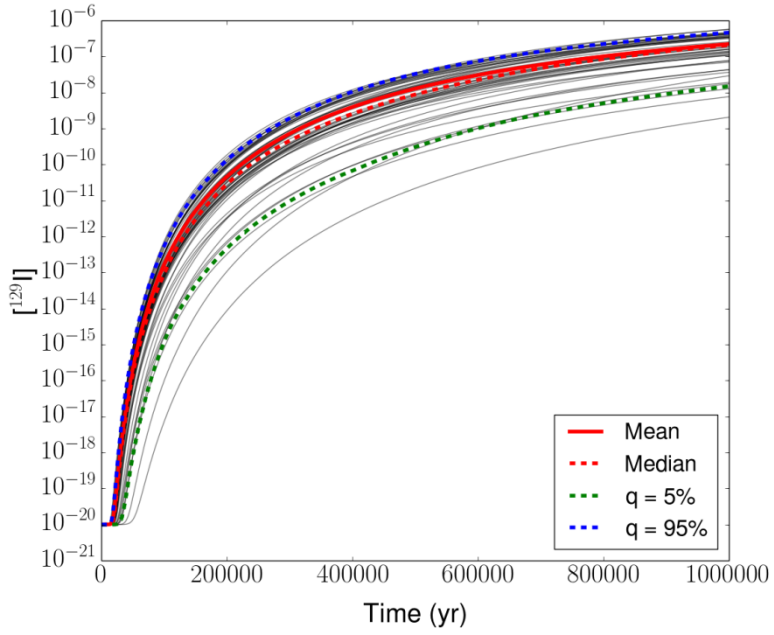

Figure 4-21a,b. Horsetail Plot of ^{129}I Dissolved Concentration at Various Observation Points for the Probabilistic *Thermal* Generic Salt Repository Simulation.

a) "Anhydrite Near": x = 6212 m, y = 10 m, z = 279.5 m

b) "Halite Near": x = 6212 m, y = 10 m, z = 375 m

c)

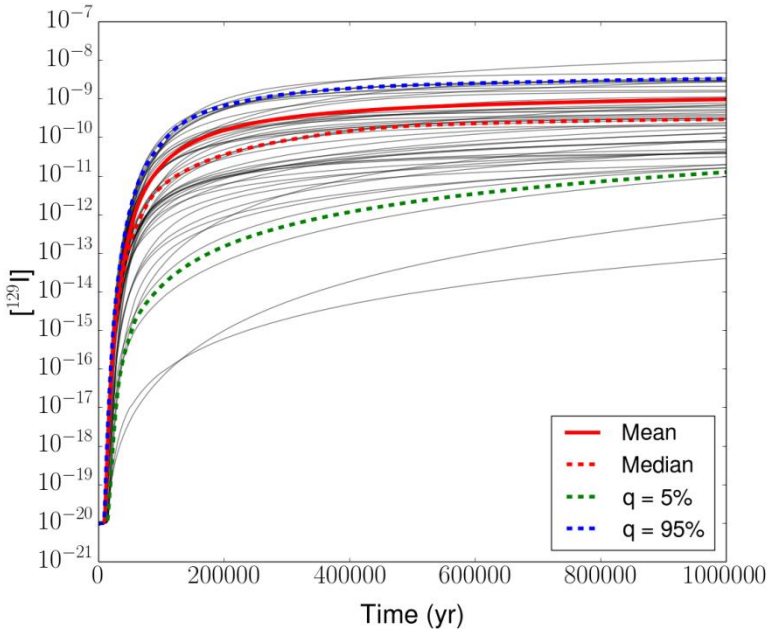

d)

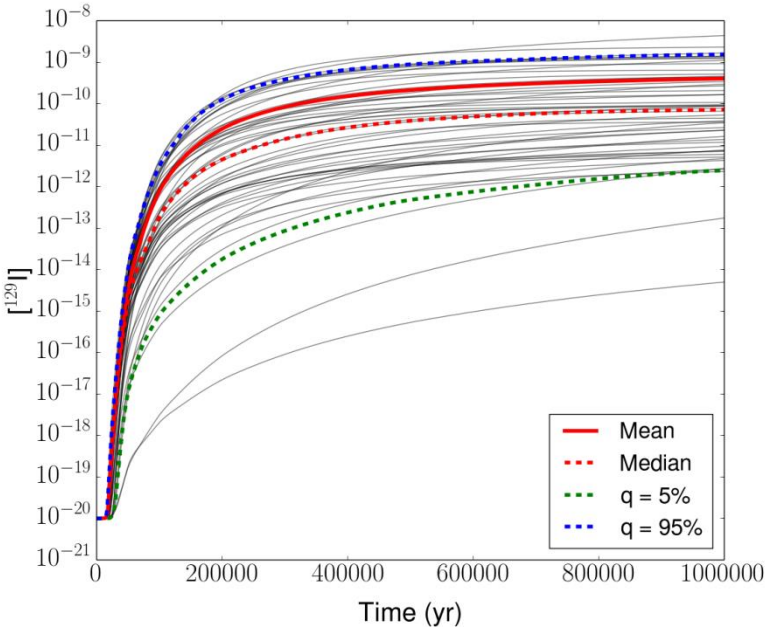

Figure 4-21c,d. Horsetail Plot of ^{129}I Dissolved Concentration at Various Observation Points for the Probabilistic *Thermal* Generic Salt Repository Simulation.

c) "Aquifer Near": x = 6212 m, y = 10 m, z = 502.5 m

d) "Sediments Near": x = 6212 m, y = 10 m, z = 600 m

e)

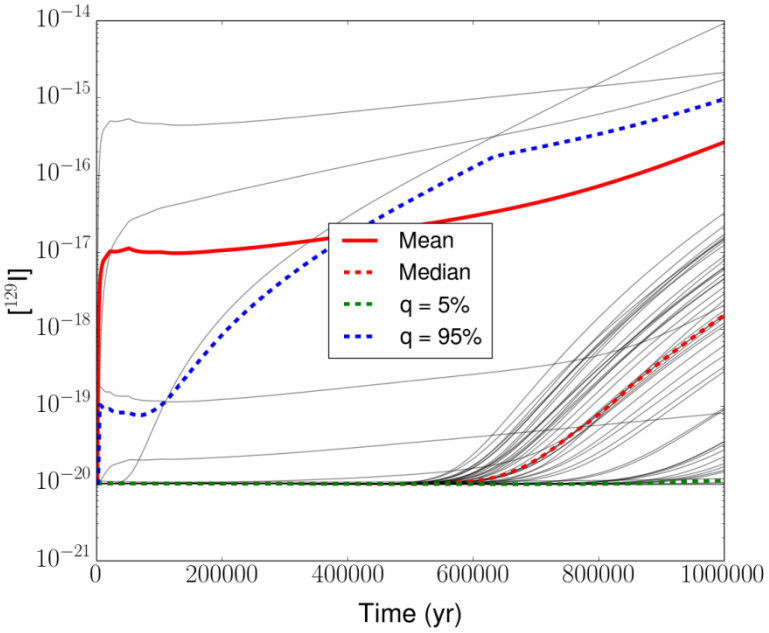

f)

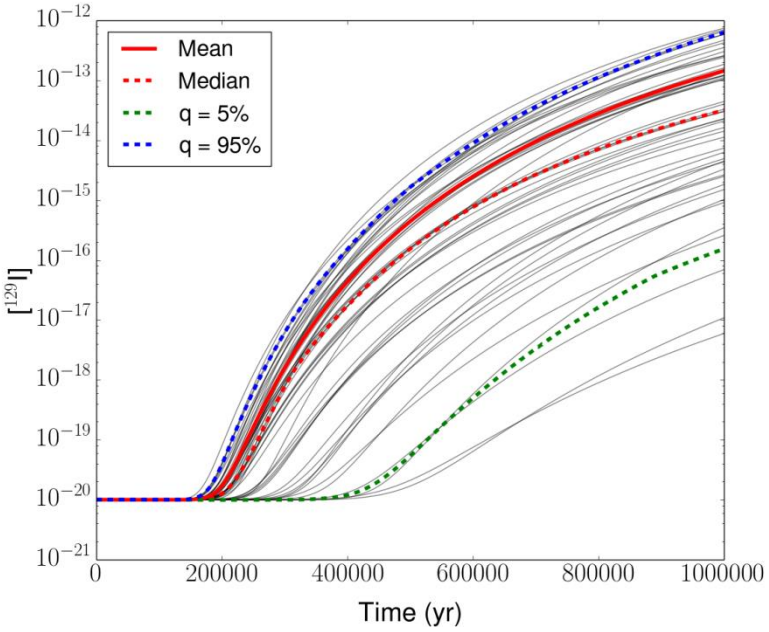

Figure 4-21e,f. Horsetail Plot of ^{129}I Dissolved Concentration at Various Observation Points for the Probabilistic *Thermal* Generic Salt Repository Simulation.

e) "Anhydrite Mid-x": x = 7500 m, y = 10 m, z = 279.5 m

f) "Halite Mid-x": x = 7500 m, y = 10 m, z = 375 m

g)

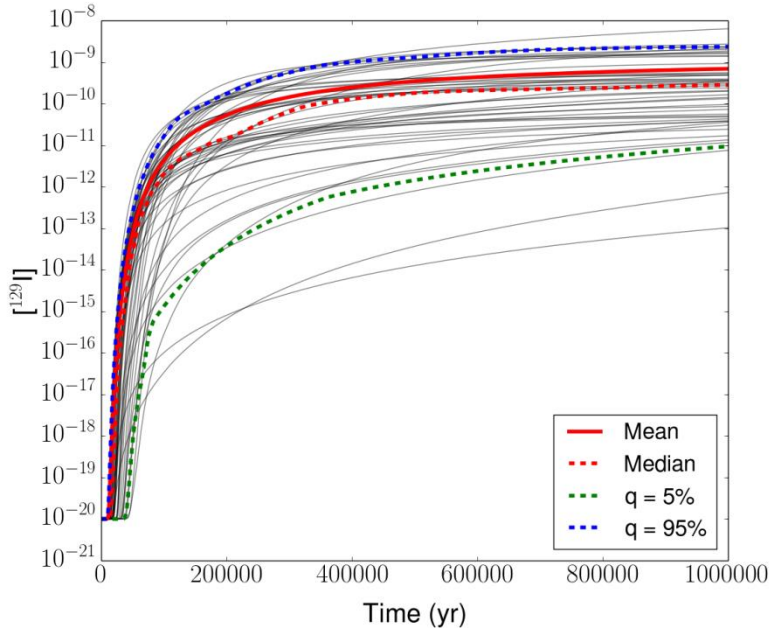

h)

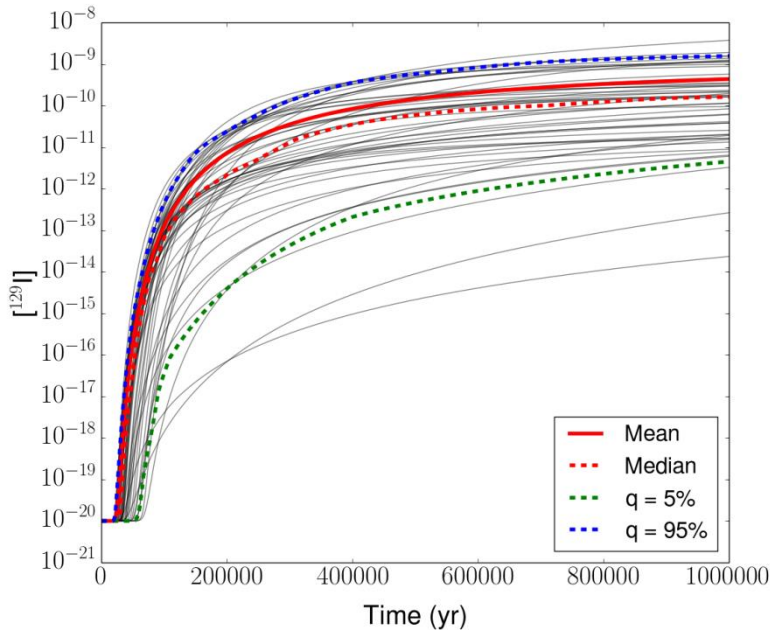

Figure 4-21g,h. Horsetail Plot of ^{129}I Dissolved Concentration at Various Observation Points for the Probabilistic *Thermal* Generic Salt Repository Simulation.

g) "Aquifer Mid-x": x = 7500 m, y = 10 m, z = 502.5 m

h) "Sediments Mid-x": x = 7500 m, y = 10 m, z = 600 m

i)

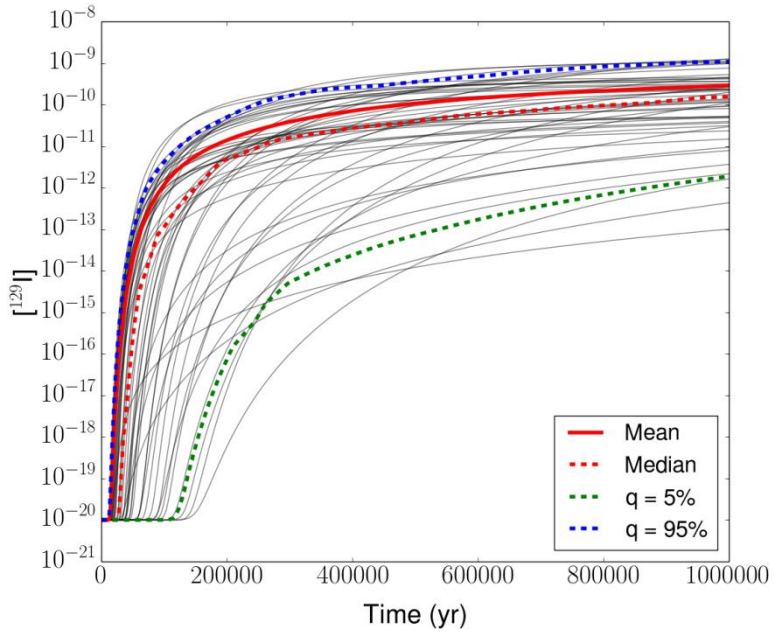

Figure 4-21i. Horsetail Plot of ^{129}I Dissolved Concentration at Various Observation Points for the Probabilistic *Thermal* Generic Salt Repository Simulation.

i) Aquifer monitor well location: x = 11,600 m, y = 10 m, z = 502.5 m

a)

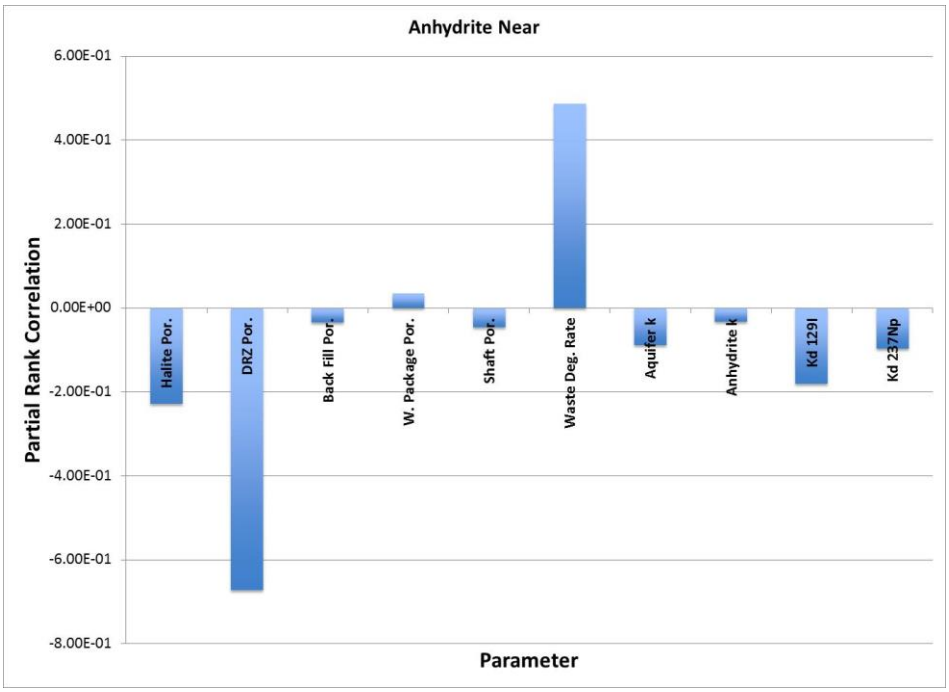

b)

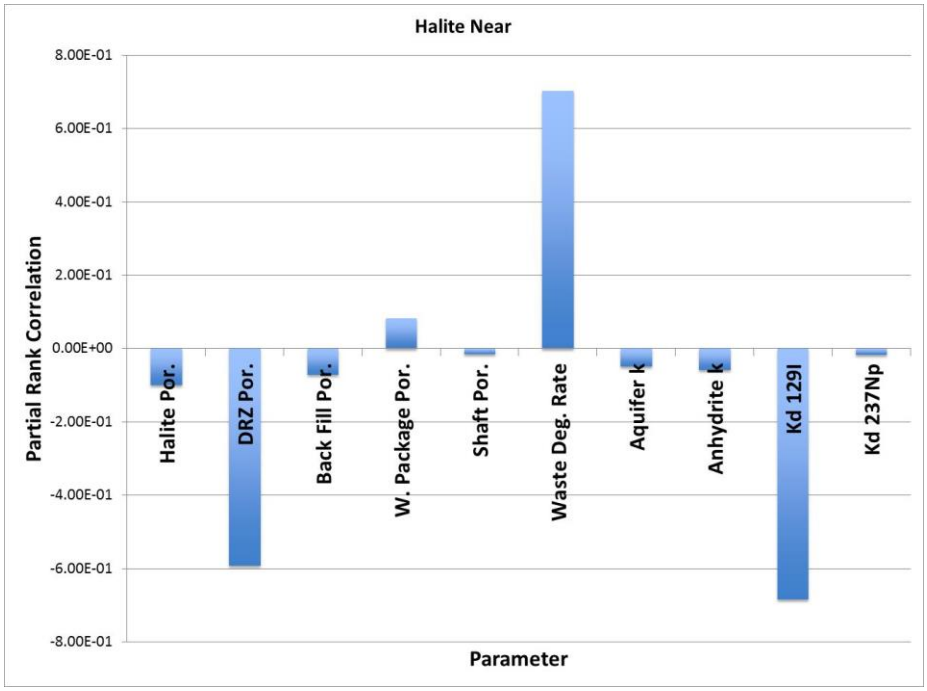

Figure 4-22a,b. Partial Rank Correlation Coefficients for ^{129}I Dissolved Concentration versus Sampled Parameters for the Probabilistic *Thermal* Generic Salt Repository Simulation.

a) "Anhydrite Near": x = 6212 m, y = 10 m, z = 279.5 m

b) "Halite Near": x = 6212 m, y = 10 m, z = 375 m

c)

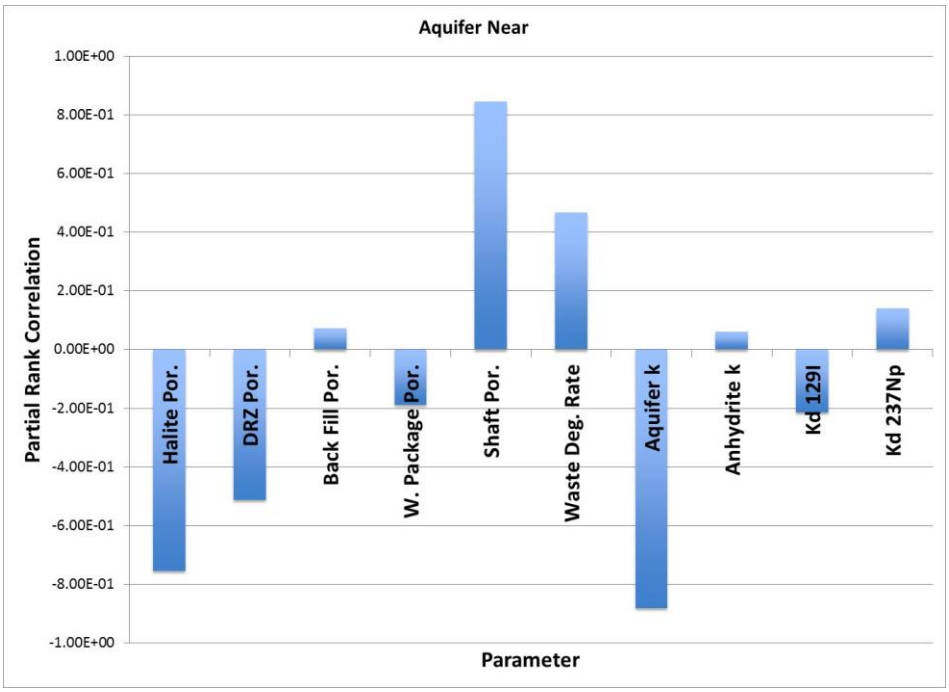

d)

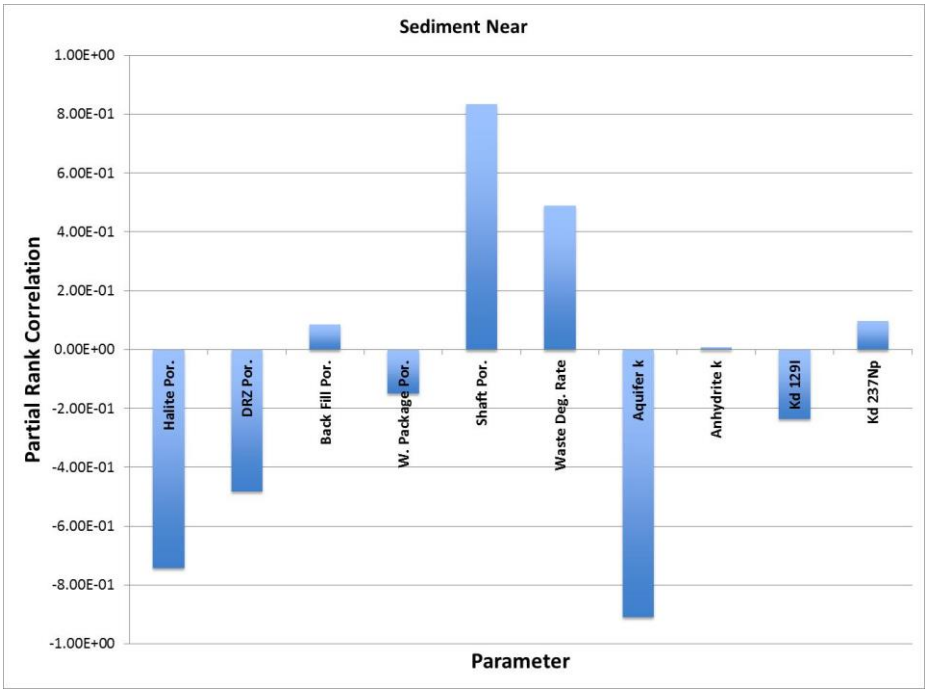

Figure 4-22c,d. Partial Rank Correlation Coefficients for ^{129}I Dissolved Concentration versus Sampled Parameters for the Probabilistic *Thermal* Generic Salt Repository Simulation.

c) "Aquifer Near": x = 6212 m, y = 10 m, z = 502.5 m

d) "Sediments Near": x = 6212 m, y = 10 m, z = 600 m

e)

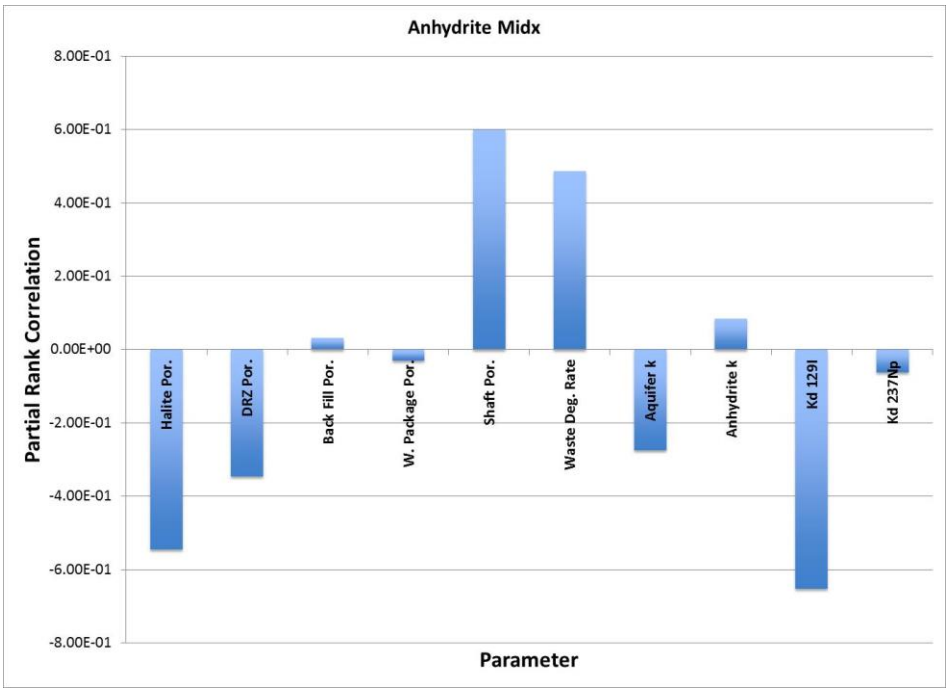

f)

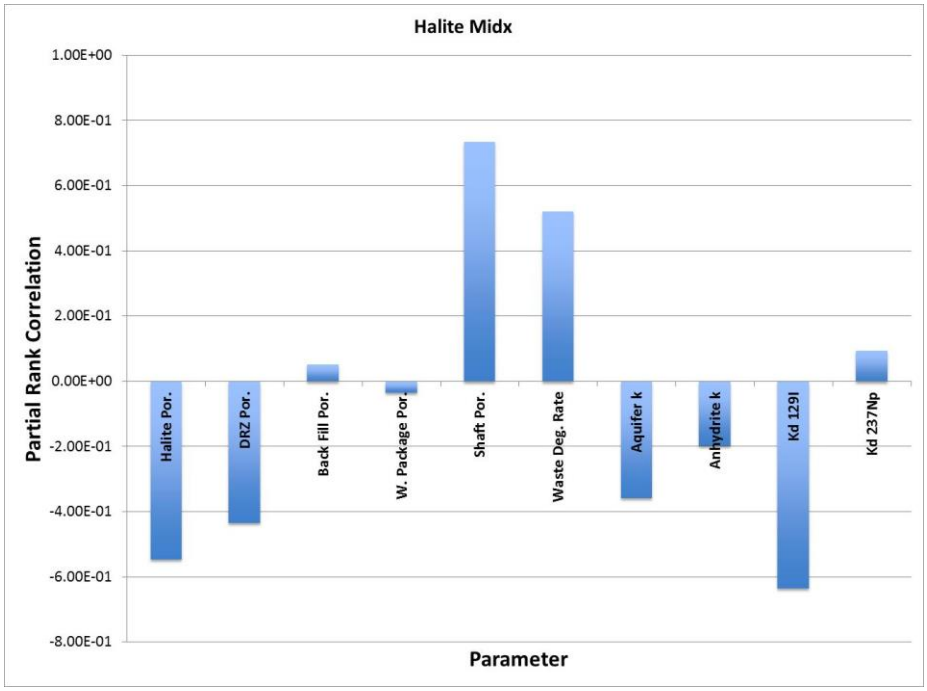

Figure 4-22e,f. Partial Rank Correlation Coefficients for ^{129}I Dissolved Concentration versus Sampled Parameters for the Probabilistic *Thermal* Generic Salt Repository Simulation.

e) "Anhydrite Mid-x": x = 7500 m, y = 10 m, z = 279.5 m

f) "Halite Mid-x": x = 7500 m, y = 10 m, z = 375 m

g)

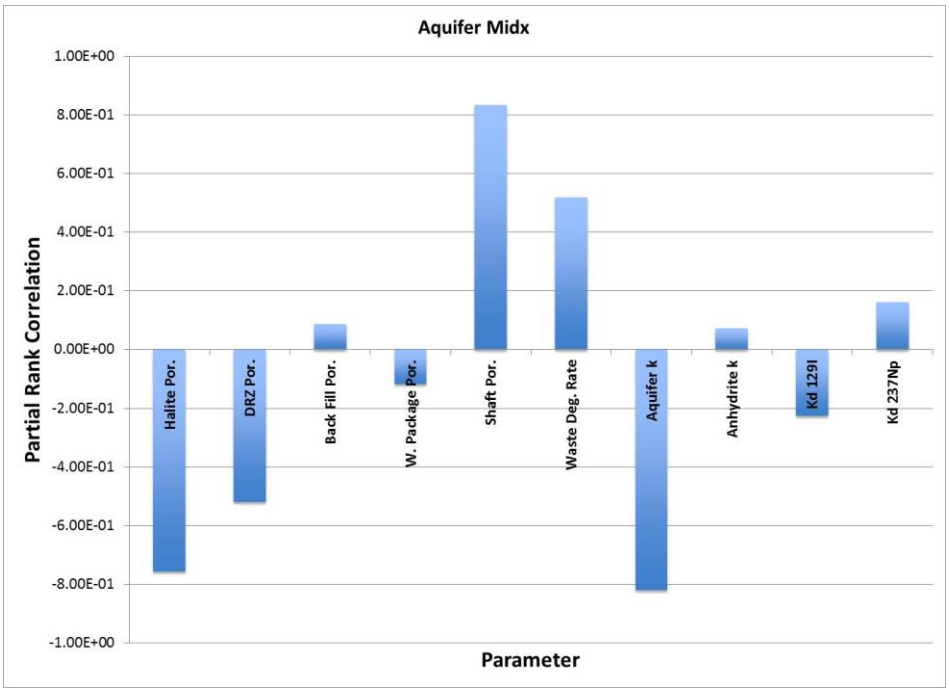

h)

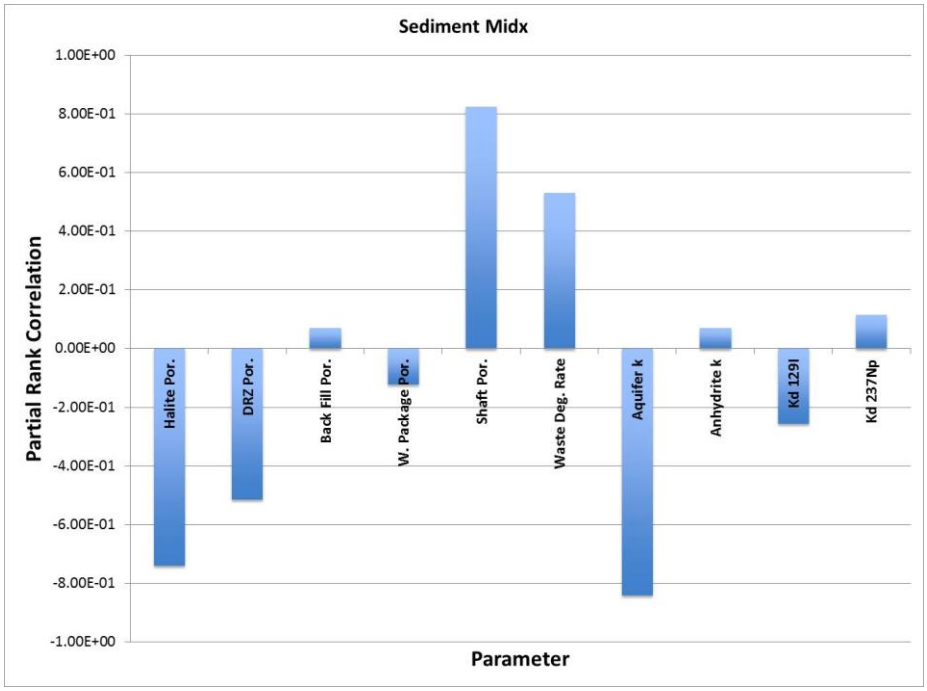

Figure 4-22g,h. Partial Rank Correlation Coefficients for ^{129}I Dissolved Concentration versus Sampled Parameters for the Probabilistic *Thermal* Generic Salt Repository Simulation.

g) "Aquifer Mid-x": x = 7500 m, y = 10 m, z = 502.5 m

h) "Sediments Mid-x": x = 7500 m, y = 10 m, z = 600 m

i)

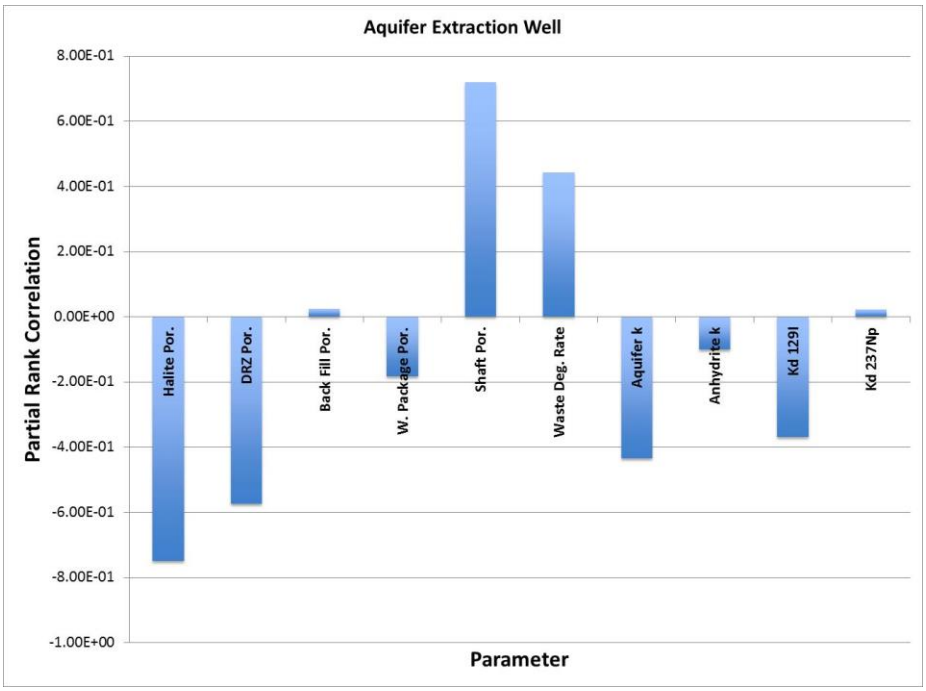

Figure 4-22i. Partial Rank Correlation Coefficients for ^{129}I Dissolved Concentration versus Sampled Parameters for the Probabilistic *Thermal* Generic Salt Repository Simulation.

i) Aquifer monitor well location: x = 11,600 m, y = 10 m, z = 502.5 m

a)

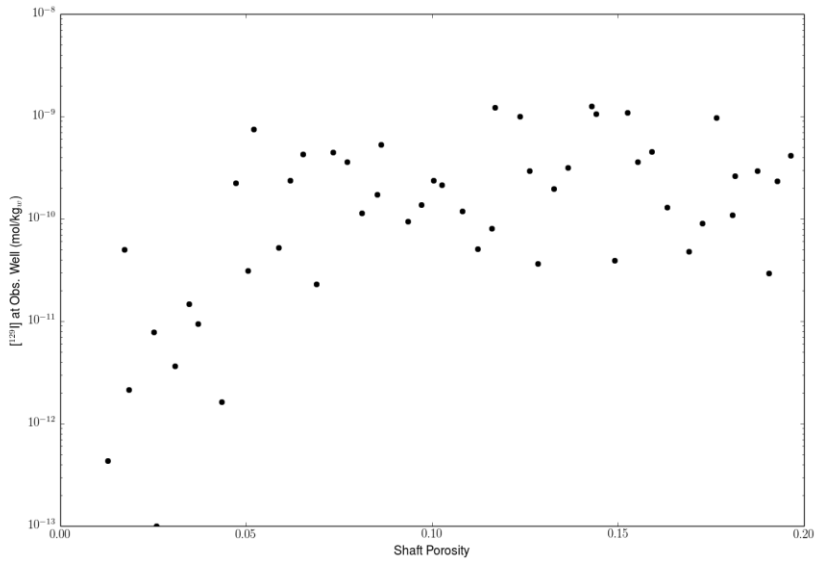

b)

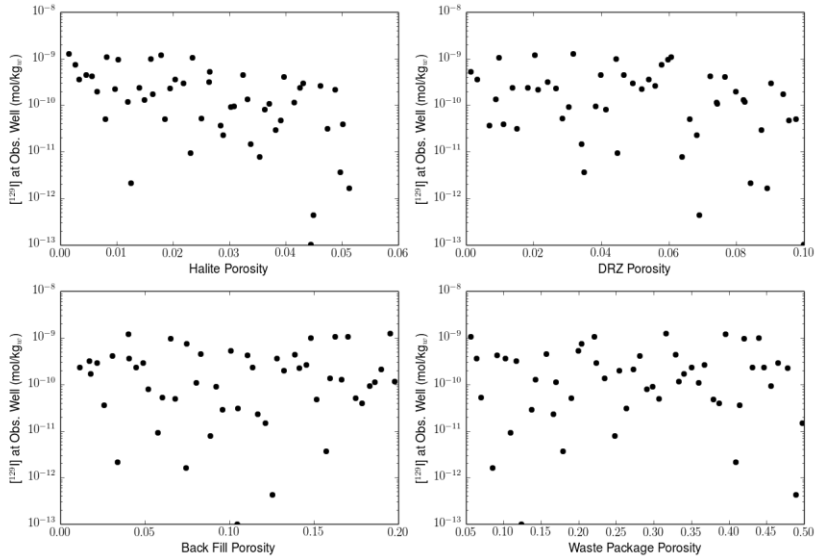

Figure 4-23a,b. Scatterplots for Maximum ^{129}I Dissolved Concentration versus Sampled Parameters for the Probabilistic *Thermal* Generic Salt Repository Simulation, at the "Aquifer Monitor Well" Observation Point.

a) ^{129}I vs. Shaft Porosity

b) ^{129}I vs. Halite Porosity; ^{129}I vs. DRZ Porosity; ^{129}I vs. Backfill Porosity; ^{129}I vs. Waste Package Porosity

c)

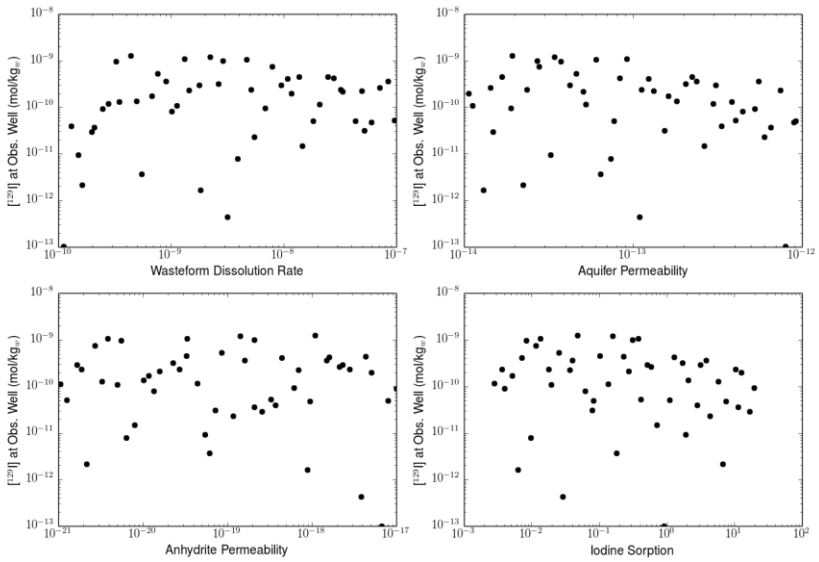

Figure 4-23c. Scatterplots for Maximum ^{129}I Dissolved Concentration versus Sampled Parameters for the Probabilistic *Thermal* Generic Salt Repository Simulation, at the "Aquifer Monitor Well" Observation Point.

c) ^{129}I vs. WF Dissolution Rate; ^{129}I vs. Aquifer *k*; ^{129}I vs. Anhydrite *k*; ^{129}I vs. Iodine K_d

5. SUMMARY AND CONCLUSIONS

This report describes specific activities in FY2014 toward the development of an enhanced generic disposal system modeling and analysis capability that utilizes high-performance computing (HPC) environments to simulate important multi-physics phenomena and couplings associated with the potential behavior of a geologic repository for UNF and HLW. This new Generic Disposal System Analysis (GDSA) Framework employs the HPC-capable PFLOTRAN multi-physics code (Hammond et al. 2014) to support the evaluation of repository and subsystem performance in the presence of coupled thermal-hydrologic-chemical processes, and the HPC-capable uncertainty sampling and propagation code DAKOTA (Adams et al. 2013a) for sensitivity analysis and multi-realization performance assessment, over a range of disposal options (e.g., salt, granite, clay, and deep borehole disposal).

In 2014 enhancements were made to the GDSA Framework process model capabilities, including the addition and testing of (1) a new multiphase fluid and heat flow process model, (2) dispersive transport through the addition of a diagonal hydrodynamic dispersion tensor, (3) a soil matrix compressibility model, (4) a hydrogen gas generation source term computed as a function of Fe corrosion and microbial degradation organics in waste packages, (5) generalization of sorption through isotherms, (6) on-the-fly swappable constitutive relations (i.e. gas and liquid equations of state, etc.), and (7) increasingly flexible radioactive decay and ingrowth within the aqueous and sorbed phases. This enhanced performance assessment (PA) modeling capability is demonstrated in FY2014 with deterministic and probabilistic simulations of a generic repository in bedded salt host rock, by comparisons of repository performance between a case with heat-generating waste (“thermal” case) and a case without heat generation (“isothermal” case). The simulation results provide preliminary insights into the multi-physics processes and couplings for the long-term behavior of a generic reference-case salt repository, but require additional refinement before being used as a definitive guide for future R&D. These preliminary results indicate that the effect of heat on radionuclide transport to the biosphere is likely not significant in a bedded salt repository, if only TH couplings are considered. However, the impact of THC, THM, and THMC coupling has not been investigated and may have important effects on transport pathways and behavior for the nominal scenario. Also, disturbed scenarios still require investigation with the GDSA Framework. (There are some effects on transport in some rock units for certain random samplings of the parameters in the multi-realization thermal (TH) case.)

In addition to the enhanced GDSA Framework capabilities and the expanded demonstration for the generic salt repository (Section 4), the salt repository reference case (Freeze et al. 2013a) was further revised in FY 2014 to include additional details (Section 3), and the reference cases for generic granite and clay/shale repositories were further advanced in FY 2014, as reported in Painter et al. (2014) and Wang et al. (2014) for granite, and Zheng et al. (2014) and Jove-Colon et al. (2014) for clay/shale.

The application of an HPC-capable GDSA Framework is a significant advancement in PA modeling capability in that it allows the important multi-physics couplings to be represented directly, rather than through simplified abstractions. It also allows for more complex representations of the source term.

Planned improvements to the GDSA Framework in FY 2015 include (1) a new capability to allow for decay of isotopes in the solid phase and equilibrium partitioning of decayed isotopes across the aqueous, mineral, and sorbed phases, (2) incorporation of updated subsystem models

into the GDSA Framework, such as the Mixed Potential UNF degradation model (Jerden et al. 2014), (3) updates to reference cases, and (4) demonstration of the GDSA Framework for other media besides salt, such as argillite.

6. REFERENCES

Adams, B.M., M.S. Ebeida, M.S. Eldred, J.D. Jakeman, L.P. Swiler, W.J. Bohnhoff, K.R. Dalbey, J.P. Eddy, K.T. Hu, D.M. Vigil, L.E. Baumann, and P.D. Hough 2013a. *Dakota, a Multilevel Parallel Object-Oriented Framework for Design Optimization, Parameter Estimation, Uncertainty Quantification, and Sensitivity Analysis, Version 5.3.1+ User's Manual.* SAND2010-2183, Updated May 22, 2013. Sandia National Laboratories, Albuquerque, NM. (http://dakota.sandia.gov/)

Adams, B.M., M.S. Ebeida, M.S. Eldred, J.D. Jakeman, L.P. Swiler, W.J. Bohnhoff, K.R. Dalbey, J.P. Eddy, K.T. Hu, D.M. Vigil, L.E. Baumann, and P.D. Hough 2013b. *Dakota, a Multilevel Parallel Object-Oriented Framework for Design Optimization, Parameter Estimation, Uncertainty Quantification, and Sensitivity Analysis, Version 5.3.1+ Theory Manual.* SAND2011-9106, Updated May 22, 2013. Sandia National Laboratories, Albuquerque, NM. (http://dakota.sandia.gov/)

Balay S., J. Brown, K. Buschelman, V. Eijkhout, W.D. Gropp, D. Kaushik, M.G. Knepley, L. Curfman McInnes, B.F. Smith and H. Zhang 2013. *PETSc Users Manual*, ANL-95/11 – Revision 3.4, Argonne National Laboratory, Argonne IL.

Carter, J. T., A. J. Luptak, J. Gastelum, C. Stockman, and A. Miller 2012. *Fuel Cycle Potential Waste Inventory for Disposition*. FCRD-USED-2010-000031, Rev. 5. U.S. Department of Energy, Office of Used Nuclear Fuel Disposition, Washington, DC.

Chen, X., H. Murakami, M. Hahn, G.E. Hammond, M.L. Rockhold, J.M. Zachara and Y. Rubin 2012. "Three-Dimensional Bayesian Geostatistical Aquifer Characterization at the Hanford 300 Area using Tracer Test Data", *Water Resources Research*, 48, doi:10.1029/2011WR010675.

Chen, X., G. Hammond, C. Murray, M. Rockhold, V. Vermeul and J. Zachara 2013. "Applications of Ensemble-based Data Assimilation Techniques for Aquifer Characterization using Tracer Data at Hanford 300 Area", *Water Resources Research*, 49, doi:10.1002/2012WR013285.

Clayton, D.J., and C.W. Gable 2009. *3-D Thermal Analyses of High-Level Waste Emplaced in a Generic Salt Repository*. AFCI-WAST-PMO-MI-DV-2009 000002. February, 2009.

Clayton, D., G. Freeze, T. Hadgu, E. Hardin, J. Lee, J. Prouty, R. Rogers, W.M. Nutt, J. Birkholzer, H.H. Liu, L. Zheng, and S. Chu 2011. *Generic Disposal System Modeling – Fiscal Year 2011 Progress Report.* FCRD-USED-2011-000184, SAND2011-5828P. U.S. Department of Energy, Office of Nuclear Energy, Used Fuel Disposition Campaign, Washington, DC.

DOE (U.S. Department of Energy) 1996. *Title 40 CFR Part 191 Compliance Certification Application for the Waste Isolation Pilot Plant.* DOE/CAO-1996-2184 (21 volumes). U.S. Department of Energy, Carlsbad Area Office, Carlsbad, NM.
(http://www.wipp.energy.gov/library/CRA/BaselineTool/Documents/Appendices/SEAL%20A.PDF)

DOE (U.S. Department of Energy) 2008. *Yucca Mountain Repository License Application Safety Analysis Report.* DOE/RW-0573, Revision 1. U.S. Department of Energy, Washington, DC.
(http://www.nrc.gov/waste/hlw-disposal/yucca-lic-app/yucca-lic-app-safety-report.html#1)

DOE (U.S. Department of Energy) 2009. *Title 40 CFR Part 191 Subparts B and C Compliance Recertification Application for the Waste Isolation Pilot Plant*. DOE/WIPP 09-3424. U.S. Department of Energy, Carlsbad Area Office, Carlsbad, NM, http://www.wipp.energy.gov/library/CRA/2009_CRA/CRA/Appendix_SOTERM/Appendix_SOTERM.htm

Fluor (Fluor Technology Inc.) 1985. *Waste Package/Repository Impact Study: Final Report*. Battelle Memorial Institute, Office of Nuclear Waste Isolation, Columbus, OH. BMI/ONWI/C-312. September, 1985.

Fluor (Fluor Technology Inc.) 1986. Site Characterization Plan Conceptual Design Report for a High-Level Nuclear Waste Repository in Salt, Vertical Emplacement Mode. U.S. Department of Energy, Office of Civilian Radioactive Waste Management, Salt Repository Office. September, 1986.

Fox, B. 2008. *Parameter Summary Report for CRA-2009, Revision 0,* WIPP:1.2.5:PA:QA-L:547488, Sandia National Laboratories, Carlsbad, NM.

Freeze, R.A. and J.A. Cherry 1979. *Groundwater*, Prentice-Hall, Englewood Cliffs, NJ.

Freeze, G. and P. Vaughn 2012. *Development of an Advanced Performance Assessment Modeling Capability for Geologic Disposal of Nuclear Waste: Methodology and Requirements.* SAND2012-10208. Sandia National Laboratories, Albuquerque, NM.

Freeze, G., P. Gardner, P. Vaughn, S.D. Sevougian, P. Mariner, V. Mousseau, and G. Hammond 2013a. *Enhancements to Generic Disposal System Modeling Capabilities.* FCRD-UFD-2014-000062. SAND2013-10532P. Sandia National Laboratories, Albuquerque, NM.

Freeze, G., M. Voegele, P. Vaughn, J. Prouty, W.M. Nutt, E. Hardin, and S.D. Sevougian 2013b. *Generic Deep Geologic Disposal Safety Case.* FCRD-UFD-2012-000146 Rev. 1, SAND2013-0974P. Sandia National Laboratories, Albuquerque, NM.

Freeze, G., S.D. Sevougian, and M. Gross 2013c. *Safety Framework for Disposal of Heat-Generating Waste in Salt: Features, Events, and Processes (FEPs) Classification.* FCRD-UFD-2013-000191. SAND2013-5220P. Sandia National Laboratories, Albuquerque, NM.

Freeze, G., S. D. Sevougian, C. Leigh, M. Gross, J. Wolf, J. Mönig, and D. Buhmann 2014. "A New Approach for Feature, Event, and Process (FEP) Analysis of UNF/HLW Disposal – 14314," in *Proceedings of the WM2014 Conference*, March 2 – 6, 2014, Phoenix, Arizona USA.

Hammond, G., P. Lichtner, and C. Lu 2007. "Subsurface multiphase flow and multicomponent reactive transport modeling using high performance computing", in *Journal of Physics: Conference Series 78*, pp. 1-10.

Hammond, G.E., P.C. Lichtner, R.T. Mills, and C. Lu 2008. "Toward petascale computing in geosciences: application to the Hanford 300 Area", in *Journal of Physics Conference Series*, 125, 012051 doi:10.1088/1742-6596/125/1/012051.

Hammond, G.E. and P.C. Lichtner 2010. "Field-Scale Modeling for the Natural Attenuation of Uranium at the Hanford 300 Area using High Performance Computing", *Water Resources Research*, 46, W09527, doi:10.1029/2009WR008819.

Hammond, G.E., P.C. Lichtner and M.L. Rockhold 2011. "Stochastic Simulation of Uranium Migration at the Hanford 300 Area", *Journal of Contaminant Hydrology*, v120-121, pp. 115-128, doi:10.1016/j.jconhyd.2010.04.005.

Hammond, G.E., P.C. Lichtner and R.T. Mills 2014. "Evaluating the Performance of Parallel Subsurface Simulators: An Illustrative Example with PFLORAN", *Water Resources Research*, 50, doi:10.1002/2012WR013483.

Hardin, E., T. Hadgu, D. Clayton, R. Howard, H. Greenberg, J. Blink, M. Sharma, M. Sutton, J. Carter, M. Dupont, and P. Rodwell 2012. *Repository Reference Disposal Concepts and Thermal Load Management Analysis.* FCRD-UFD-2012-000219 Rev. 2. U.S. Department of Energy, Office of Used Nuclear Fuel Disposition, Washington, DC.

Hardin, E. L., D. J. Clayton, R. L. Howard, J. M. Scaglione, E. Pierce, K. Banerjee, M. D. Voegele, H. R. Greenberg, J. Wen, T. A. Buscheck, J. T. Carter, T. Severynse, and W. M. Nutt 2013. *Preliminary Report on Dual-Purpose Canister Disposal Alternatives (FY13)*. FCRD-UFD-2013-000171 Rev. 0, U.S. Department of Energy, Office of Used Nuclear Fuel Disposition, Washington, DC.

Jerden J., K. E. Frey, J. M. Copple, and W. Ebert 2014. *ANL Mixed Potential Model For Used Fuel Degradation: Application to Argillite and Crystalline Rock Environments*, FCRD-UFD-2014-000490, U.S. Department of Energy, Office of Used Nuclear Fuel Disposition, Washington, DC, July 14, 2014.

Jové Colón, C., L. Zheng, J. Houseworth, et al. 2014. *Evaluation of Used Fuel Disposition in Clay-Bearing Rock*, FCRD-UFD-2014-000056, U.S. Department of Energy, Office of Used Nuclear Fuel Disposition, Washington, DC.

Kienzler, B., M. Altmaier, C. Bube, and V. Metz 2012. *Radionuclide Source Term for HLW Glass, Spent Nuclear Fuel, and Compacted Hulls and End Pieces (CSD-C Waste)*, KIT Scientific Publishing, Report-Nr. KIT-SR 7624, Karlsruher Institut für Technologie (KIT), Straße am Forum 2, D-76131 Karlsruhe, www.ksp.kit.edu

Lake, Larry W. 1989. *Enhanced Oil Recovery*, Prentice-Hall, Englewood Cliffs, NJ 07632.

Lichtner, P.C. and G.E. Hammond. 2012a. "Using High Performance Computing to Understand Roles of Labile and Nonlabile U(VI) on Hanford 300 Area Plume Longevity", *Vadose Zone Journal*, v11, n2, doi:10.2136/vzj2011.0097.

Lichtner, P. C. 2014. *PFLOTRAN: Technical Design Documentation for Two-Phase Air-Water System*, draft, May 7, 2014.

Lichtner, P. C., G. E. Hammond, C. Lu, S. Karra, G. Bisht, B. Andre, R. Mills, and J. Kumar 2014. *PFLOTRAN User Manual: A Massively Parallel Reactive Flow and Transport Model for Describing Surface and Subsurface Processes*, http://www.pflotran.org/docs/user_manual.pdf

LLNL (Lawrence Livermore National Laboratory) 2005. *VisIt User's Manual, Version 1.5, October 2005*. UCRL-SM-220449. Lawrence Livermore National Laboratory, Livermore, CA. (www.visitusers.org)

Lu, C. and P.C. Lichtner 2007. "High resolution numerical investigation on the effect of convective instability on long term CO2 storage in saline aquifers", *Journal of Physics Conference Series*, 78, doi:10.1088/1742-6596/78/1/012042.

Mills, R., C. Lu, P.C. Lichtner, and G. Hammond 2007. Simulating Subsurface Flow and Transport on Ultrascale Computers using PFLOTRAN, *Journal of Physics Conference Series*, 78, 012051 doi:10.1088/1742-6596/78/1/012051.

Navarre-Sitchler, A., R.M. Maxwell, E.R. Siirila, G.E. Hammond and P.C. Lichtner 2013. "Elucidating geochemical response of shallow heterogeneous aquifers to CO_2 leakage using high-performance computing: implications for monitoring CO_2 sequestration", *Advances in Water Resources*, v53, pp. 45-55, doi:10.1016/j.advwatres.2012.10.005.

Olivella S. 1995. *Nonisothermal Multiphase Flow of Brine and Gas Through Saline Media*, Doctoral Thesis, Technical University of Catalunya, Barcelona, Spain, June 1995.

Painter, S. L., Chu S., Harp, D., Perry, F. V., and Y. Wang 2014. *Generic Crystalline Disposal Reference Case*, FCRD-UFD-2014-00500, LA-UR-14-26449. Los Alamos National Laboratory, Los Alamos, NM, August 2014.

Pruess, K, 1991. *TOUGH2 – A General Purpose Numerical Simulator for Multiphase Fluid and Heat Flow*, LBL-29400, Lawrence Berkeley Laboratory, CA.

Sassani D. et al. 2012. *Integration of EBS Models with Generic Disposal System Models*. FCRD-UFD-2012-000277, SAND2012-7762P. Sandia National Laboratories, Albuquerque, NM, September 7, 2012.

Sevougian, S. D. and R. J. MacKinnon 2014. "A Decision Methodology for Prioritizing R&D Supporting Geologic Disposal of SNF/HLW in Salt – 14030," in *Proceedings of the WM2014 Conference*, March 2 – 6, 2014, Phoenix, Arizona USA.

Sevougian, S.D., G.A. Freeze, M.B. Gross, J. Lee, C.D. Leigh, P. Mariner, R.J. MacKinnon, and P. Vaughn 2012. *TSPA Model Development and Sensitivity Analysis of Processes Affecting Performance of a Salt Repository for Disposal of Heat-Generating Nuclear Waste*. FCRD-UFD-2012-000320 Rev. 0, U.S. Department of Energy, Office of Used Nuclear Fuel Disposition, Washington, DC.

Sevougian, S. D., R. J. MacKinnon, C. D. Leigh, and F. D. Hansen 2013a. "A Safety Case Approach for Deep Geologic Disposal of DOE HLW and DOE SNF in Bedded Salt – 13350," in *Proceedings of the WM2013 Conference*, February 24 – 28, 2013, Phoenix, Arizona USA.

Sevougian, S.D., G.A. Freeze, P. Vaughn, P. Mariner, and W.P. Gardner 2013b. *Update to the Salt R&D Reference Case*. FCRD-UFD-2013-000368, SAND2013-8255P. Sandia National Laboratories, Albuquerque, NM.

Sevougian, S. D., G. Freeze, M. Gross, J. Wolf, J. Mönig, and D. Buhmann 2014. "Generic Salt FEPs Catalogue – Volume I," Rev. 0, March 31, 2014, Carlsbad, NM: Sandia National Laboratories, Waste Isolation Pilot Plant (WIPP) Records Center, Sandia Level Three Milestone: No. INT-14-01.

SKB (Svensk Kärnbränslehantering AB) 2010. *Data Report for the Safety Assessment SR-Site*. Technical Report TR-10-52. Swedish Nuclear Fuel and Waste Management Co., Stockholm, Sweden.

Smyth, J.R., B. M. Crowe, P. M. Halleck and A. W. Reed 1979. *A Preliminary Evaluation of the Radioactive Waste Isolation Potential of the Alluvium-Filled Valleys of the Great Basin*. Los Alamos National Laboratory. LA-7962-MS.

SNL 2008. *Total System Performance Assessment Model/Analysis for the License Application*, Volume 1, MDL-WIS-PA-000005 REV 00 ADD 01 ERD 4. Las Vegas, Nevada: Sandia National Laboratories. ACC: DOC.20080312.0001, DIRS 183478.

SNL (Sandia National Laboratories) 2013. *Cubit 14.0 User Documentation.* Sandia National Laboratories, Albuquerque, NM. (https://cubit.sandia.gov)

Vaughn, P., G. Freeze, J. Lee, S. Chu, K.D. Huff, W.M. Nutt, T. Hadgu, R. Rogers, J. Prouty, E. Hardin, B. Arnold, E. Kalinina, W.P. Gardner, M. Bianchi, H.H. Liu, and J. Birkholzer 2013a. *Generic Disposal System Model: Architecture, Implementation, and Demonstration.* FCRD-UFD-2012-000430 Rev. 1, SAND2013-1539P. Sandia National Laboratories, Albuquerque, NM.

Vaughn, P., S. D. Sevougian, E. L. Hardin, P. Mariner, and M. B. Gross 2013b. "Reference Case For Generic Disposal of HLW and SNF in Salt," in *Proceedings of the 2013 International High-Level Radioactive Waste Management Conference*, Albuquerque, NM, April 28 – May 2, 2013, American Nuclear Society, La Grange Park, IL. (www.ans.org)

Wang, Y., E. Matteo, Rutqvist, J. Davis, L. Zheng, V. Vilarrasa, J. Houseworth, J. Birkholzer, T. Dittrich, C. W. Gable, S. Karra, N. Makedonska, S. Chu, D. Harp, S. L. Painter, P. Reimus, F. Perry, P. Zhao, J. Begg, M. Zavarin, S. J. Tumey, Z. Dai, A. B. Kersting, J. Jerden, K. Frey, J. M. Copple, W. Ebert 2014. *Used Fuel Disposal in Crystalline Rocks: Status and FY14 Progress*, FCRD-UFD-2014-000060, U.S. Department of Energy, Office of Used Nuclear Fuel Disposition, Washington, DC., September 2014.

WIPP PA 1997. User's Manual for NUTS Version 2.05. Sandia National Laboratories, Carlsbad, NM. ERMS #246002

WIPP PA 2013a. User's Manual for BRAGFLO Version 6.02. Sandia National Laboratories, Carlsbad, NM. ERMS #558663

WIPP PA 2013b. Requirements Document and Verification and Validation Plan for BRAGFLO Version 6.02. Sandia National Laboratories, Carlsbad, NM. ERMS #558659

Zheng L., C. Jove-Colon, M. Bianchi, and J. Birkholzer 2014. *Generic Agillite/Shale Disposal Reference Case*, FCRD-UFDC-2014-000319, U.S. Department of Energy, Office of Used Nuclear Fuel Disposition, Washington, DC., August 2014.